MSc Thesis

Design of Ferritic-Bainitic High Strength Steels: A Physical Metallurgy Guided Machine Learning

MS53035

Miquel Ayllón García

Delft University of Technology

TU Delft

MSc Thesis

Design of Ferritic-Bainitic High Strength Steels: A Physical Metallurgy Guided Machine Learning

by

Miquel Ayllón García

to obtain the degree of MSc Materials Science & Engineering
at the Delft University of Technology,
to be defended publicly Thursday 26th October 2023 at 15:00

Student Number:	5623340
Supervisor, TU Delft:	Dr. Sid Kumar
Supervisor, TU Delft, TATA steel:	Dr. Hussein Farahani
Project Duration:	Nov, 2022 - Oct, 2023
Faculty:	Faculty of Mechanical, Maritime and Materials Engineering, TU Delft

Cover: Ferritic-bainitic steels used in the automotive industry
Style: TU Delft Report

TU Delft

Acknowledgements

This thesis marks an end to an amazing 2 years journey studying at TU Delft. Given the effort made, this comes with an overall feeling of accomplishment and satisfaction. Coming to the Netherlands to follow my studies has enabled me to develop a professional and social life that has been well worth it. It turned out to be a fantastic decision. I am proud to confirm that I have succeeded in every aspect: social, educational and professional.

I would like to first express my gratitude to my thesis supervisors, Sid Kumar and Hussein Farahani, for their help and assistance throughout the project. They have played an essential role in the accomplishment of my thesis, with their attention and advice during the past year, making this project a great period.

I would like to thank everyone I have met for the past two years. I am extremely grateful to the Gee Whiz, who have been the core of my daily life. The great times and help have made everything easier and better. They are bit wizards. Special thanks to Gerard, for being like Pumba in every adventure possible. To that house next to the station, leaving unforgettable memories. Most importantly, thanks to my parents, brother, girlfriend and family, for their support and belief in my capabilities, which have made each challenge more manageable. Us estimo!

Miquel Ayllón García
Delft, October 2023

Abstract

Bainite steels are in high demand in many application areas owing to their outstanding mechanical properties, mainly due to the presence of a combination of fine bainite plates and retained austenite. Understanding the complicated mechanism of bainite transformation is crucial to creating an optimum design. Researchers have addressed this challenge via computational modelling, where the transformation start temperatures of bainite (B_S) and martensite (M_S) are key indexes when designing high-performance steels and their heat treatments.

This thesis aims to explore the potential that data collection has to create a model, using experimental results of the bainite transformation process. A list of metallurgical accepted claims is elaborated to assess the quality of the data. Principal component analysis and clustering techniques are used to identify patterns, most important features and main relationships in the dataset. The results confirm the exponential carbon dependence that bainite and martensite transformation temperatures have, therefore requiring nonlinear models to predict them.

Following, regression models and machine learning algorithms based solely on the chemical composition are used to predict B_S and M_S. Train-test split series and cross-validation are used to evaluate the prediction and consistency of each model. The results show that the ensemble learning algorithms outperform the regression techniques. Random forest and gradient boosting decision tree provide excellent M_S prediction on the validation set with R^2 values of 0.92 and 0.93. The smaller dataset size adds up to the complexity of bainite transformation, resulting in worse prediction models of B_S, where the random forest and gradient boosting decision tree R^2 values are 0.68 and 0.67 respectively. Even though the models are showing signs of learning, the impact that outliers have demonstrates that the data is not good by itself to create a predictive model. The incorporation of microstructural and process parameters would provide significant advances to the models for designing bainitic steels.

Contents

List of Figures

List of Tables

Nomenclature

Nomenclature used in this thesis, in alphabetical order

Abbreviations

Abbreviation	Definition
AHSS	Advanced high-strength steels.
AI	Artificial intelligence.
bcc	Body-centered cubic.
bct	Body-centered tetragonal.
BHT	Bainite holding temperature.
BIW	Body-in-white.
CCT	Continuous-cooling-transformation.
CFB	Carbide-free bainitic.
CIAV	Charpy impact absorbed value.
CP	Complex phase.
DP	Dual-phase.
DRX	Dynamic recrystallization.
EDA	Exploratory data analysis.
FB	Ferritic-bainitic.
fcc	Face-centered Cubic.
GBDT	Gradient-boosting decision tree.
HE	Hole expansion.
HSS	High-strength steels.
ICT	Incomplete transformation.
LB	Lower bainite.
M/A	Martensite/Austenite.
MAE	Mean absolute error.
ML	Machine learning.
OLS	Ordinary least squares.
PCA	Principal component analysis.
PM	Physical metallurgy.
QP	Quenching and partitioning.
R2	Regression coefficient.
RA	Retained austenite.
RF	Random forest.
RMSE	Root mean square error.
SDLE	Solute drag-like effect.
TBF	TRIP-assisted bainitic ferrite.
TRIP	Transformation-induced plasticity.
TTT	Time-temperature-transformation.
TWIP	Twinning-induced plasticity.
UB	Upper bainite.
UMAP	Uniform manifold approximation and projection.

Symbols

Symbol	Definition	Unit
B_F	Bainite transformation finish temperature.	[ºC]
B_S	Bainite transformation start temperature.	[ºC]
CR	Cooling rate.	[ºC/s]
$f_{bainite}$	bainite phase fraction.	[%]
$f_{M/A}$	martensite/austenite phase fraction.	[%]
F_S	Ferrite transformation start temperature.	[ºC]
HV	Hardness Vickers.	[HV]
M_S	Martensite transformation start temperature.	[ºC]
T_B	Bay temperature.	[ºC]
TEl	Total elongation.	[%]
UEl	Uniform elongation.	[%]
UTS	Ultimate tensile strength.	[MPa]
YS	Yield strength.	[MPa]
$f_{\alpha 0}$	ferrite phase fraction.	[%]
$f_{\gamma 0}$	initial volume fraction of retained austenite.	[vol%]
$C_{\gamma 0}$	carbon concentration of retained austenite.	[mass%]
D^{γ}	austenite grain size.	[m]

1

Introduction

Bainite steels have gained significant attention across various industrial sectors due to their remarkable properties, including exceptional tensile strength, impact toughness, and weldability. These steels exhibit ultimate tensile strengths reaching up to 2.2 GPa, coupled with impressive toughness values of up to 130 MPa $m^{1/2}$. The key to their outstanding mechanical attributes lies in the microstructure composed of fine bainite plates, which, thanks to the presence of ductile-phase austenite, strike an optimal balance between strength and ductility. The transformation behaviour of bainite, a crucial aspect of understanding and optimizing these steels, has been recently the focus of extensive research. Various methodologies have been employed to investigate the phase transformation temperatures associated with bainite formation.

Materials development is currently undergoing large changes with a transition from the previously dominating empirical methods toward the development of methodologies with more computational components. The use of data and machine learning is increasingly used in the field of steel materials. An optimum design of high-performance steels requires a careful proportion of phases. In the alloy and heat treatment design process, the bainite start temperature and the martensite start temperature are critical parameters. Therefore, significant attention has been paid to their modelling in recent research, via different methodologies such as linear regression, thermodynamics-based modelling, or artificial neural network modelling. These methods are referred to as ML, computational techniques that enable the computer to learn from data and recognize patterns.

This thesis aims to gain a better understanding of the phase-transformation bainitic steels and ascertain whether or not it is sustainable to gain insights from published data. Initially, a literature review will be conducted, with an overview of the current state of the art in steel technology, covering bainitic steel phase-transformation mechanisms. Following, data will be collected and analysed through Exploratory Data Analysis and meta-analysis, to gain insight into the behaviour and main patterns of the dataset. Numerous visualization and data analysis techniques are used before modelling of bainitic transformation properties through machine learning techniques. Results and discussions for the machine learning algorithms are then presented followed by the conclusions of the study and recommendations for future research.

2

State of the art

2.1. Overview on advanced high-strength steels for the automotive industry

The automobile industry is confronting three major worldwide challenges: global warming, the constant need for energy from fossil fuels as a finite natural resource, and customers high expectations for quality products. Reducing fuel usage helps to protect fossil fuels, reduce dependence on fossil fuels, and reduce CO_2 emissions, which contribute to global warming. One potential answer that the automobile industry may invest in is the so-called Body-In-White (BIW) technology, which reduces the weight of cars. According to estimates, a 10% decrease in overall vehicle weight would result in an 8–10% increase in fuel economy [1]. However, other competing factors must be taken into account in combination with weight reduction, such as passenger safety and car formability. Governmental measures are often focused on improving vehicle safety. Therefore, design goals for cars must include their safety and integrity during a crash scenario. This is often evaluated by the car BIW's ability to absorb energy during a crash occurrence, or crashworthiness. For material producers and engineers, the task of simultaneously maximizing weight reduction, crashworthiness, and formability is challenging. Since decades ago, in response to these difficulties, new methods have been developed to enhance the mechanical qualities of steels, the primary metal used in BIW, or to add new lightweight materials such as alloys of aluminium and magnesium. This served as the driving force to develop the creation of Advanced High-Strength Steels (AHSS), which made vehicles more sustainable, safe, energy-efficient, and less polluting. The goal of the research was to raise the strength-ductility ratio in comparison to ordinary high-strength steels (HSS). Meaning, high strength values are desired in AHSS without losing toughness and formability.

Some base values that define the AHSS are a yield strength (YS) $\geq$ 300 MPa and an ultimate tensile strength (UTS) $\geq$ 600 MPa. Furthermore, other automotive analyses include, according to a safety-based automotive body design, two primary ranges for tensile strength. These take into consideration the structural function of the different components. Values for UTS $\leq$ 1000 MPa are established for components with a high energy absorption capacity for dynamic loading occurring during automobile collisions, and values UTS $\geq$ 1200 MPa with a high rigidity, anti-intrusion barrier for the safety of passengers [2]. The following empirical equations relating strength with hardness are proposed, as a rough estimate, when strength numbers in the literature are not reported:

$$UTS = -99.8 + 3.734\text{HV} \tag{2.1}$$

$$YS = -90.7 + 2.876\text{HV} \tag{2.2}$$

where both strength values are in units of MPa, and HV is the diamond pyramid hardness Vickers, in units kgf/mm^2. The standard error in these equations is $\leq$ 112 MPa [3].

The strain hardening capacity, which is attributed to the multi-phase nature of AHSS, as opposed to traditional HSSs, is the base of its magnificent performance. Three categories of AHSS have been

developed up to date since the late 1970s, obtaining an increasingly optimum combination of high strength and ductility. Built on a ferrite matrix that secures ductility, the first generation of AHSS includes different proportions of other microstructural components like martensite, bainite, and retained austenite, giving strength, extra ductility and offering improved formability in comparison with HSSs. However, because the microstructural components have such large hardness variations, there may be difficulties with local formability in some particular applications. A nice summary of the first generation can be found in the literature [4]: dual phase (DP), ferritic bainitic (FB), complex phase (CP), hot press forming, or press hardening (HPF, PHS), martensitic (MS), and transformation-induced plasticity (TRIP) steels.

Continuously, the following generation of AHSS includes principally high-Mn TRIP and Twinning-Induced Plasticity (TWIP) steels. Relying on a twinning deformation mechanism for strength and ductility, they present virtually a total austenitic microstructure. Due to their similarities, austenitic stainless steels are occasionally included in this category as well. The counterpart of this generation of steels is frequently their large cost. Due to its complicated mill processing and high alloy content, which presents welding issues, it is more expensive [5].

Starting in the last decade, the need to make the production of ultra-high-strength steels compatible with cold forming operations for the manufacturing of more complex shapes [4], caused together with economic reasons the creation of a third, and last to date, generation of AHSS. It expects to fill the gaps and solve the drawbacks of the two previous generations i.e., steels with a strength-ductility combination significantly higher than the exhibited by the first generation, but at a cost significantly lower than required for the second generation. The World Steel Association (AISBL) has not set a worldwide accepted minimum value of strength and ductility, or specific balances of microstructural components. International consortia focused on the creation of two products: a high-strength grade steel having 25% elongation and 1500 MPa tensile strength, and a high-ductility grade steel with a target elongation of 30% and tensile strength of 1200 MPa. The 3rd generation of AHSS consists of multi-phase steels designed to exhibit improved formability, that relies on a significant amount of ductile retained austenite that improves the work-hardening of the structure by TRIP effect, in a high strength phase as bainite or martensite, as well as ferrite and/or other precipitates, all in specified proportions and distributions.

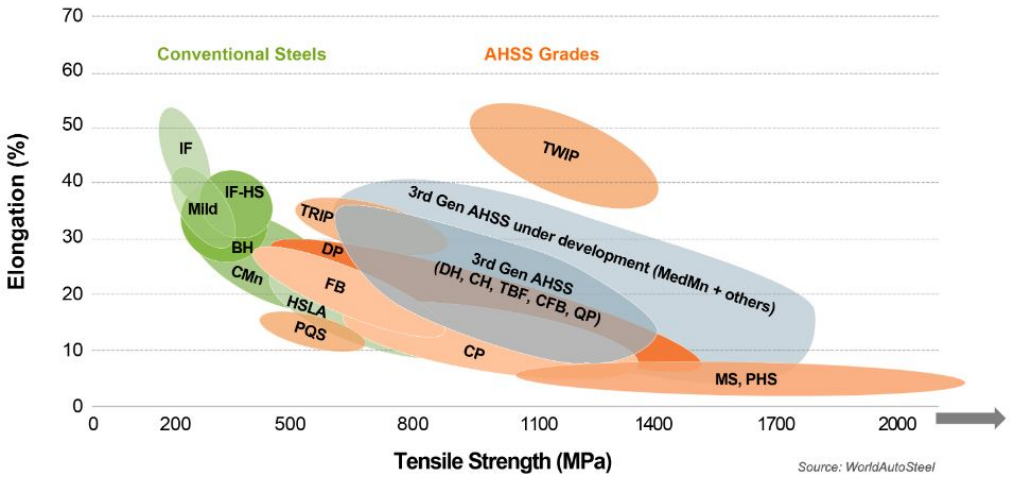

Figure 2.1: Comparison of the mechanical performance of conventional steels and AHSS - adapted from [4]

To guarantee outstanding press formability, a high hole expansion (HE) ratio, index of stretch-flangeability, is also needed [6]. While the HE strain might be adversely impacted by a low YS for the same tensile strength levels, the uniform elongation (UEl) normally rises with a low yield-to-tensile ratio [7]. It is a challenge to design steel with an optimum combination of these properties.

The 3rd generation of AHSS has established the control of the mechanical properties by the adjust-

ment of the phase volume fractions through the thermomechanical route [8]. A remarkably important design parameter to adjust regarding the phase volume fractions is the amount of retained austenite at room temperature. The retained austenite is the main responsible for the ductility of the microstructure, attributable to the TRIP effect. Three different broad categories of third-generation steels are now on the market or being tested. The TRIP effect is used in all of them. Additional high-performance grades might be created by using the quenching and partitioning (QP) procedure for the following grades: medium-Mn TRIP steels, QP steels and TRIP-Assisted bainitic ferrite (TBF) and Carbide-Free Bainitic (CFB) steels.

Medium-Mn TRIP steels are composed of a high content of Mn ranging from 3 wt.% to 12 wt.% together with other alloying elements such as Si, Al and microalloying additions. Since manganese has a lower density than iron, alloys containing this element produce lightweight products. With a lower density, aluminium further reduces the weight. Without an established chemistry of processing method, several investigations suggest as the easiest route performing hot-rolling above the A_3 temperature followed by quenching below the martensite start (M_S) temperature, cold rolling and following a subsequent intercritical annealing to enhance the formation of retained austenite and ferrite. Alternative treatments involve a series of intercritical annealing, with a consecutive quenching below M_S, which brings a greater martensite content in the resulting microstructure [9]. Compared to similar AHSS, with the same strength levels, the increased manganese content of Medium-Mn steels promotes greater quantities of retained austenite and thus better ductility through the TRIP effect.

QP steels have a simple heat treatment method consisting of quenching down to a predetermined temperature between M_S and M_d to produce a microstructure made of martensite and austenite, followed by overaging to cause the partitioning of carbon from austenite. It can be a one-step QP steel, with the holding done at the ultimate quenching temperature, or even at a higher temperature in a two-step QP steel. C enrichment stabilizes austenite throughout the isothermal holding or overaging process, resulting in a proper proportion of retained austenite at ambient temperature.

The last family of the third AHSS generation involve the bainitic steels. These have some characteristics in common with the QP microstructure, because the major phase is created when austenite is transformed into a BCC/BCT structure (bainitic ferrite or martensite), and a smaller portion of carbon-enriched austenite persists as the second phase. The good strength-ductility combination is attributed to the TRIP effect, giving rise to the name of these steels as TRIP-assisted bainitic-ferritic and CFB steels. When a YS criterion must be reached, CFB steels outperform medium-Mn TRIP steels in terms of stretch-flangeability.

Conventional bainitic steels generated during isothermal holding are distinguished by the large presence of cementite, either within or at the borders of the bainitic ferrite plates, where depending on the temperature of the treatment two different microstructures arise: lower (lower-bainite, LB) or higher (upper-bainite, UB). Another morphology in low-C steels that transforms with continued cooling is granular bainite. In contrast to ordinary bainite, one of its distinguishing features is the absence of carbides in the microstructure. C partitions from bainitic ferrite into the surrounding residual austenite and stabilizes it, resulting in this phase becoming enriched in C in a solid solution. As a result, the final microstructure includes both preserved austenite and potentially hazardous fresh martensite with a high C concentration in a solid solution. Normally, these two phases are combined and produce the called M/A (martensite/austenite) islands.

If alloying elements are sensibly added it is also feasible to create CFB steels with diverse morphologies and increased C-content. Some basic compositions are based on the combination Fe-C-Mn-Si. Si has limited solubility in this phase, serving as an alloying element that prevents cementite precipitation, competing therefore with carbon diffusion into austenite. When the microstructures are produced using an isothermal heat-process technique, that results in full bainitic transformation, leaving the martensitic transformation blocked after final cooling. The mechanical characteristics in that situation are similar to those of quenched and tempered processes. It has also been proposed that the isothermal holding might result in specific healing of quenching-induced microcracks by fine cementite precipitation [2].

2.2. Steel phase-transformations

Understanding the many allotropic transformations of elemental iron is necessary to characterize martensite and martensitic transformation, which is a phase that needs to be taken into consideration in bainitic steels. When pure iron is heated or cooled, it undergoes a phase transformation, changing its crystal structure or atom arrangement, which alters its physical characteristics. At ambient temperature, pure iron has a body-centred cubic structure, in which each unit cell has one atom at the body centre and one atom at each of the cube corners. Ferrite, or α-phase, refers to this homogeneous and isotropic phase. When heating above 1063K, ferrite shifts its magnetic characteristics from ferro- to para-magnetism, reflected by the α-β-phase transitioning. There is however no structural modification or reorganization of the atoms, having the β-phase the same bcc crystal structure. When heated even more to around 1183 K, the paramagnetic bcc β-phase changes into the face-centred cubic structure known as the γ-phase, where atoms are located on the face side of every one of the cube's eight faces and one atom is located at each of the cubes four corners. It is common to refer to this homogeneous, isotropic fcc phase as austenite. At 1673 K, the fcc γ-phase evolves again into the bcc structure known as the δ-phase, being this the final solid-state phase transition that takes place [10]. The Fe-C phase diagram in figure 2.2 shows what is the stable phase at a range of temperatures and carbon content in steel.

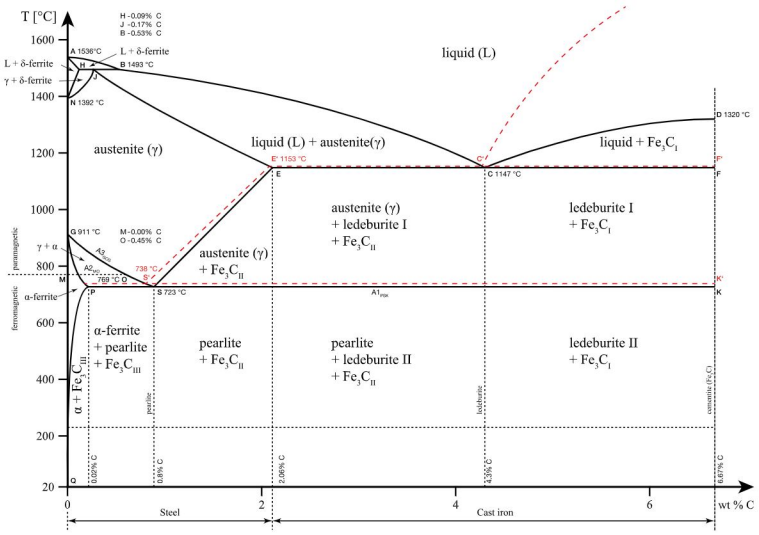

Figure 2.2: Iron-Carbon Phase Diagram

Fully austenitic phases transform into other phases with a different microstructure and hardness upon cooling at constant or varying cooling rates. The cooling rate will allow carbon steels to overcome a stable or metastable transformation. In Figure 2.3 several cooling rate routes are shown in a hypothetical time-temperature diagram. Coarse and fine pearlite, UB and LB, and martensite are some of the most typical outcome microstructures upon cooling. Several other factors influence here, such as alloying elements and previous austenite grain size, which will be addressed in future sections.

Martensitic transformation

Rapid quenching of the material from the A_3 temperature causes the austenite to change into the martensite crystal structure. The term "Martensite start temperature" refers to the temperature at which the first martensite sheaves form inside an austenite grain as a result of fast cooling. Because stable bcc α-Fe can dissolve less C, the metastable fcc austenite tries to reject the C maintained in a solid solution upon quenching. However, because the temperature is falling quickly, carbon cannot simply escape, instead, it is held inside the austenite, straining it to the point where a shear-like, diffusionless transition from fcc to a bct structure occurs, involving the cooperative movement of atoms over distances less than one atomic diameter and supported by a macroscopic change in shape of the transformed volume. This transformation is known as martensitic transformation. The resulting structure is

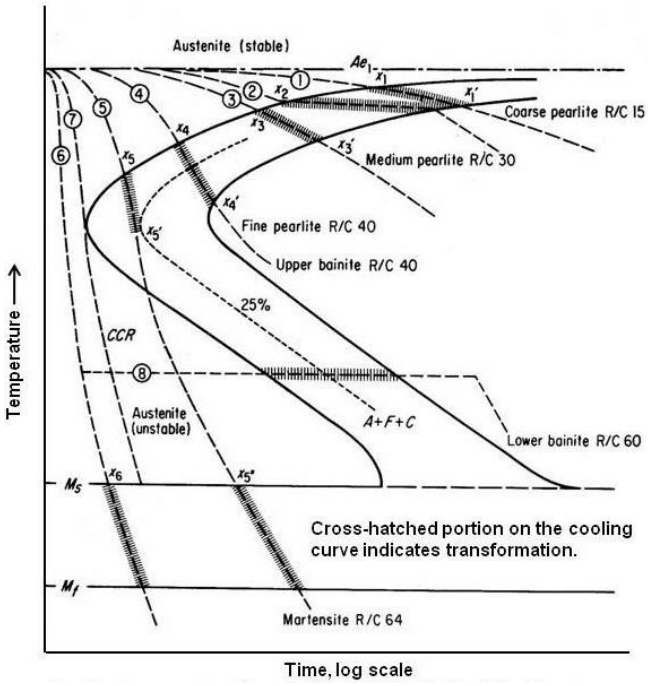

Figure 2.3: Cooling curves superimposed on a hypothetical t-T diagram - adapted from [11]

known as martensite, which is a metastable supersaturated phase. The martensite transformation has developed interest among researchers and several theories have been published after some empirical observations have been discovered [12].

Crystallography of Martensitic Transformation

Earlier theories developed by scientists tried to explain the crystallography of the martensitic transformation, relating lattice orientation between parent and product phases, shape alterations and morphologies dependent on the habit plane and the nature of interfaces. The different morphologies are affected by the direction and size of habit planes, and by the crucial role in the shape change caused by the cooperative displacive movement of atoms. This change is contributed by the shear and a subsequent volume variation. Without initial success, the theories by Kurdjumov-Sachs [13], Nishiyama [14] and Bain [15] were the fundamental base of newer theories [16][17], which would concentrate the research on the interface-orientation relationship between parent and product phases and with surface dislocations that lead to the invariant plane theory.

Kurdjumov-Sachs correspondence proposes the fcc to bcc transformation by a double shear mechanism, without reconstruction of the crystal structure. Bain's conclusion that the fcc and bcc lattices are equivalent was not supported by his shear theories solely and failed to explain the empirically observed surface tilts during transformation, caused by an invariant plane, known as the habit plane. The invariant plane theory has added a further deformation in the form of shear to make up for the fact that Bain's strain alone cannot yield an undistorted habit plane. The "inhomogeneous" or "complementary" shear effectively shortens lattice vectors that have been stretched by the Bain strain. Even though the result of these combined deformations is an undistorted plane, this plane is rotated from its initial position, requiring the introduction of a rigid body rotation to fully describe the crystallographic theory of martensite transformation [18] [19] (see figure 2.4).

Some studies [21] show a temperature dependence of the lattice parameters in martensite. In the martensitic phase, the lattice parameter varies significantly with temperature along the c-axis.

Many have tried to establish a relationship between the carbon content and the lattice parameters both in experimental and modelling research. The separation of the (002) and (200) peaks on X-ray

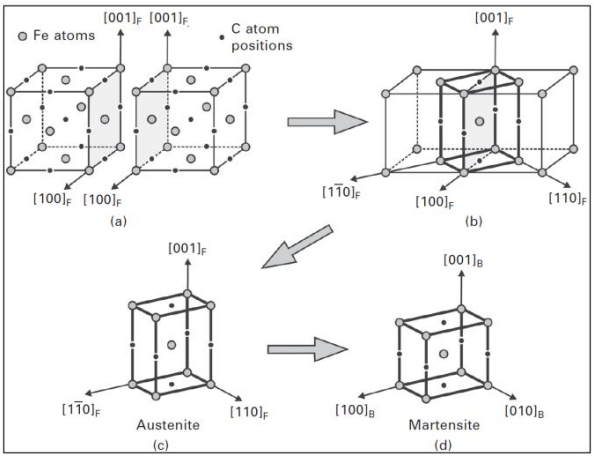

Figure 2.4: Schematic illustration of the Bain correspondence for martensite in steels. (a) shows a pair of unit cells of the fcc_F austenite structure. As the two unit cells are joined, a bct arrangement emerges as highlighted in (b), and selectively distinguished in (c). The bct unit cell in (c) is transformed into a bcc_B (d) via contraction along the direction $[001]_F$, and expansion along the directions $[1-10]_F$ and $[110]_F$. The distortion applied between (c) and (d) corresponds to the Bain strain [20]

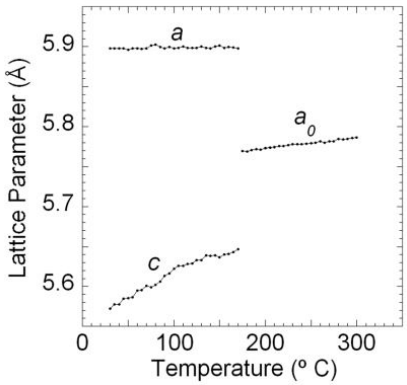

Figure 2.5: Evolution of the lattice parameters a and c of tetragonal martensite during heating showing a transformation into the cubic austenite (a_0) - adapted from [21]

diffractograms was the initial proof of martensite lattice tetragonality [22]. It has been proven that the a lattice parameter of the α-phase (0.286 nm) is always smaller compared with the a lattice parameter of martensite (0.285 nm). On the other hand, the c lattice parameter of martensite rose from 0.291 to 0.302 nm, corresponding to changes in the c/a ratio from 1.024 to 1.058, while the carbon content of the material grew from 0.8 to 1.2 wt.%.

Greninger and Troiano [23] focused their attention on the surface tilts observation of the shape strain preceding the transition. To explain the combined impact of Bain's correspondence and shape strains along the habit plane involved in the transition from fcc to bcc/bct lattices, the modern Phenomenological Theory of Martensitic Crystallography (PTMC) was developed. The Lattice Invariant strain (LIS), which is incorporated into PTMC, does not modify the crystal structure of any phase but alters the geometry of the changed volume. The volume change is connected to a shear-initiated slide or twinning mechanism.

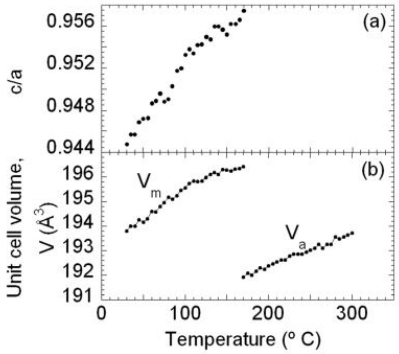

Figure 2.6: Temperature dependence of the martensitic lattice distortion, c/a (a) and unit cell volume of austenite, V_a, and martensite, V_m (b) during heating. Whereas the behaviour of lattice distortion is reminiscent of the one in a bulk, a large volume contraction during the transformation from martensite to austenite is inverse in comparison with the volume expansion observed in bulk Ni-Mn-Ga alloys - adapted from [21]

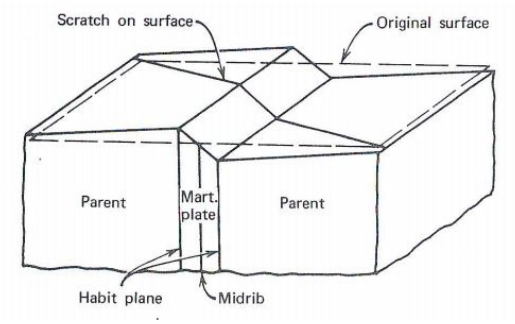

Figure 2.7: Martensite transformation involves shape and volume change [24]

2.3. Bainitic Steels

2.3.1. Nucleation kinetics

Whether it is upper or lower, bainite is an aggregate of plates of ferrite that are separated by martensite, untransformed austenite or cementite. The aggregation of those ferritic plates are termed sheaves, while a single ferritic plate in the sheave is termed a sub-unit. All sub-units are crystallographically aligned with each other. A wedge-like shape with a thicker side characterises these sheaves, with the thicker side being where the austenitic nucleation starts. Sub-units only nucleate over a previously nucleated one and are nucleated until a specific size and have limited growth.

The time-temperature-transformation (TTT) diagram in figure 2.8 shows the highest temperature T_H at which displacive transformation to bainite is observed. There is evidence [25] that bainite and Widmanstätten ferrite nucleate by the same mechanism as martensite but with the requirement of carbon to partition during the nucleation of bainite. The nucleation principally occurs in sites confined to the austenite grain surfaces. Bhadeshia found that the activation energy for nucleation varies linearly with the driving force. He then went on to demonstrate that the straight line can be justified theoretically by the dissociation of dislocation clusters.

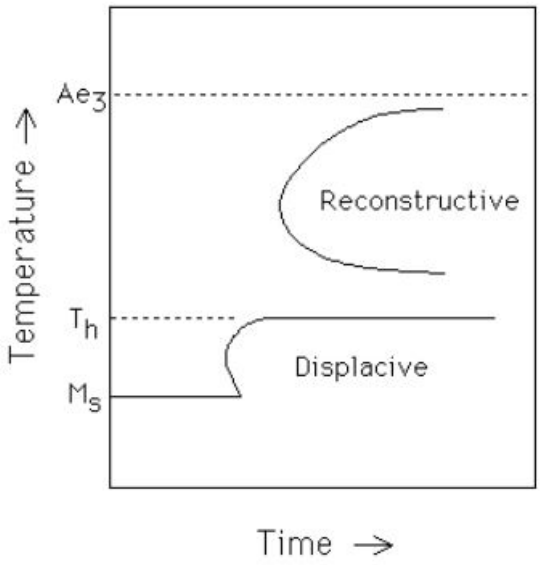

Figure 2.8: Schematic TTT diagram illustrating two C-curves and the temperature T_H.

2.3.2. Bainite growth kinetics

At temperatures between those of pearlite and martensite, austenite undergoes a phase transformation that results in the phase product known as bainite. Hultgren gave it the name ”Troostite” after seeing that it was composed of cementite and ferrite [26]. Later, it was given its current name after Bain, in recognition as he was the person who discovered its TTT behaviour [27]. With the finding, a brand-new area of study was opened, leading to the creation of steels with remarkable qualities. Bainite in steel is a plate-like, non-lamellar mixture of ferrite and cementite. Its remarkable properties such as good strength, hardness, toughness and wear resistance are retained or even benefited when in combination with other phases as in DP or TRIP steels. Industry finds use as forged sheet steel automotive parts, with high requirements in strength, formability and energy absorption at fast deformation rates.

It is important to understand the kinetics and mechanism of bainite formation for an optimum design of bainitic steels. Despite several explanations for this, there is still disagreement amongst researchers, even though it has been the focus of decades worth of research, and opposing viewpoints have arisen. All previous efforts to characterize the transformation mechanism of bainite have been categorized under two competing mechanisms, the diffusional hypothesis and the diffusionless hypothesis, both presented below. One of the conflicting ideas that separate the views into two mechanisms is the presence of a surface relief when a unit of Widmanstätten ferrite or bainite forms.

Diffusional approach

In the diffusional case, carbon diffusion in austenite is assumed to control bainite growth and the challenge is to determine the carbon concentration at the interface and the degree of supersaturation in ferrite. Hultgren proposed a diffusional approach in which bainite forms as plates of Widmanstätten ferrite [28] and the edgewise growth is controlled by the diffusion of carbon in austenite. The Widmanstätten ferrite transition and the bainitic ferrite transformation have the same diffusional process, while the reaction of carbide generation in UB and LB occurs after the main growth.

The lengthening rate is larger than the lateral growth, attributed to the low mobility of the coherent interfaces. The α-γ interface grows with C concentration that deviates from equilibrium and is affected by kinetics, capillarity and interactions with alloying elements. There is no partitioning of substitutional alloying elements, a condition referred to as paraequilibrium. The transformation products of Widmanstätten ferrite and acicular ferrite in the two varieties of upper and lower bainite, following supporters of the diffusional model, create a continuous set of products [29]. Hillert observed a morphological similarity between the Widmanstätten ferrite and bainite, where the lengthening rates of both

varied equally with temperature, concluding that it is the same transformation mechanism [30]. The presence of the surface relief is explained to be caused by a ledge mechanism [31]. The observed sub-units are ledges propagating along the broad faces of bainitic plates. They further claimed a direct relationship between ledges and sub-units. Additionally, the apparent lengthening kinetics are consistent with a diffusion-controlled growth mechanism. Aaronson and Kinsman presented evidence to invalidate the displacive mechanism. Bhadeshia and Edmonds [32] observed that the sheaf of UB consisted of smaller sub-units that could not possibly be compared with ledges since the individual sub-units were isolated by carbon-enriched retained austenite (RA) films.

Some studies [33] have tried to model the lengthening kinetics of bainitic ferrite laths with the effect of holding temperature, C content and crystallography, showing that there is a deviation between the orientation of bainitic ferrite concerning the parent austenite and that this deviation is temperature and C content dependent. Figure 2.9 shows the results, where the lengthening rates of the laths increase with the increasing temperature and decreasing amount of C. The same study concluded that the lengthening kinetics of an individual lath may be dependent on its orientation concerning the parent austenite. A good fit of the experimental results was obtained when introducing the misorientation effect on the interface mobility.

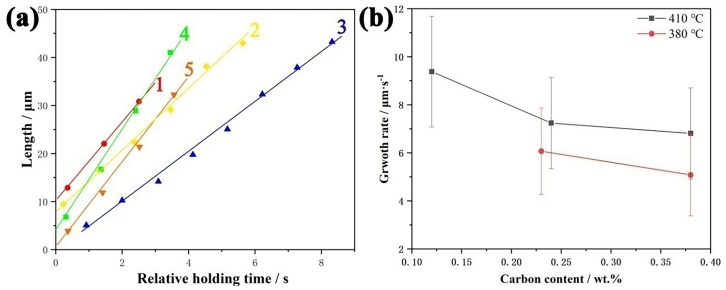

Figure 2.9: (a) Length change of individual BF as a function of the holding time in the region with 0.38 wt.% C during holding at 419ºC ; (b) measured growth rates of BF under different combinations of C content and holding temperature - adapted from [33].

Diffusionless approach

For the diffusionless-control mode, the carbon is assumed to be trapped in bainitic ferrite during growth. The rate is thus controlled by repeated nucleation at the tip of the plate. One of the key reasons for the diffusionless hypothesis is the likeness of bainite to martensite. It is said that bainite is generated by a displacive process and that the transformation boundary behaves similarly to the martensitic interface. Oblak and Hehemann [34] proposed, after examining Widmanstätten ferrite, UB and LB, that it is not a continuous series of transformation products, but a repeated nucleation of martensitic subunits growing to a size determined by the strain accumulation, with a continued growth limited by strain relaxation. Bainitic ferrite grows by the propagation of discrete martensitic sub-units, giving rise to a plate-like morphology. Immediately after the supersaturated ferritic component is formed, the partitioning of C into the residual austenite gives the formation of carbides. As in martensite, the surface relief can be explained by the lattice change occurring by a displacive mechanism, however not only this mechanism can give rise to this effect.

Bainite start temperature

One may predict a critical line in the Fe-C phase diagram where the thermodynamic parameters allow the transition to bainite to occur from the barrier for growth. Based on Zener and his diffusionless growth of bainitic ferrite [35], Bhadeshia presented the T_0 line [32], the temperature at which austenite and ferrite with the same composition present the same Gibbs energy (see figure 2.10).

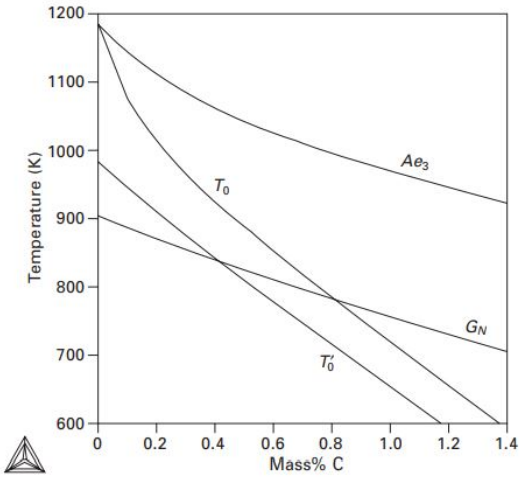

Figure 2.10: Schematic showing the barriers to the development of bainitic ferrite using the diffusionless theory. B_S is predicted to be controlled by nucleation above the intersection of G_N and T_0 and by growth below that point.

Bhadeshia predicted back in 1981 that a 400 $Jmol^{-1}$ barrier needs to be exceeded during growth, meaning that for the microstructure to be able to grow it requires this chemical driving force, leading to the T_0' line in figure 2.10. Following the diffusionless approach the start of bainite formation, B_S, does depend both on the barrier needed for nucleation and on the barrier for growth. The B_S temperature should not be used only for evaluating the barrier for nucleation. The microstructure therefore cannot be observed unless the driving force is sufficient for nucleation as well as for growth.

The development of cementite on the sidewalls of ferritic plates signals the start of a second stage of transformation. Cementite may form in carbon-enriched austenite over longer periods or at lower temperatures, either as a result of carbon being rejected from supersaturated ferrite plates by the diffusionless hypothesis or as a result of carbon escaping from the moving ferrite/austenite interface under the diffusional hypothesis. Following the diffusional hypothesis, simultaneous growth of cementite and ferrite leads to a mixture of ferrite and coarse cementite, representing UB. On the other hand, it is less clear if the ferritic constituent in the diffusionless hypothesis is formed under diffusion of C or by displacive and diffusionless growth.

Following Hillert diffusional hypothesis, it is seen that at a lower temperature, the LB mixture forms as the the plates of ferrite are thinner, with wider spaces between the primary plates. A thick layer of ferrite and cementite grows with a cooperative mechanism [36]. On the other side, LB is not formed via this mechanism but by the precipitation of cementite inside the supersaturated ferrite, similar to the tempering of martensite, which proposes the diffusionless approach. Kingsman and Aaronson reported the process of C rejection from supersaturated ferrite into the surrounding austenite without the austenite/ferrite interface moving.

The difficulty in defining bainite should be underlined in this context. The diffusional theory states that Widmanstätten and bainitic ferrites are identical, but bainite is the final result after the second phase of the eutectoid transition. At high temperatures, there may be a noticeable time difference, and Widmanstätten ferrite may as well be formed without ever being followed by cementite.

It was proposed by Kuo and Hultgren that when bainite forms, solute atoms do not partition between ferrite and cementite. It is now generally agreed that bainite forms under paraequilibrium, implying that the amount of the alloy content relative to Fe on both sides of the moving phase is the same, which from the thermodynamics point of view is like if the Fe atoms were substituted by an element with different thermodynamic properties. For example, Al or Si are less soluble in cementite and the tendency to form cementite will therefore decrease or even be prevented with the addition of these, which would result in CFB steels. If the amount of Si and Al are lower, it will only delay temporarily the transformation. Illustrated in figure 2.11, a temporarily incomplete transformation in which only with a long heat treat-

ment will the carbides appear. The plateau represents the CFB steels. In the plateau, the C content in the austenite combined with the heat treatment temperature defines a point on the B_S line, making it an experimental way of determining the B_S for an alloy with a determined carbon and initial alloy content.

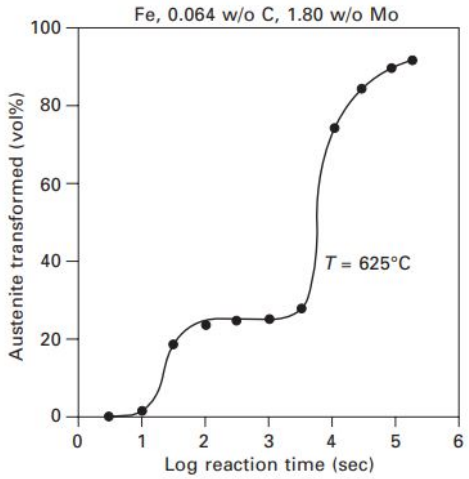

Figure 2.11: Degree of transformation as a function of time with incomplete transformation - adapted from [37].

Steven and Haynes proposed an analytical expression able to predict the B_S using the content of alloying elements:

$$B_S = 830–270C–90Mn–37Ni–70Cr–83Mo(°C) \tag{2.3}$$

where The chemical elements are in quantities of mass percentage in the austenite phase. This empirical relation is limited to small composition intervals. Many attempts have been made to analyze the effect of alloying elements on B_S based solely on binary models. When Hillert introduced the barrier of growth, he treated it as independent of composition. When his work was revised [38] the independence of C and Mn content were accepted. However, experimental analysis on Cr and Mo showed a proportional increase of the barrier with the solute content (see figure 2.12). It was proposed that carbide-forming elements may have an effect, and it is now known as the solute drag-like effect (SDLE).

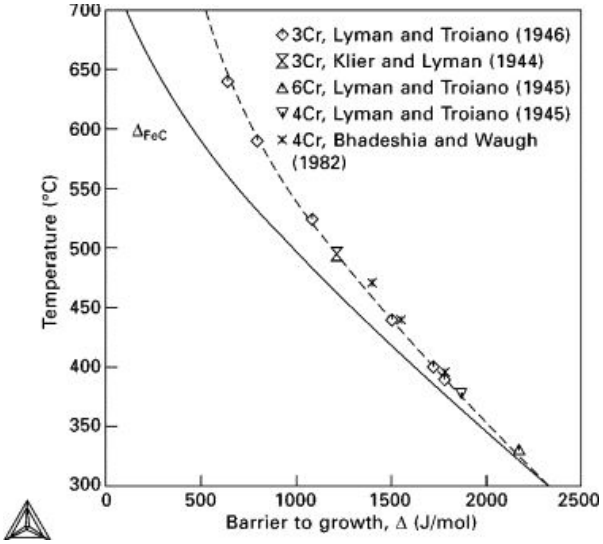

Figure 2.12: The evaluated barrier for acicular growth of ferrite with 3 wt.% Cr. ΔFeC represents the driving force for the Fe-C system.

2.3.3. Upper and Lower Bainite

Still without a successful attempt to generalise a definition of bainite, many accept it as a microstructure consisting of a non-lamellar mixture of ferrite and carbides. Two families can be differentiated: upper and lower bainite, which display different mechanical properties. Formed at higher temperatures, UB is formed as aggregates of small plates or laths of ferrite, free of precipitation. Carbides do grow between the plates of ferrite, from the carbon-enriched residual austenite. Contrarily, in LB carbide particles grow, in addition to the same kind of precipitation in the upper form of bainite.

It has been proven that the transition between UB and LB can be predicted with models by comparing the rates of decarburisation and precipitation. A narrow range of temperatures separates the formation of both forms, allowing them to occur simultaneously [39]. During an isothermal transformation, a competition between the rate at which carbides precipitate from ferrite, which is dependent on multiple factors such as time, temperature and chemical composition, and the speed with which C atoms are partitioned from the supersaturated ferrite into austenite, allows both forms to coexist at some extent. With a higher diffusion, UB permits the C to partition before it can precipitate in the ferrite, while a slower diffusion at lower transformation temperatures allows some C to precipitate in the supersaturated ferrite. The illustration in figure 2.13 can be expressed quantitatively by comparing the time required to decarburise supersaturated ferrite against the time interval necessary to obtain a detectable amount of cementite precipitation in the ferrite [32], giving a reasonable way to interpret the transition from LB to UB.

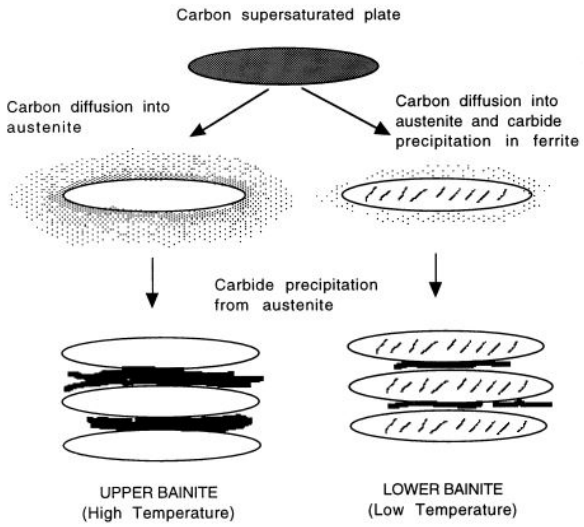

Figure 2.13: Schematic representation of the transition from upper to lower bainite - adapted from [32].

With some assumptions, and in agreement with experimental data, the theory concludes that lower bainite cannot form in plain carbon steels with less than 0.3 wt.% carbon, while upper bainite is not formed when the carbon concentration is larger than 0.4 wt.% carbon in plain carbon steels.

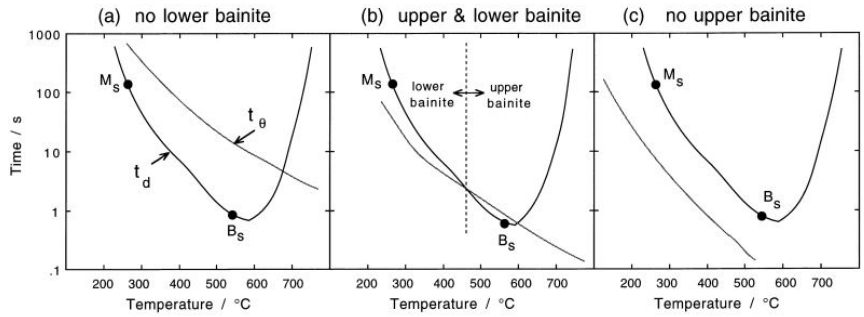

Figure 2.14: This figure shows how a small variation of the decarburisation time t_d and the precipitation time t_θ can lead to: (a) steel incapable of transforming to lower bainite ; (b) steel which under appropriate conditions is capable of transforming to both upper and lower bainite ; (c) steel which always transforms to LB - adapted from [32].

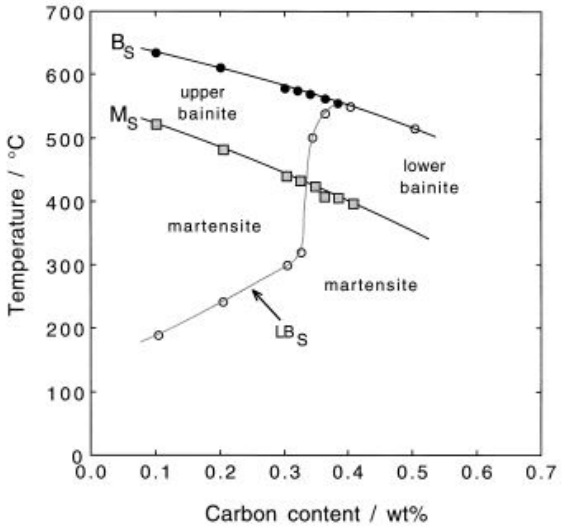

Figure 2.15: Calculated LB transformation start temperatures for plain carbon steels, as a function of the transformation temperature - adapted from [32].

When bainite laths grow in UB, the high diffusivity of C enables its partition between ferrite and austenite, forming a low carbon-content ferrite and resulting in the enrichment of carbon in austenite. In low-carbon steels, the carbides are present as discrete particles at the lath boundaries.

LB, similarly to tempered martensite, is generated by an autotempering process, therefore a comparison between these microstructures should be made. Studies found that in both high-carbon martensite and LB, the initial precipitate is normally a transition phase, ϵ-carbide, which subsequently is replaced by a more stable cementite. In LB during a prolonged holding at the isothermal transformation temperature, the same transition occurs. The probability of formation for the ϵ-carbide first in LB increases by lowering the transformation temperature, because the time needed to decarburise a supersaturated plate of bainite increases. High C concentration can remain in the ferritic matrix for more time and allows the formation of the ϵ-carbide, only occurring if the carbon concentration is lower than approximately 0.25 wt.%. This illustrates why a medium carbon Fe-0.43C-3Mn-2Si wt.% steel transforms to LB, which contains cementite particles.

Even resembling martensite, studies show that the carbides in LB have the same crystallographic orientation while in the tempered martensite, the cementite precipitates form with a different crystallographic orientation. The carbides in LB have a rod-like morphology and are aligned almost parallel to each other, similar to what can be seen in figure 2.13.

2.3.4. Carbide-Free Bainitic Steels

When slowly cooling austenite, it transforms into a microstructure containing ferrite and an iron carbide with composition Fe_3C, termed cementite. Controlled cooling can produce bainite, consisting of a dislocation-rich ferrite surrounded by austenite, martensite and cementite. With the right chemistry and the application of specialized thermal profiles capable of holding at particular temperatures, the size of these components can be controlled to some extent. It is possible to prevent the formation of the low-ductile cementite phase. As shown in figure 2.16, thin fine laths of untransformed retained austenite can be obtained instead of the classical structure of interlath carbides, resulting in a higher strength associated with the grain size. Due to the fine size and greater dislocation density, the ferritic component leads to an additional improvement in local formability. The RA promotes the TRIP effect, resulting in greater UEl and global formability. These characteristics combined give this microstructure the name of TRIP Assisted Bainitic Ferrite or Carbide-Free Bainite.

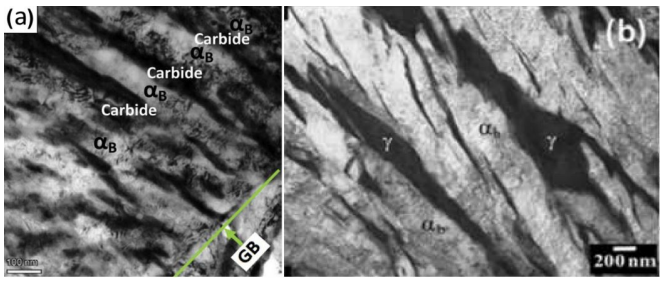

Figure 2.16: On the left the classic bainitic structure with bainitic ferrite laths (α_b) and interlath carbide. On the right, the microstructure of TBF / CFB shows bainitic ferrite laths interwoven with thin films of untransformed retained austenite (γ).

Recent developments in the creation of high-performance steels with enhanced strength and ductility depend on the TRIP effect, which consists of the mechanically induced martensitic transformation of the remaining retained austenite scattered in a soft ferrite-based matrix. For a long time it has been known that during mechanical loading, austenite undergoes a martensitic transformation. As a result, the stabilization and retention of austenite at ambient temperature has been for some studies a priority, giving rise to steel grades and thermomechanical treatments that have been particularly created for this aim. In particular, it was discovered [40] that preserving austenite was greatly aided by C enrichment of the material during intercritical annealing and bainite transition, as carbon is one of the strongest austenite stabiliser elements. The work hardening rate significantly increases as a result of the metastable austenite gradually transforming straining. This postpones the onset of necking and therefore improves the formability. Increasing the austenite content enhances the strain-hardening rate and overall performance of the steel, whereas the fracture strain, cut-edge sensitivity and bendability (bending degree) seem to be controlled by the number of second phases (M/A).

If small grains of austenite are retained at room temperature and dispersed in a soft ferritic matrix, the TRIP effect can take place. The stabilisation of austenite at room temperature is controlled by the amount of carbon. During the intercritical annealing, the first C enrichment of the austenite accompanies the nucleation and growth of the phases. A second hold together with the presence of particular alloying elements enhances the formation of C-saturated austenite instead of cementite precipitates, promoting the prevention of martensitic transformation upon quenching, and the stabilisation of austenite at room temperature. Aluminum seems to be an effective compound even though lower levels of strength are exhibited. Silicon influences strongly through the solid solution strengthening effect. A mixed Al-Si CFB steel shows a good combination of the processing requirements, the desired mechanical properties and industrial constraints [41]. Si inhibits the precipitation of cementite [38] during bainitic transformation, due to its low solubility in this phase. It is enough to add to the steel 1.5%wt Si to suppress the growth of cementite from austenite. C rejected from the bainitic ferrite enriches the residual austenite, thereby stabilising it down to ambient temperature, resulting in a microstructure of fine plates of bainitic ferrite separated by C-enriched regions of austenite. However, it is also challenging regarding final surface quality [42]. Partial replacement of Si by Al helps solve this problem [43] [44] [45]. Other studies consider Cu [46], P [47] or Ni [48] as possible alternatives.

Besides specific chemical compositions, the austenite grain size [49] and the austenite prior deformation [50] influence as well the austenite retention at ambient temperature and are under current investigation. Reducing the austenite grain size changes the growth process from autocatalytic nucleation to grain boundary nucleation, and the morphology from a sheaf structure to adjacent plates, leading to a variation of the transformation rate. The austenite prior hot deformation also influences greatly the morphology of the bainite / retained austenite microstructure.

As already mentioned, the enhancement of strength without compromising the UEl is the primary goal behind the creation of TRIP-assisted multiphase steels. These two qualities, however, are opposed. It is quite challenging to raise the amount of stress that a material can withstand without lowering its resistance to localized deformation and subsequent fracture. The work hardening rate, or the ratio of increased stress to increased strain, $\Delta\sigma/\Delta\epsilon$, is connected to these two qualities of strength and deformation. The balance between the formation and annihilation of dislocations, which occurs at the microscopic level, determines the work hardening rate. By carefully combining several processes of strengthening and softening, TRIP-aided steels enable to increase in the work hardening rate concerning other steel grades and microstructures. Using the Hill elastic-plastic analysis of the expansion of a spherical particle in an infinite medium, a study [51] shows that the increment of the work-hardening rate and therefore the strength-ductility balance at the onset of necking is influenced by the rate of dislocation strengthening as a consequence of the TRIP effect. It is concluded that the transformation rate of retained austenite and thus its mechanical stability are the key factors influencing the work-hardening behaviour of TBF steels.

The high degree of strength displayed by the TRIP steels cannot however be solely attributed to the rise in dislocation density. The composite nature of the steel microstructure is another important feature. With a mixture of phases of opposing characteristics, the YS of these can be measured thanks to neutron diffraction. Values ranging from 500 MPa to 2000 MPa were found for ferrite, bainite, austenite and martensite [52] [53]. Neutron diffraction enlightens the stress partitioning occurring between soft ferrite and hard martensite during loading. Analysis of SEM micrographs allows the measurement of the strain partitioning. The large variability among the phases permits stress and strain partitioning during the loading and dictates the macroscopic stress-strain response.

A possible route to obtaining this microstructure is to perform an intercritical annealing between the A_1 and A_3 temperatures, cooling slightly to enhance the transformation of ferrite, then quenching to a temperature just below B_S but above M_S. After an isothermal hold, a certain amount of bainite will have formed, and the process ends with a rapid quench to ambient temperature.

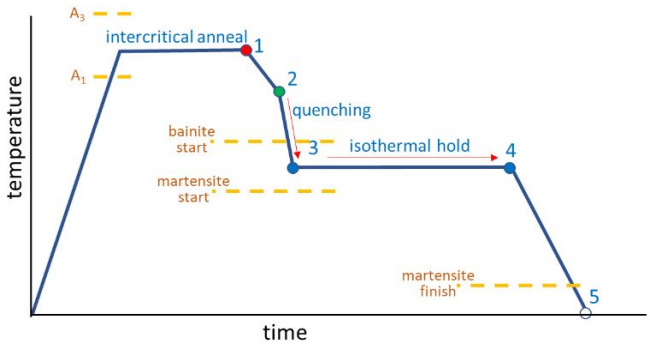

Figure 2.17: Possible thermal cycle to produce Carbide-Free Bainite steels.

The steels exhibit a strong equilibrium between global formability and strength, measured by high TSxEL, UEl, and total elongation (TEl) together with low YS/UTS, versus local formability, evaluated by bend angle and the HE ratio. Due to its consistent fine lath structure, CFB steels are likely to exhibit exceptionally good stretch-flangeability. Besides, the presence of martensite provides heterogeneities in hardness, enabling the steel to achieve excellent deep drawability [54]. The absence of fine carbides

provides the steel with high resistance to cleavage fracture and void formation. It is possible to further enhance the toughness by the TRIP effect and improve the toughness with an ultrafine grain size of the bainitic ferrite plates.

Effect of the chemical composition

Regarding alloying elements, Al has been proposed as a substitute for Si for final surface quality reasons in intercritically annealed conventional TRIP steels. In TBF steels, Cr and Mo are seen as an optimum alternative to Al to achieve full austenitization at an industrial scale. A careful quantification of the alloying elements allowed a 0.9Si wt.% and a combination of Mn, Cr and Mo up to 2.9 wt.% to present YS values of 1100 MPa, a total elongation above 10% and HE strain above 30%, with a heat treatment consisting of a quenching down to 350ºC and a holding temperature of 400ºC [55]. TBF steels with Nb contents below 0.05 wt.% have been produced for the automotive industry, giving a general refinement of the microstructure. Ti, V and Nb are sometimes added in small amounts to enhance strength and hardenability. At higher temperatures, vanadium is seen to significantly impede the formation of bainite, possibly due to the segregation of V atoms in the grain boundaries, and consequently reduction of the bainitic nucleation rate [56].

The combination of strength and total elongation (TElxUTS) increases as the austenite stabilizer elements (C + Mn + Cu + Ni) amount increases, confirming results by Sugimoto et al. [57]. Mn and C stabilize a higher fraction of M/A islands and retained austenite for bainitic transformation. Cu and Ni show similar final properties as Mn but slows down the bainitic transformation rate, which is not desired in industrial applications.

Effect of bainite holding temperature

Studies have analysed how the bainite holding temperature (BHT) affects the properties of CFB steels [58]. In figure 2.18, the effect of the BHT on strength, ductility and formability is displayed, showing how the BHT is a very relevant parameter to optimize the formability-strength balance of the final product. In the studied steels, holding temperatures above M_S and close to 400ºC should be selected to reach an optimum UEl, while lower BHT should be used to produce high HE materials. In any case, the results give better performances than expected for conventional DP steels. Too high BHT, 450ºC in this precise case, are better to be avoided as it can lead to insufficient transformed fractions. Another design parameter is the control of the duration of the bainitic transformation. It is shown that a too-short bainitic holding time would result in a too-high fraction of fresh martensite, which can lead to poor properties. A too-high fraction of martensite significantly reduces the damaging performance of the microstructure.

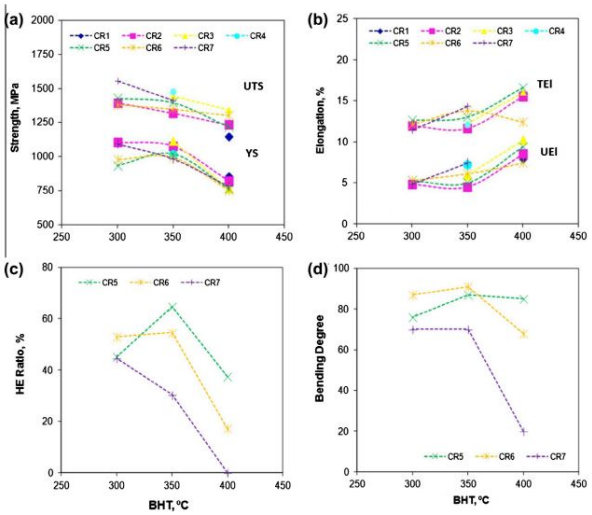

Figure 2.18: (a) Strength, (b) elongation, (c) hole expansion ratio, and (d) maximum bending angle before fracture, of cold rolled bainitic steels after CAL process as a function of BHT - adapted from [58].

Incomplete bainite transformation

The incomplete transformation phenomenon is always present when applying a cooling rate in the process of austenite transformation. When transforming to bainite, a transformation stasis can take place, known as the incomplete bainite transformation (ICT) phenomenon. Both the diffusional and displacive hypotheses can give evidence about it. Zener [35] suggested, according to the displacive mechanism of bainite transformation, that in particular given conditions, austenite would not transform into bainite. This happens when the C content in austenite reaches the composition corresponding to the T_0, in which austenite and ferrite have the same free energy. At this point, bainitic ferrite inherits all the carbon of the austenite and C atoms are enriched in untransformed austenite, thus, ICT occurs. The other view suggests that ICT is the consequence of energy dissipation in bainite transformation [59]. Alloying elements including Mn, Mo and Cr at the ferrite/austenite interface result in SDLE, which leads to energy losses and the development of ICT [60] [61].

Other studies have attempted to study the ICT of bainite during continuous cooling. A multiple-step transformation stage is visible in the bainite ICT, ranging from a three-stage transition at low cooling rates to a two-stage transformation at intermediate and rapid cooling rates [62]. When the bainite transformation is incomplete and under continuous cooling conditions, the products consist of UB, granular bainite, acicular bainite, LB, lath and twin martensite. In a CrMnV steel, Grupta et al. [63] concluded that the second step happened due to the formation of precipitations or secondary island constituents, agreeing with Reisinger et al. [64], who also concluded studying a CrMoV steel that the formation of M/A constituents was caused by the transformation stasis, which results in an incomplete transformation. Furuhara [65] added that Nb addition promoted M/A formation, therefore leading to an incompleteness of the transformation. However, Qiao et al. [66] do not agree and propose that the ICT phenomenon is attributed to the formation of twin martensite, investigating a CrNiMoV steel. There are still significant disagreements and doubts about the transformation products and the formation mechanisms.

In a MnCrNiMo steel with a slow cooling rate, the ICT phenomenon occurs in the second stage and is due to the formation of coarsen carbide precipitates along grain boundaries, which consequently produce an increase of volume misfit-strain energy between austenite and bainite and inhibit bainite transformation. In a faster cooling rate, it is the martensitic transformation that inhibits LB transformation, owing to the variation of chemical and mechanical stabilization of austenite.

The SDLE has been a focus of research recently and numerous explanations have evolved since its discovery. These elements affect the overall transformation kinetics by altering ferrite nucleation kinetics and by reducing ferrite growth kinetics. A hypothesis holds that the incomplete transformation and the shape of the TTT diagram are special effects of certain alloying elements on the precipitation of proeutectoid ferrite and carbides and not a peculiar mechanism of the bainitic transformation. A study [60] analysed a series of high-purity Fe-C-Mo alloys containing 0.06 to 0.27 wt.% C and 0.23 to 4.28 wt.% Mo, establishing that the ICT phenomenon is not a general feature of the bainitic reaction itself, but depends on the concentrations of C and Mo. It assumes that the substitutional elements do not partition between austenite and ferrite, which has been demonstrated to be true by most alloying elements at temperatures almost up to the A_3 temperature [67]. Enomoto and Aaronson [68] have shown that Mo accelerates ferrite nucleation at higher temperatures, due to the stabilization of ferrite by Mo, but this is reduced when approaching the bay temperature T_b. Lower nucleation rates near the bay are caused by solute segregation to austenite grain boundaries, reducing the effectiveness of these sites for ferrite nucleation. The growth kinetics of ferrite and carbides pass through a minimum at the T_b. Growth resumes after a period called ”growth stasis” [69], which increases with the amount of C and Mo in the alloy.

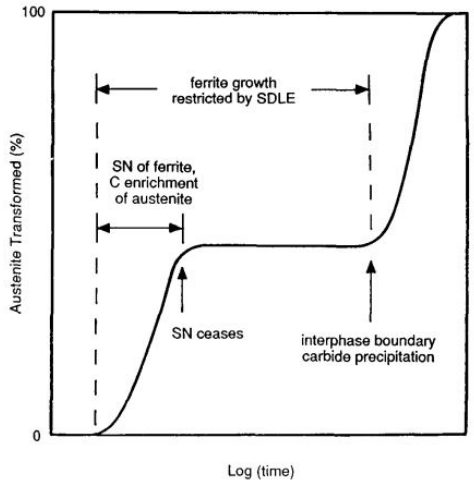

Figure 2.19: Schematic representation of the transformation sequence at temperatures below T_b.

Other elements have been investigated for their influence on the ICT to bainite at reaction temperatures between B_S and the bainite finish temperature, B_f. It has been demonstrated that incompleteness is characteristic of the proeutectoid ferrite reaction. Mn, Si, Cr and Mo were studied [37] as possible elements that alter the ferrite nucleation kinetics and reduce the ferrite growth kinetics through SDLE. Non-equilibrium concentrations between the substitutional solute element and the interstitial element, C, change the chemical potential and control the diffusional growth of ferrite. Stasis occurs when SDLE is strong enough to eliminate the concentration gradient driving ferrite growth. The strength depends on the nature of the substitutional atom X as well as the composition of the $\alpha : \gamma$ boundary. When using Si, Ni and Cu the ICT phenomenon was not observed, while with Mn in the lower carbon alloy Fe-C-Mn it occurred. The alternate hypothesis attributes the inability to observe ICT in low-alloy steels to the overlap of the pearlite and bainite C-curves. If the two reactions occur simultaneously at a certain temperature, the incomplete nature of the bainite reaction is known to be prived by the formation of pearlite.

2.3.5. From UltraFine to Nanoscale structures

The modern steel industry is becoming more aware of the potential advantages of nanoengineering, and major steel research and development institutes and companies are strongly investing in the study of nanostructured steels to achieve ultra-high strength. Suitable in many demanding engineering applications such as rail-wheel systems, bearings, gears and the automotive industry, new powerful processing techniques are now capable of reducing the steel grain size down to 100 nm, termed as "ultrafine grained". In the case of ferritic steel, the bainite reaction at low temperatures permits the creation of a microstructure consisting of 20-40 nm thick plates of ferrite and retained austenite [70]. It is achieved through an isothermal reaction to bainite in steels with higher contents of Si and C and with a M_S temperature of about 120ºC. The largest strength/toughness combinations have been recorded with these steels (2.5 GPa / 40 MPa $m^{1/2}$ [71]). Toughness can be increased to as much as 128 MPa $m^{1/2}$ for tensile strength values of 1.6 GPa when correctly applying the thermo-mechanical heat-treatment procedure. The design procedure involves a transformation at the lowest temperature possible but in a reasonable time, to obtain the finest possible structure. Thermodynamics calculations show that it is possible to obtain bainite at room temperature, but the transformation would take 100 years [72][73]. The so-called NANOBAIN steel [74] has seen to decrease in the bainite transformation temperature, and an increase in the maximum bainite volume fraction and the hardenability of the steel.

There are still important improvements to be made in this industry: developing nanosteels appropriate for large-scale applications, being able to manufacture in 3D, and being cost-effective. After mechanical milling and alloying, it has not been achieved to adequately suppress grain growth during sintering and hot pressing. An acceptable transformation time can be decreased by accelerating the transformation with controlled additions of small quantities of Al and Co. Another transformation rate increment can be achieved by reducing manganese, chromium and molybdenum contents and by

refining the previous austenite grain size with the help of niobium [75]. With research increasingly taking place, the extremely fine microstructure of bainitic nanosteels shows mechanical properties never achieved before (see Figure 2.20) in bainitic steels, and many are the potential uses of these steels.

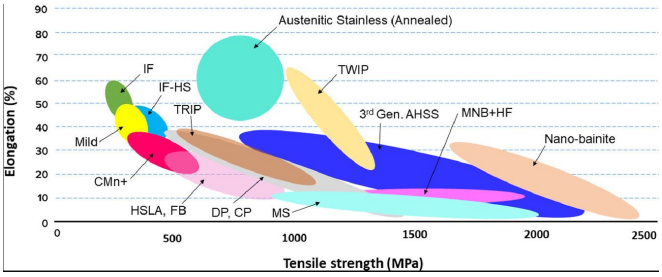

Figure 2.20: Mechanical performance of conventional steels, AHSS and nanosteels.

2.4. Hybrid PM/ML models

Understanding complicated multiphase microstructures to improve the macroscopic mechanical response and formability for automotive applications is crucial and challenging. Many researchers have addressed this challenge via computational modelling. Regardless of the promising advantages that AHSS bainitic steels offer, the bainitic ferrite-austenite microstructure has failed often to develop its full potential, mainly because of the instability of the large regions of austenite, which is sometimes trapped between sheaves of bainite. These are susceptible to change into high-C untempered martensite under the presence of minor stresses, which has an embrittling effect. On the contrary, the confined films of austenite between ferritic plates are more stable, thanks to the rich carbon content and the restriction to transform imposed by the ferrite platelets around them. Therefore, it is necessary to focus on reducing the fraction of blocky austenite present and increasing its stability with respect to martensitic transformation. Alloy design is key and should aim to maximise the permitted degree of transformation to bainitic ferrite. Other constraints are present, such as the need for a sufficient hardenability of the steel for industrial production [76].

Physical metallurgy (PM) is a branch of materials science, including steel technology. Its models are increasingly used for alloy design as an efficient alternative to the traditional experimental trial-and-error approach. Combining PM models with thermodynamics, the relationship between composition, processing, microstructure and physical and mechanical properties, guide alloy design as a tool that has achieved improved grades of properties. Machine learning (ML) is a field of artificial intelligence (AI) and computer science that uses data and algorithms to simulate how people learn, progressively increasing the accuracy of the algorithm. In practice, it extracts and learns relationships from data and applies this knowledge to new data. Some of the most common ML techniques include decision trees, support vector machines, and neural networks. ML is being emergingly applied in materials design, though it is limited by insufficient high-quality datasets, which tend to lead to unrealistic materials design outside the properties limits. An initial understanding of the mechanism with datasets is needed, which are eventually used as new training for the new group of alloys. A virtual lab paired with the predictive abilities of machine learning algorithms and artificial intelligence may speed up the creation of newer steel grades with distinctive processing routes without requiring an excessive amount of trials [77].

It is required to combine the strengths of PM and ML approaches to assess and maximize the real design power of each when designing new steel grades. While PM techniques are very sensitive to the alloy system and cannot hence explore new domains, they do offer a clearer view of the link between the overall composition and microstructure attributes. In contrast, ML produces less clear physical knowledge while producing predictions with higher accuracy for large-scale data. Hybrid PM/ML models offer solutions that maximize accuracy while producing the necessary attributes and a clearer physical image.

The project aims to apply ML approaches guided by PM models for designing a Ferritic-Bainitic High Strength Steel, featuring a microstructure that exhibits optimal mechanical properties, desirable for application in the automotive industry.

2.5. Conclusions

The main challenge in this project is applying machine learning approaches to design ferritic-bainitic high-strength steel. Furthermore, a prototype alloy will be produced, with composition and heat treatment parameters satisfying industrial requirements. This literature review has highlighted the key factors that influence the microstructure and properties of bainitic steels, including alloying elements, processing parameters, and cooling rates during quenching. The application of ML techniques offers significant advantages combined with PM models by providing faster and more accurate predictions and enabling the optimization of steel compositions and processing conditions.

In chapter 2, the literature review is introduced with an overview of the third generation of AHSS. Then, in chapter 2.2 the theoretical base on the phase transformation that steel overcomes is briefly explained. In chapter 2.3 the nucleation and growth kinetics of bainitic steel are presented, with an attempt to define the B_S temperature through different theories. Two types of bainite, upper and lower, are described, to further explain the possibility of creating CFB steels. Finally, in chapter 2.4 a brief explanation of PM and ML models is presented.

The main conclusions that concisely list the main findings of the review are listed below:

- Without a successful attempt to generalise a definition, bainite in steel is accepted by many as a plate-like, non-lamellar mixture of ferrite and cementite. The industry finds use in applications with high requirements in strength, formability, hardness and energy absorption at fast deformation rates.
- Two families are differentiated, upper and lower bainite. The transition can be predicted by comparing the rate at which carbides precipitate from ferrite and the speed at which carbon atoms are partitioned from supersaturated ferrite.
- It is possible to prevent the formation of the low-ductile cementite phase with the right chemistry and thermal profile, resulting in CFB steels. The retained austenite is the main responsible for the ductility of the microstructure, attributable to the TRIP effect.
- Sub units, single ferritic plates, only nucleate over a previously nucleated one and are nucleated until a specific size delimited by the kinetics. The nucleation principally takes place in sites confined to the austenite grain surfaces.
- There is disagreement on the mechanism of bainite formation, which has been categorized as either a diffusional or diffusionless hypothesis. In the diffusional case, carbon diffusion in austenite is assumed to control bainite growth. The lengthening rate is larger than the lateral growth. In the diffusionless mode, the carbon is assumed to be trapped in bainitic ferrite during growth. Growth is controlled by repeated nucleation at the tip of the plate.
- It has been shown that a driving force of 400 J mol^{-1} must be exceeded for the microstructure to be able to start growing.
- The austenite grain size and the austenite prior deformation influence the austenite retention at ambient temperature.
- A careful quantification of the alloying elements provides a general refinement of the microstructure, which enhances the strength and hardenability of the microstructure. The combination of strength and total elongation increases with the amount of austenite stabilizer elements.
- The BHT and holding time are important parameters to optimize the formability-strength balance.
- When transforming to bainite, a transformation stasis can take place. The SDLE and other theories try to explain this phenomenon.

2.5.1. Research questions

However, there are still challenges to be addressed in applying ML to the design of ferritic-bainitic high-strength steels. These include the need for large and diverse datasets, the selection of appropriate

features and algorithms, and the interpretation of the results. Addressing these challenges will require the development of new tools and techniques for data collection, processing, and analysis. The use of ML guided by PM principles has the potential to introduce a new design tool leading to improved properties. The scientific objective of the project is to propose a new material design method, where intermediate parameters are generated based on original inputs and PM principles. The model is to be applied while being compatible with industrial production, using a database extracted from the Thermo-Calc software. Specifically, the following research questions have been formulated to help achieve the main objective of this work:

- What is the effect/role of carbon and different alloying elements on the microstructure and mechanical properties of FB AHSS? Can ML models be used to optimize their composition?
- How does the cooling rate affect the microstructure and mechanical properties of FB AHSS? Can ML models be used to predict these relationships?
- What are the key PM factors that influence the mechanical properties of FB AHSS?
- How does the microstructure of FB AHSS affect their mechanical properties? Can ML models be trained to predict these relationships?
- How do different processing routes, such as hot rolling and quenching, affect the microstructure and properties of FB AHSS? Can ML models be used to predict these relationships?
- What are the limitations and challenges associated with using ML in the design of FB AHSS? Can ML models be computationally efficient?

3

Methodology

In the context of data analysis, Exploratory Data Analysis (EDA) is an essential process used to summarize and visualize features and relationships in the data, before formal modelling can be done. It involves several steps that need to be carefully completed for the following ones to function correctly. In this work, the following six steps of data treatment and analysis are extensively described:

- Data Collection: Modelling requires data, therefore the first step is the research of data using various sources. In this case, the data involves parameters related to bainitic transformation, which is documented in a datafile.
- Data Cleaning: This crucial step involves the handling of empty data, outliers or incorrect values in the dataset, as they require special attention and treatment. Inconsistencies, errors or discrepancies lead to quality issues, undesired in ML. This can involve checking for data integrity, validating data formats, or detecting duplicate entries. Cleaning and preprocessing the data are crucial steps to ensure the quality and usability of the data, and to prepare the data for further analysis.
- Feature Selection: Data summarizing the main characteristics of the dataset, including descriptive statistics, provide an initial understanding of the central tendencies, variabilities, and distributions of the variables, and help in the selection of parameters.
- Meta-Analysis: To get a general understanding of the parameters and the relationships within each other in the context of the existing literature. By exploring the data and observing patterns or trends, a formulation of initial claims is made to be analyzed in further steps.
- Data Visualization: Various types of plots, such as scatter plots, pair plots, or correlation matrices, are commonly used to explore and visualize the relationships, correlations, and distributions of the variables. It allows for the identification of trends, remaining outliers, or unusual patterns that may require further investigation. Provides evidence if data supports the existing literature or not. Understanding the dependencies between variables is crucial for model building.
- Anomaly Detection: use machine learning techniques such as PCA, clustering or UMAP to detect unusual patterns and understand the importance of each parameter. Helps in feature selection for the modelling process.

3.1. Data collection

An appropriate collection of data is vital in many domains since it allows one to obtain reliable information and makes it more likely to make intelligent choices. The information gathered influences the quality of what is studied and determines the judgments made during the interpretation of results. When basing all the study on data collected from elsewhere, all the conclusions made will only be valid if the data you started with is correct. Even more when creating models, which are very sensible to data quality. Mistakes in this step can result in a waste of time, apart from incorrect interpretation of results which can have consequences if other scientists use your findings in their research. Strong data provides the foundation for smart judgments and discoveries.

The data used in this project has been collected from various sources. It contains 930 data points, where each data point refers to a specific steel and process, with measurement values for as many parameters as possible. Therefore, each datapoint contains information for multiple parameters. The variables that are recorded are described in this chapter. Out of the 79 variables, a selection has been made as some of them are not as relevant, or there are not enough recorded values, remaining many columns quite empty. The shape of the dataset is therefore 930 x 79, where 930 is the total number of observations and 79 is the number of attributes. The consistency between datapoints is good enough so that importing this file is possible with not much adaption.

In the input side of the features (independent variables), factors affecting the results of mechanical properties and morphological outcomes are first selected and assigned as input variables. These include information on the microstructure, the alloy composition and process parameters. There are 15 chemical elements in the dataset, including C, Mn, Si, and Cr, as well as austenite grain size, initial deformation at high temperature, the time between deformation and cooling, austenitizing temperature and time, and cooling rate, among others. However, some parameters as the amount of deformation or the grain size are most frequently left out. The output side of the process (dependent variables) includes variables related mainly to microstructure and properties. Here are found fractions of each phase, austenite grain size after the heat treatment, mechanical properties, or phase transformation temperatures. Moreover, the only categorical variable of the dataset is found, which gives information about the morphology of the sample after transformation. ML relies heavily on data pre-processing since it may enhance both the quality of the dataset and the effectiveness of the machine learning model [78]. Pre-processing techniques often include data cleaning, parameters selection, data normalization and data transformation.

For more details on how the data was collected refer to Appendix A.1. Next, the processing of data is addressed.

3.1.1. Data cleaning

There were some issues with the data that are worth mentioning. The first refers to experiments where the heat treatment process has several cooling steps, meaning, there are several values for instance in the temperature (e.g. Tempering 780 + 400 ºC), holding time, and CR after the step. As one-step cooling processes are not comparable to multiple steps under the same parameter, these have been separated into different parameters when possible, or excluded, so that in the end the data remains only as numerical values.

In this context, it is important to remark on the issues of comparing a single-step cooling rate with a multi-step process. Heat treatment techniques have the purpose of changing the microstructure of a material, which has immediate effects on its physical properties, which take place gradually. Every intermediate stage in a heat treatment process causes a particular change in the microstructure of the material, as can involve phase transitions such as solidification, precipitation or diffusion. When comparing a single-step process to a multi-step process, the microstructures will most likely change, as multiple steps allow the material to undergo several phase transformations that cannot be expected when using only one step. With a careful and controlled sequence of heating, cooling and intermediate temperatures, it is more likely to obtain more optimal properties when applying several steps, if optimized correctly. With different outcomes, these processes can lead to an invalid comparison.

Another simple correction made came from the fact that when a paper included a considerably large number of data in the format of a table, a tool to pull data straight from PDF tables into Excel spreadsheets was used. The decimal format had to be changed from points to commas. A similar error was encountered with the digitized data from WebPlotDigitizer. When Excel tools were used to automatically convert to numeric, some values were thousands of times larger than a realistic measurement, as can be finding temperatures of 800 million degrees Celsius, which is logically not a real recorded temperature. This created the suspicion that something must have gone wrong with either the decimal separators or the consequence of human error. In the end, these were repaired manually after carefully double-checking.

Another change to be made was in the data that included together with the mean value a deviation (e.g. 0.022 ± 0.004), a consequence of several measurements. These are important as we need to take into account the error that this measurement includes. A copy of the file was made, so that it is possible to come back and import these errors, while in the original data file, the error was removed so that a numerical value is recorded.

Finally, some assumptions had to be made to convert all the cooling rates to numerical values. These are mostly given under three descriptive variables ”Oil Quenching”, ”Water/Ice Quenching”, and ”Air Cooling”. The following values have been assumed for these cooling rates, after consultation in the literature, even though it is not precisely a constant value: oil quenching as 101ºC/s, ice quenching as 60,1ºC/s, and air cooling as 20,1ºC/s. However, it is not correct to approximate a cooling rate to a constant value as these are not linear from the start to the end of the process but would be closer to an exponential heat loss instead [79].

Additionally, it is worth mentioning that sometimes data was found in different units. However, it was always noted in the same units, using the international system to convert into the desired units. This way, there were no issues regarding units.

3.1.2. Parameters selection

With a completed cleaning of the data, where mainly structural errors and handling of unwanted outliers are addressed, it is decided that a parameter should meet at least the following requirements to be taken into account for further analysis:

- There is a significant amount of data, at least 50 observations are recorded.
- All measurements are either numeric values or empty cells.
- The information comes from, at least, two different studies.
- It is relevant and comparable to the study

These requirements are important for ensuring that the chosen parameters contribute meaningfully to further analysis and align well with the objectives. The first is necessary for several reasons. In ML, a large dataset leads to more accurate results and is statistically more reliable. Therefore, the larger the sample size, the more precise the estimates and correlations tend to be. This also reduces the impact of human or sampling errors.

Numeric values are necessary for quantitative analysis, as other types of data would create mathematical problems when applying different analysis techniques. It is important to remark that only one variable is categorical, the morphology of the phases, but it is descriptive text, meaning that every stored information is different and therefore classification is challenging. Empty cells represent missing data, which handling is possible but needs to be appropriate to avoid inaccuracies in analysis.

Similarly to the first requirement, the third one is necessary to avoid possible cases where a study does not accurately represent the entire population. The goal of machine learning models and analysis techniques is to generalize the findings using data. If it does not represent the entire population, the likelihood that the model build will not generalize well increases significantly. Several studies are required to better capture patterns, as gathering data from multiple studies enhances the parameters validity. It also makes it possible to detect rare events, outliers or incorrect patterns, apart from minimizing the risk of drawing conclusions based on particular characteristics of a single study, which could not be representative. Finally, the parameters that are directly relevant to the focus of the study and research questions are also considered. Relevance to the aims of the study ensures that the parameters insights can be meaningfully integrated into the overall analysis.

From the above-mentioned requirements, 29 parameters remain. Descriptive statistics of each feature are generated, including a summary of the central tendency, dispersion and shape of each distribution, where NaN values are excluded. Table 3.1 summarizes the main characteristics of the input

parameters of the dataset, including descriptive statistics such as mean, median, standard deviation, and quartiles. It helps provide an initial understanding of some tendencies, variabilities, and distributions of the variables, but also outliers.

Table 3.1: Descriptive statistics of main independent features.

	count	mean	std	min	25%	50%	75%	max
C (%)	929	0.29	0.24	0.02	0.15	0.20	0.38	1.86
Al (%)	667	0.28	0.48	0.01	0.03	0.04	0.06	1.70
Si (%)	880	0.89	0.64	0.00	0.25	0.98	1.49	2.50
Cr (%)	368	0.87	0.77	0.00	0.27	0.97	1.12	4.00
Mn (%)	922	1.59	0.97	0.00	1.20	1.50	1.57	5.50
Nb (%)	305	0.03	0.02	0.00	0.00	0.03	0.05	0.07
Mo (%)	364	0.19	0.22	0.00	0.02	0.18	0.23	1.18
Cu (%)	73	0.16	0.60	0.01	0.01	0.03	0.03	3.01
Ni (%)	326	0.99	1.49	0.00	0.00	0.16	1.52	7.25
Aust$_T$ (ºC)	701	863.67	120.51	670.00	780.00	850.00	900.00	1300.00
Aust$_t$ (s)	644	704.44	775.41	60.00	300.00	300.00	1200.00	10800.00
Aust$_{CR}$ (ºC/s)	346	42.34	43.84	0.01	10.00	20.00	100.00	374.33
Isot$_T$ (ºC)	587	394.28	110.73	24.75	350.00	400.00	450.00	840.00
Isot$_t$ (s)	413	1111.25	2458.94	0.00	120.00	300.00	1000.00	21600.00
Isot$_{CR}$ (ºC/s)	339	47.27	38.55	1.00	20.10	20.10	101.00	101.00

By observing these statistics, we see that in some of the chemical elements the minimum value is 0. This is not wrong, as in some experiments the values of some chemical elements were explicitly given as 0, so it is correct to introduce a zero instead of a missing value. However, this can lead to inaccurate interpretation of the data when analyzing the results, such as the correlation between variables. On the other hand, filling the empty data with zeros would provide non-useful information in some cases.

The two options to be followed for a consistent analysis of the experiments are, either removing all the values in experiments where a chemical element is not present or filling in all the empty concentrations with zeros. the first approach is described in Table 3.2, while the second approach is in Table 3.3. Using nickel to make a comparison between the two approaches, if zero values are removed, the descriptive statistics tell us that 244 out of the 930 datapoints are recorded, with an average value of 1.33 wt% Ni. On the other hand, if the cells are filled in with 0 where there is no nickel present in the steel sample, there are 930 recorded values that show an average value of 0.348 wt% Ni, and a 70% percentile of 0. These are two different approaches to analysing the same data, where both of them offer useful and different information. From the first approach, we can get a better insight, with the mean value, of the amount of nickel that is typically added in steels that are designed for applications where the bainitic phase is desired. On the other side, the mean value in the second approach does not tell anything, but we can see that at least 70% of these steels do not contain nickel, suggesting that it is not that common to add nickel in these types of steels.

Both approaches are correct and give the same information differently, so both will be considered during the analysis. In every case, it will be considered what information can give a better understanding of the analysis and how they affect each type of representation. Considering this, 7114 empty cells have been filled with 0 on the alloying elements. Table 3.3 shows a summary of the second approach, including percentiles:

Table 3.2: Descriptive statistics of chemical elements, by removing empty values.

	count	mean	std	min	10%	25%	40%	50%	60%	75%	90%	max
C (%)	929	0.29	0.24	0.02	0.13	0.15	0.18	0.20	0.21	0.38	0.58	1.86
Al (%)	667	0.28	0.48	0.01	0.03	0.03	0.04	0.04	0.04	0.06	1.00	1.70
Si (%)	878	0.89	0.64	0.00	0.11	0.25	0.49	0.99	1.46	1.49	1.52	2.50
Cr (%)	344	0.94	0.76	0.01	0.10	0.31	0.64	1.00	1.00	1.15	1.65	4.00
Mn (%)	922	1.59	0.97	0.00	0.52	1.20	1.48	1.50	1.50	1.57	2.98	5.50
Nb (%)	269	0.03	0.02	0.00	0.00	0.02	0.02	0.03	0.05	0.05	0.05	0.07
Mo (%)	297	0.23	0.22	0.01	0.04	0.09	0.19	0.20	0.20	0.26	0.49	1.18
Cu (%)	73	0.16	0.60	0.01	0.01	0.01	0.03	0.03	0.03	0.03	0.15	3.01
Ni (%)	244	1.33	1.58	0.01	0.01	0.16	0.17	0.32	1.49	2.02	4.06	7.25

Table 3.3: Descriptive statistics of main chemical elements, after filling empty values with zeros.

	count	mean	std	min	10%	25%	40%	50%	60%	75%	90%	max
C (%)	930	0.29	0.24	0.00	0.13	0.15	0.18	0.20	0.21	0.38	0.58	1.86
Al (%)	930	0.20	0.42	0.00	0.00	0.00	0.03	0.04	0.04	0.04	1.00	1.70
Si (%)	930	0.84	0.66	0.00	0.04	0.22	0.38	0.53	1.46	1.49	1.52	2.50
Cr (%)	930	0.35	0.64	0.00	0.00	0.00	0.00	0.00	0.00	0.50	1.12	4.00
Mn (%)	930	1.57	0.98	0.00	0.50	1.20	1.48	1.50	1.50	1.57	2.98	5.50
Nb (%)	930	0.01	0.02	0.00	0.00	0.00	0.00	0.00	0.00	0.00	0.05	0.07
Mo (%)	930	0.07	0.16	0.00	0.00	0.00	0.00	0.00	0.00	0.09	0.23	1.18
Cu (%)	930	0.01	0.17	0.00	0.00	0.00	0.00	0.00	0.00	0.00	0.00	3.01
Ni (%)	930	0.35	1.00	0.00	0.00	0.00	0.00	0.00	0.00	0.01	1.52	7.25

An additional observation regarding the dataset is the presence of some negligible values of some chemical elements. Observing the wt% of Al content in Table 3.3, most literature studies report the value (667 out of 930 experiments), however, the presence of aluminium is negligible in at least three-quarters of the data, with a 0.75 percentile of 0.06 wt% Al. This situation when a very small amount is reported is very similar to a zero value, however removing this data would make it necessary to draw a line for every element on where to cut the data. Therefore, the presence of a negligible amount of some alloying elements will have to be considered when interpreting the results later on.

Figure 3.1 depicts in a histogram representation the distribution of all the chemical elements, when present in the sample. In the x-axis, the concentration in weight percentage of the 15 chemical elements is represented, and the y-axis represents the number of observations for a given composition. The exclusion of certain elements, such as nitrogen, phosphorous and sulfur is because they are commonly not the focus of attention for steels. They are often considered as unavoidable impurities in steel. Their presence is inherent to the raw materials and to the manufacturing process, therefore they cannot be easily removed without a complex and expensive refining process. Focus is rather done on elements that can be easier to control or modify during steel production.

Finally, Table 3.4 below depicts the descriptive statistics of the main dependent variables that are interesting for further analysis. 14 features have been selected for the following steps. An exception has been made by including the CIAV, which includes slightly less than 50 observations. This parameter is the main representative of the toughness of the material, which is a very important mechanical property in these types of steels, and it is therefore interesting to include it for the analysis. The reason why only 47 observations were collected is that there are multiple ways of measuring the toughness, therefore the distribution has been wider, ending with the Charpy test as the most representative within the collected data.

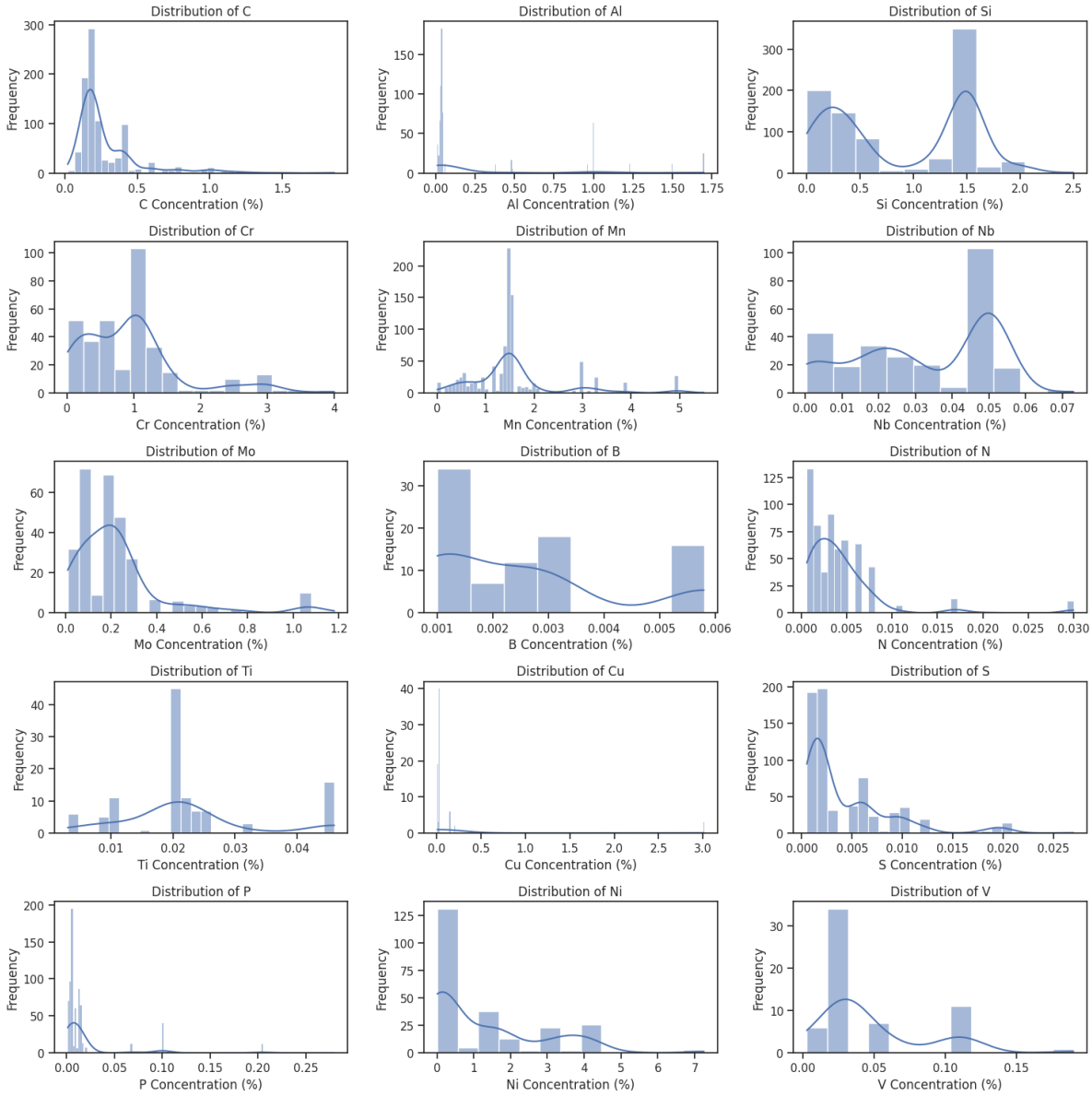

Figure 3.1: Distribution of chemical element concentrations.

Table 3.4: Descriptive statistics of dependent variables.

	count	mean	std	min	25%	50%	75%	max
$f_{ferrite}$ (%)	65	26.86	23.52	0.00	9.00	9.00	42.00	76.00
$f_{bainite}$ (%)	121	38.00	30.72	0.00	20.00	28.00	51.00	100.00
$f_{RA/M}$ (%)	245	10.31	13.67	0.00	4.30	8.40	11.20	100.00
$C_{\gamma 0}$ (mass%)	159	0.98	0.39	0.03	0.73	0.97	1.26	1.88
$f_{\gamma 0}$ (vol%)	195	14.55	6.83	0.00	9.00	13.26	20.75	25.50
Hardness Vickers (HV)	105	376.07	113.00	186.67	282.00	375.00	437.00	744.00
YS (MPa)	305	656.41	228.72	307.57	457.91	608.00	847.94	1307.00
UTS (MPa)	302	971.99	307.89	538.00	711.20	921.50	1170.75	2036.00
TEl (%)	315	22.41	8.20	1.70	15.62	23.42	27.23	57.00
UEl (%)	202	15.53	6.83	1.70	9.30	16.57	20.09	31.40
CIAV (MPa $m^{1/2}$)	47	84.05	45.79	7.35	48.94	104.46	122.13	150.00
F_S (ºC)	116	924.55	174.92	610.03	748.35	1014.00	1070.00	1120.00
B_S (ºC)	172	527.78	72.09	339.00	491.23	520.00	586.61	734.97
M_S (ºC)	380	378.73	155.61	50.00	289.25	369.50	437.00	693.00

3.2. Meta-analysis

Scientists have known for centuries that a single study will not resolve a major issue. Indeed, a small sample study will not even resolve a minor issue. Thus, the foundation of science is the accumulation of knowledge from the results of many studies [80].

A statistical method known as meta-analysis is used in research to gather and analyze data from several independent studies on a certain issue. By providing a quantitative overview of the results from many investigations, it hopes to improve the statistical significance and generalizability of the findings. Instead of depending on the results of a single research, by considering a bigger sample size meta-analysis improves the reliability and precision of estimated results. Meta-analysis is widely used in various fields, including medicine, psychology, education, and social sciences, to synthesize and summarize research findings, identify patterns or trends, and provide a more robust and reliable evidence base for decision-making [81] .

In this project, some of the steps of a typical meta-analysis have been performed, while others have been left out. The article ”How to conduct a meta-analysis in eight steps” [82] gives a practical guide on how to correctly perform an extended meta-analysis.

The process of conducting this meta-analysis involves several steps. The initial step in conducting a meta-analysis is defining the research question and the objectives of the investigation. Following, systematic literature research is done, in which different strategies to search relevant studies can be followed. Previous meta-analyses on the same or similar topic can be the starting point to provide studies that are relevant to the research. Keyword search in electronic databases [83] is another typical search strategy, which can also lead to less relevant studies. To avoid these, Boolean operators are advisable for a more precise search [84]. The track of forward citations and influential studies can also help in identifying some of the following interesting articles.

Next, it must be decided which studies to include in the meta-analysis. Renowned academic journals ensure a better quality of the findings, whilst reviews with large available datasets can also be desired [85]. In this step, it is important to include different types of studies to prevent selection biases. The selected studies are then critically evaluated and data is extracted where possible and available.

An individual analysis follows article by article, where a collection of findings is noted and compared both with the dataset and with other studies. Different aspects are pointed out, as are the main findings of the paper, the results, and personal interpretation. From these, a list of claims that are both interesting to analyze and relevant to our research questions is elaborated. These claims are then compared with the collected data, and checked if it is possible to make a good enough analysis, as sometimes it involves parameters with not enough amount of datapoints or outside the range. In these cases, some or left apart, and do not make it to the following analysis steps.

Based on the outcomes of the meta-analysis performed on the collected data and in alignment with the existing literature, the list of claims has been established.

3.2.1. List of claims in meta-analysis

- **Claim 1: There is a weak inverse relation between the B_S temperature and the carbon content in steel, while in the case of the M_S temperature, a strong inverse exponential dependence of carbon content exists.**

In agreement with published literature, it is observed that the start temperatures of bainite and martensite formation exhibit an inverse exponential carbon dependence, as this element influences the kinetics of phase transformation and therefore the resulting microstructure [86]. Carbon has a powerful austenite stabilizing effect on steel [87], which rises with carbon concentration. As a result, the austenitic phase that is present at high temperatures during austenitization can be held at lower temperatures upon cooling, and the bainitic and martensitic phases' transformation is delayed. Carbon in the

austenite phase inhibits other C atoms migration, making bainite production more likely at lower temperatures. Martensite is formed by quickly cooling austenite. Carbon atoms occupy interstitial locations inside the iron crystal lattice, distorting the lattice and making it more vulnerable to shear transformation. The addition of carbon enhances the rate at which carbon atoms diffuse inside the austenite. During cooling, this increased diffusion promotes the nucleation and development of new phases (martensite or bainite), resulting in lower start temperatures for their formation.

- **Claim 2: Manganese increases the fraction of retained austenite after the heat treatment, and decreases the amount of bainite transformed. For bainite to be formed, the maximum amount of Mn should be 3.6%. A great combination of strength-ductility is achieved at around 3% Mn, as well as an increased toughness. The best strength combination is achieved with additions of approximately 1.5% Mn. Finally, in the UTS range above 1.5GPa, quantities of 3% Mn exhibit a better toughness-strength combination.**

The literature affirms that the increase of manganese leads to a lower bainite fraction after the isothermal stage [88]. This implies a higher fraction of other phases, such as retained austenite or martensite. The less bainite formed, the higher the fraction of residual austenite, which carbon enrichment is low. This occurs through an alteration of the kinetics of phase transformation, as manganese has the ability to delay the transition of austenite to other phases. The incubation time is increased together with the increased manganese content. The precise process by which Mn influences transformation kinetics is complicated but relies on a drop of chemical driving force for the austenite to transform into bainite. According to some studies, the level of manganese should be limited to 3.6% for the transformation to bainite to be completed in a time acceptable in an industrial context.

Furthermore, Mn reacts with carbon in steel, producing carbides, and limiting the amount of carbon available for diffusion into the austenite phase. As a result, the production of other phases such as martensite and pearlite becomes difficult, and the retained austenite proportion rises.

Medium manganese steels containing around 3% Mn have gained popularity due to their optimum combination of strength and ductility at low manufacturing costs. A good combination of strength and ductility is achieved when the 10-15% retained austenite remains in the bainitic or martensitic matrices [89] [90].

- **Claim 3: Silicon improves the strength and total elongation between 1-2 wt%. B_S decreases harshly from 600ºC to 500ºC by adding Si up to 0.2 wt%. When further adding more, the tendency remains almost unchanged. Silicon increases the initial volume fraction of retained austenite and stabilizes the residual austenite by carbon enrichment**

The presence of silicon retards the kinetics of bainite transformation. The strength and ductility of bainitic steels rises as the Si content increases in the range of 1.0 to 2.0 wt%, resulting in a more filmy austenitic phase and less cementite [91] [92]. Some studies have analysed the relationship between Si and B_S using different ML algorithms, finding that the B_S temperatures vary significantly with increasing Si. By increasing the silicon content to 0.2 wt%, B_S decreased from 596ºC to 513ºC. After 0.2% the tendency remains almost unchanged when adding Si [93].

As already mentioned in Chapter 2.3, Si-rich samples lead to CFB steels suppressing cementite during bainite formation, which benefits the mechanical properties. Silicon retards the bainite kinetics and stabilizes the residual austenite by carbon enrichment. During an incomplete bainitic transformation, austenite is stabilized due to carbon rejection from bainitic ferrite into residual austenite and to the prevention of cementite precipitation from austenite [94]. Because silicon has a very poor solubility in cementite, it can completely prevent its solubility when about 2% Si is added [95].o The result is a combination of CFB ferrite and carbon-rich residual austenite. Because of the large amount of C present in this remaining austenite, the M_S temperature is lower than the ambient temperature [96]. As a result, even though silicon has an influence on carbon activity in both ferrite and austenite, standard TRIP-assisted multiphase steels always contain 1.5-2.5% Si to avoid cementite precipitation. They also

contain 0.1-0.4% C and 1.5-2.5% Mn (to promote hardenability) [53].

- **Claim 4: The partial substitution of silicon by aluminium is said to increase the initial volume fraction of retained austenite, stabilizing the retained austenite by carbon enrichment, and therefore increasing the strength and total elongation by TRIP process.**

As well as silicon, aluminium presents a low solubility in the cementite phase, being able to completely prevent it if added enough. The high silicon levels that are needed are not well suited to the industrial practice. Aluminum has been proposed as the most promising alloying element for TRIP-aided steels [44] [45]. When completely substituting Si with Al, a deterioration of the strength-ductility balance is reported [97] [43], as, in contrast to silicon, aluminium is not a strong solid-solution strengthening element. This leads to TRIP-aided steels presenting low strength levels. Instead, a mixed Al–Si TRIP-assisted multiphase steel offers an efficient balance between the processing practice of these steels, the exhibited mechanical properties and the industrial requirements [43].

- **Claim 5: Mo and Cr are strong carbide-forming elements, simultaneously improving the strength and hardness, due to the formation of carbides. Cr delays the start of bainite formation.**

Chromium and molybdenum are gaining popularity to enhance the hardenability of steel. Both of them are strong carbide-forming elements [98] and at the same time weak austenite stabilisers. Sometimes rapid cooling after the annealing process is not possible, in situation in which adding Mn, Cr or Mo are needed to delay the bainitic transformation. This allows for a wider range of cooling rates to obtain bainitic microstructures [94]. Moreover, Cr and Mo are elements that difficult the diffusion of carbon in steel difficult, resulting in SDLE [99] [100]. This effect reduces the ferrite growth kinetics and results in the incomplete reaction phenomenon. However, combinations of two carbide former elements can alter the transformation stasis if carbides are formed too quickly [101].

It has been shown that this bay of ICT occurs at temperatures between 450-550ºC, whilst Cr decreases the start temperature of bainite formation B_S [102]. A more homogeneous and fine microstructure is produced after continuous cooling, due to a narrower region of the transition temperature. This finer microstructure also contributes to improved mechanical properties. After the isothermal transformation, martensite islands are developed due to the ICT. With an increase in the stability of RA, a higher amount can be retained at room temperature, allowing to maintain or even enhance the ductility upon mechanical loading. At the same time, strength and hardness are improved due to the formation of carbides. Additionally, Mo improves the high-temperature performance of bainitic TRIP-assisted steels.

- **Claim 6: Single additions of Cr can show better properties than when combined with Mo. Single additions display better ductility and strength-ductility while the combination displays a larger yield stress and tensile strength.**

It has been proven that single additions of Cr display lower amounts of pro eutectoid ferrite, achieving a larger quantity of RA. Instead, when combined with molybdenum a mixed microstructure of uniform BF matrix with BF is developed [103]. With this, the multiple additions of both chemical elements increase the strength of the steel, while the single addition of Cr maximizes the total elongation and combinations of strength-ductility, thanks to the dual-phase mixed structure. Not only this, but the toughness and strength-toughness combinations bring also larger results when combined.

- **Claim 7: By increasing the amount of niobium to around 0.05%, the ferrite start temperature and the fraction of ferrite decrease. However, by further adding Nb (0.075%) the fraction increases dramatically, due to the formation of NbC. There seems to be an ideal point of 0.05 wt%Nb in these steels where less ferrite is formed.**

Niobium is added in steels to influence the microstructure and phase transformations. Depending on the composition it can have different effects. The addition of Nb can lead to a decrease in the ferrite start temperature (F_S) and the ferrite phase fraction (f_α). Niobium is a strong austenite stabilizer that is added as a microalloying element, leading to a delay in ferrite transformation during cooling. By increasing the content further from 0.05 wt% to around 0.075 wt% Nb, it combines with C and forms niobium carbides, NbC, which act as nucleation sites for ferrite formation [103]. This means that as Nb content increases, more sites are present for ferrite nucleation and a higher fraction is transformed in the microstructure.

Even though the amount is only an approximation, it is around 0.05 wt%Nb where the effects of niobium on austenite stabilization and ferrite nucleation are in balance, resulting in a controlled and perhaps ideal amount of ferrite. However, the specific composition and behaviour do vary depending on other variables such as the steel composition, temperature, cooling rate, and processing treatments.

- **Claim 8: Complex additions of 0.5% Al and 0.05% Nb increase the strength-elongation and the total elongation.**

While Al mechanically stabilizes the RA through increasing the C concentration in conventional TRIP-aided steels, microalloying by Nb further refines the matrix and RA due to NbC precipitates, although when the last forms it lowers the mechanical stability of retained austenite. This improves the strength-elongation ratio [104]. Excellent elongation values have been linked to the combined presence of Al and Nb and a posterior austempering at temperatures above M_S.

Complex additions of 0.5% Al and 0.05% Nb in steel with chemical composition of 0.2% C, 1.5% Si, and 1.5% Mn, show optimum total elongation and stretch-flangeability [105], even in high UTS ranges. Outstanding stretch-flange-ability has been attributed to several reasons: refined previous austenitic grain by NbC precipitates, consistent fine mixed matrix microstructure of bainitic ferrite and martensite, and TRIP effect of metastable retained austenite.

- **Claim 9: Single molybdenum addition promotes bainite transformation and therefore enhances strength in low-C bainitic steels. Nb retards bainite transformation but improves strength by refining the microstructure. However, these strength levels are not reached in combination.**

According to a review of the literature, several researchers have described the impact of individual Nb or Mo addition on microstructure and behaviour in low-C bainitic steels. Nevertheless, few investigations have been undertaken to date on the impact of combined Nb and Mo additions on the transformation, microstructure, and properties of low-carbon bainitic steels. Studies reveal that individual Nb addition slows down the bainitic transformation in low-C bainitic steels while refining the microstructure and therefore improving strength. Furthermore, Mo addition strengthens the same type of steel by boosting bainitic transformation [106].

Single Mo addition has a stronger strengthening impact than single Nb addition [107]. Furthermore, Nb addition refines bainite while preventing bainitic transition due to smaller austenite grains. As a result, the composite strengthening effect of complex additions of Mo and Nb in low-carbon bainitic steels shows little or no benefit when compared with a single Mo addition, even if both improve strength. This occurs because the Nb addition weakens the promotion function of Mo on bainite transformation. Therefore, Nb addition could be avoided in Mo-containing low-C bainitic steels if the outcome is to design a high-strength steel.

4

Data Analysis

4.1. Visualization techniques

The step that follows the meta-analysis is the visualization of the data, which helps uncover patterns and detect outliers, and is the first step to validate hypotheses. The main trends and relationships in the data are more easily detected previous to the modelling steps. The representation in Figure 4.1 shows a pair plot visualization of the dataset distribution, frequently employed in EDA. It shows the pairwise relationship between the input (independent) and output (dependent) variables selected in Chapter 3.1.2. In the x-axis, chemical composition and process parameters are labelled, and the y-axis contains microstructural parameters, mechanical properties and transformation temperatures. This way, it makes it easier to spot trends that may assist in feature selection and further model construction. The data contains only continuous variables, there are no categorical values. Coloured, the datapoints have been separated into 6 clusters, representing the amount of carbon, to facilitate the detection of patterns.

As this step is performed after the preprocessing of the data mentioned in subsection 3.1.1, evident outliers have already been suppressed. The pair plot confirms that no evident outliers are standing out. It is probably in the austenization holding time where a larger variance is seen, confirming what is seen in Table 3.1 where the deviation value is large, due to some very long holding times.

Pair plots are particularly useful as a first exploration of patterns and correlations. From the bottom left part of the representation, we infer that a correlation between carbon content and the phase transformation temperatures B_S and M_S exists. By observing the chromium content, it seems like the ductility levels of steel are not too high when chromium is added in large quantities, but strength levels are benefited, due to its strong carbide-forming behaviour. In the manganese vs volume fraction of retained austenite relationship, a clear inverse relationship is spotted.

Correlation matrix

A correlation matrix of the dataset is computed and displayed in Figure 4.2. Shortly, it computes the Pearson correlation coefficient, which quantifies the degree of linearity between every pairwise of variables. It is important to mention this, as non-linear relations of data are therefore not predicted with this particular correlation. The formula of the Pearson correlation coefficient (r) is as follows:

$$r = \frac{\sum_{i=1}^{n}(X_i - \bar{X})(Y_i - \bar{Y})}{\sqrt{\sum_{i=1}^{n}(X_i - \bar{X})^2}\sqrt{\sum_{i=1}^{n}(Y_i - \bar{Y})^2}} \tag{4.1}$$

where n is the number of data points, X_i and Y_i are the individual data points of variables X and Y respectively, and $\bar{X}$ and $\bar{Y}$ are the mean values of variables X and Y respectively.

Similarly to the pair plot, on this occasion in the x-axis, the dependent parameters are represented, and in the y-axis the independent variables. The stronger correlations have a larger absolute value,

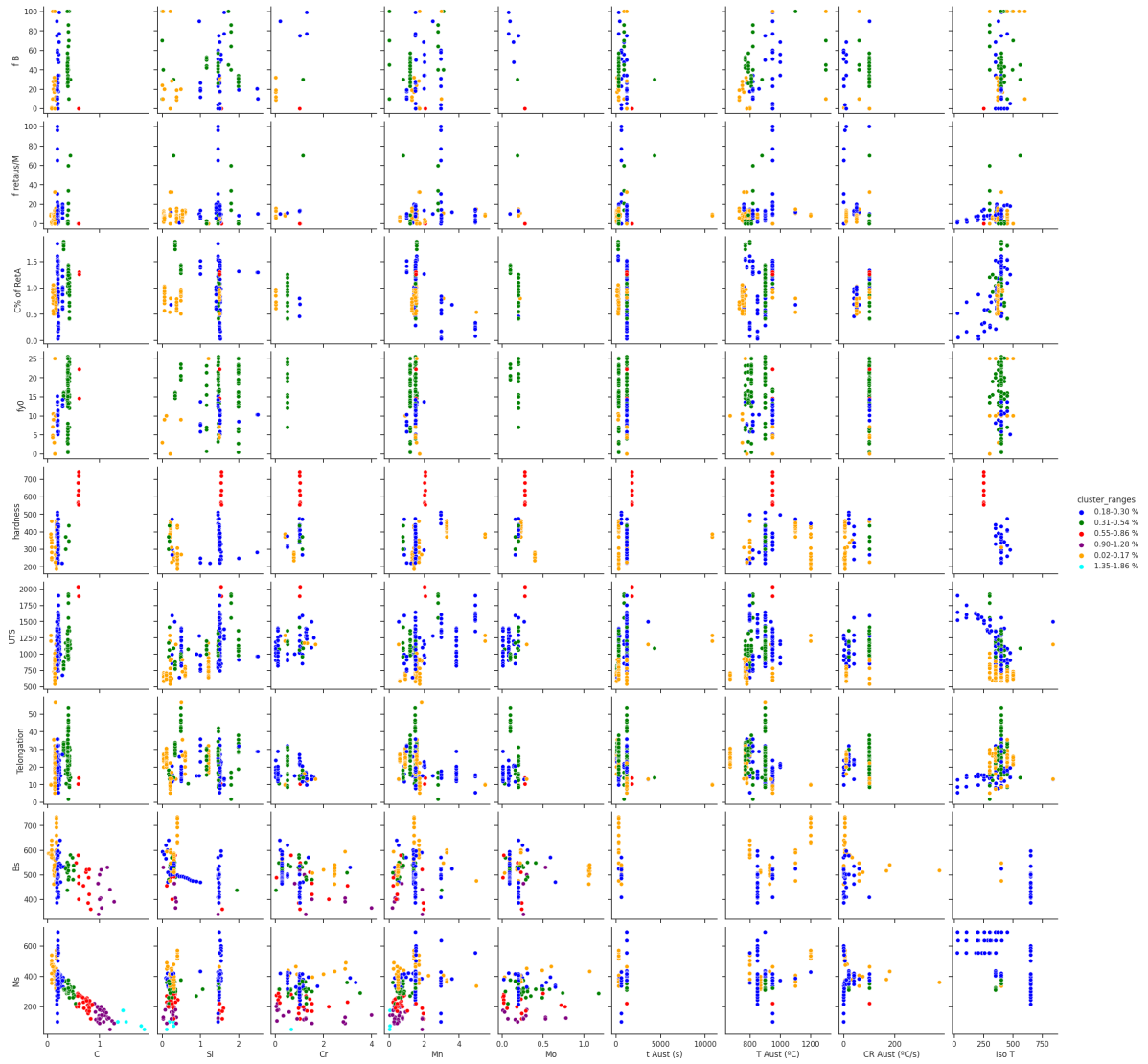

Figure 4.1: Pair Plot representation

while the colour represents the direction of the correlation. Warmer colors are positively correlated variables and colder colors are negative correlations. Blank cells appear where there are less than 10 observations, to show a minimal representative meaning. Zero values of chemical elements are not considered.

For more insights into correlation matrices, refer to Appendix A.2. The correlation matrix that includes the range of zeros for chemical components can be found in Figure A.2.

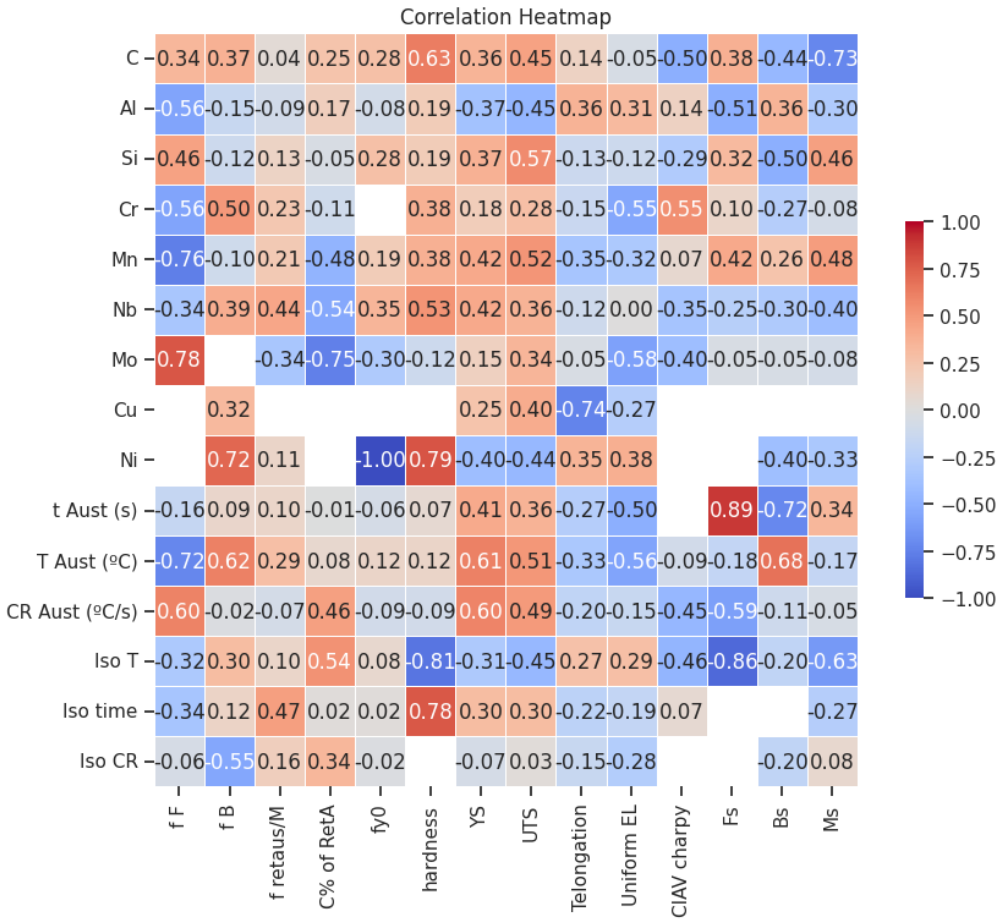

Figure 4.2: Correlation Matrix of the dataset, where missing values of chemical elements are excluded

There are some potential situations of misleading results involving correlation matrices that need to be mentioned. Its reliability depends on many factors, as can be sample size or the presence of outliers. Correlations with a small number of observations may be unstable and vulnerable to random fluctuations, while larger sample sizes produce more consistent and statistically meaningful findings. For example, we see that the strongest relationship is between the amount of nickel and $f_{\gamma 0}$. Numerically, there is a perfect inverse relationship between these variables. The following illustration shows the relationship between these variables.

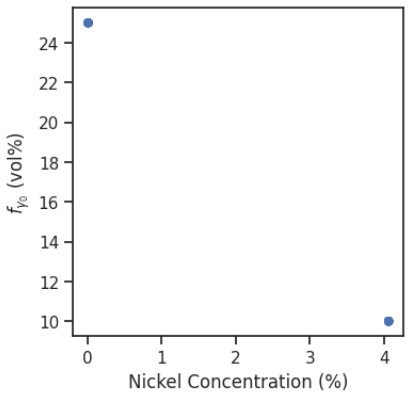

Figure 4.3: Experiments involving nickel and initial volume fraction of retained austenite.

In this representation, there are 46 datapoints. However, these are only in two different coordinates, which makes it have a -1.00 correlation. This occurs because the 46 observations come from only 2 different studies. Two points is indeed not enough in terms of sample size, it does not show a statistically significant result. Even nickel is known to stabilize austenite in steel alloys and improve austenite retention at room temperature. As an austenite-forming element, the possibility of maintaining austenite after cooling is often improved by increasing the nickel concentration in a steel alloy. While nickel concentration can influence the production of RA, it is not the only cause. Other factors affect $f_{\gamma 0}$ in steel, including alloy composition, such as carbon, manganese, and chromium, heat treatment conditions, or cooling rate. It should be carefully checked before reaching any conclusion with only the correlation matrix, which can be misleading, or not representative as demonstrated in this situation.

The dataset including zero values in chemical elements does not solve this situation unfortunately, as too much weight is given to values where a chemical element is not present. To better explain it with an example, we find that a positive correlation of 0.09 is given between the weight percentage of molybdenum and the fraction of bainite, while in Figure 4.4 there is a clear inverse relation between these two parameters (with an actual correlation value of -0.85).

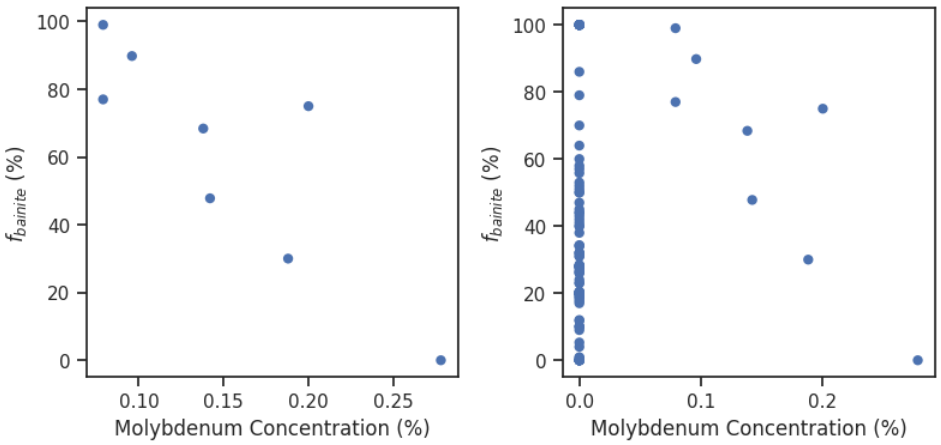

Figure 4.4: Molybdenum concentration and bainite fraction relationship. The left figure shows the experiments where molybdenum is present in the steel (r = -0.85), while in the right figure, all experiments are represented (r = 0.09).

The correlation matrix is therefore a useful analysis tool, but cannot be used on its own to draw any conclusions. It provides insights into potential relationships between variables. Complementing correlation matrices with other visualization techniques like pair plots does give a better insight into determining patterns in a system.

4.1.1. Principal Component Analysis

Principal Component Analysis (PCA) is applied in the dataset, to identify the main patterns and the most important features. It reduces the size of the dataset into lower dimensions while retaining as much important information as possible. For more details on what PCA does and how it works, please see Appendix A.3.

The principal components analysis of the main parameters of the dataset is visualized in Figure 4.5. It consists of two parts, the capture of explained variance and the loadings of principal components. In the left subplot, the PCs are found, with their respective explained variance. The orange line denotes the cumulative explained variance. In the right subplot, the correlations between the principal components and a list of selected features are displayed.

To this end, two points are interesting, where involving another PC would contribute significantly less than the previous one. This is after the fourth one, as the first 4 PCs account for 56,76% of explained

variance, or after the seventh, as those first seven make up 79,18% of the total explained variance. The following, PC8, would contribute only a little bit more than 5% in explained variance.

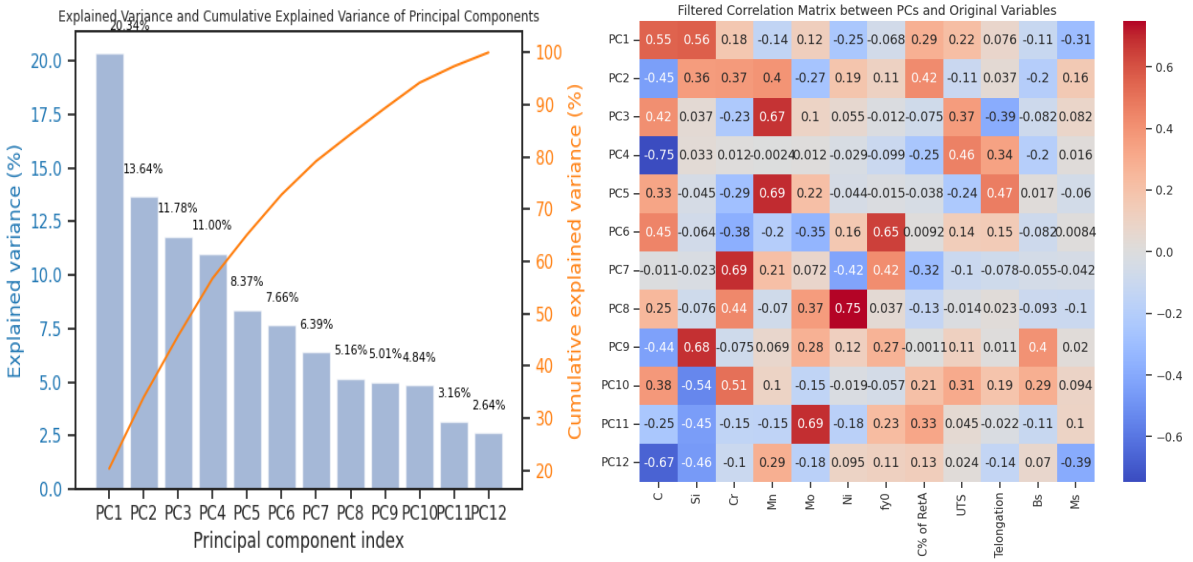

Figure 4.5: PCA Analysis of the collected data. The left figure is the capture of explained variance by PC and on the right the loadings of these PCs.

Looking at the PC loadings gives insights into processes occurring during bainitic transformations. The first PC is dominated by carbon and silicon, inversely related to M_S, and slightly dominated as well by $C_{\gamma 0}$. The relationship between C and M_S is expected, as carbon has a powerful austenite stabilizing effect on steel. The austenitic phase can therefore be maintained at higher temperatures, delaying the transformation of other phases like the martensitic. Silicon on the other hand has a limited solubility in the cementite phase, delaying the transformation and stabilizing the residual austenite by carbon enrichment, which explains the positive correlation mentioned above. In addition to silicon, this is also explained by the direct relation with carbon, as the more carbon there is, the more carbon will be present in the retained austenite.

The first two principal components capture a significant portion of the total variance in the data. Analysing these two components allows for a good understanding of the major patterns and variations in the dataset. As PCA is used for dimensionality reduction, choosing two PCs simplifies visualization and interpretation while retaining much of the information. Keeping the first two principal components has a balance between simplifying the data for visualization in two dimensions and retaining meaningful information.

Figure 4.6 displays the principal component analysis keeping the main two components. In the left subfigure, a biplot of the principal components and the original features is represented. In the right sub figure the loadings are represented in a matrix format. A biplot helps provide insights into the relationships between the original variables and the principal components, in this case, the two with a larger explained variance. The direction of the loading represents the correlation between the original feature and the PC, therefore in this situation, it is the carbon content that is strongly positively correlated with both principal components, while M_S is strongly negatively correlated with both. On the other hand, the manganese content strongly negatively correlated with PC1 but has no correlation with PC2. The length of the line represents the contribution of the feature to the PC, the loading. A longer line means a higher influence of the variable on that PC. In this case, $f_{\gamma 0}$ does not correlate with the main two components.

The angle between loadings indicates the correlation between features. Tensile strength exhibits a negative correlation with tensile elongation, as they point in opposite directions, a positive correlation with silicon, and is not correlated with carbon or the martensite start temperature. This representation

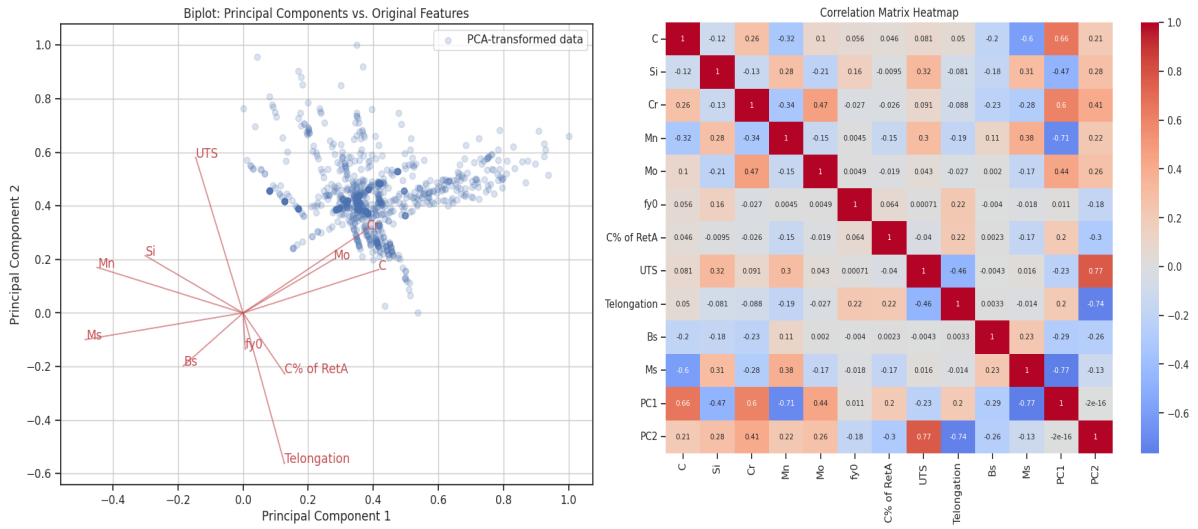

Figure 4.6: PCA Analysis. The left figure is a biplot of PCs and original features and on the right is the correlation matrix heatmap.

visually helps understanding the relation between features, and potentially identifying patterns.

The representation suggests that both Silicon and Manganese are an alternative to C. These are added to compensate for steels with lower carbon content, mainly Mn. Manganese and carbon are in opposite directions because the more manganese is added, the less carbon is required. The total carbon concentration has a direct relationship with the C concentration in RA, they increase simultaneously. But it does not necessarily mean that the $C_{\gamma 0}$ becomes less when there is more Mn, this is because there is less carbon in the alloy. Chromium and Molybdenum are usually not added simultaneously, but only one is added.

A biplot can lead to misleading interpretations and can be not sufficiently informative. A metallurgical knowledge of the data is needed for a correct interpretation, and non-orthogonal components, nonlinear relationships, and scaling can bias the visualization and the results. When using only two components, you essentially compress the data by projecting it into a lower dimensional space. Higher dimensional information is lost, and complicated relationships may be oversimplified or ignored. The data collected limits the availability of information that you can get from it.

If more parameters are included, there is less explained variance when keeping two principal components. Figure 4.7 exemplifies this with the addition of nickel. However, it can still give interesting information on the other features. For example, when Mn is added, Si is added too. And when Mn is not added, Nickel is the chemical element that compensates. Nickel has a direct correlation with elongation because it is a strong austenite stabilizer element, and when applying the TRIP effect it enhances the ductile characteristics of steel. By adding the loadings label, it is possible to make a quantitative comparison between features. For example, the first two principal components carbon (0.67), manganese (0.75) and chromium (0.73) have almost the same length. They show the same effect, despite the fact the range of C is 0-1 wt.% while manganese content is up to 5.5%, meaning that carbon is more or less 5 times more effective by its weight percentage than Mn.

4.1.2. Clustering

In the machine learning context, clustering refers to the task of grouping similar data points based on their inherent similarities or patterns. It is an unsupervised learning technique, meaning that it does not rely on predefined labels or target variables. Instead, clustering algorithms automatically identify the underlying structure in the data and group similar instances into clusters.

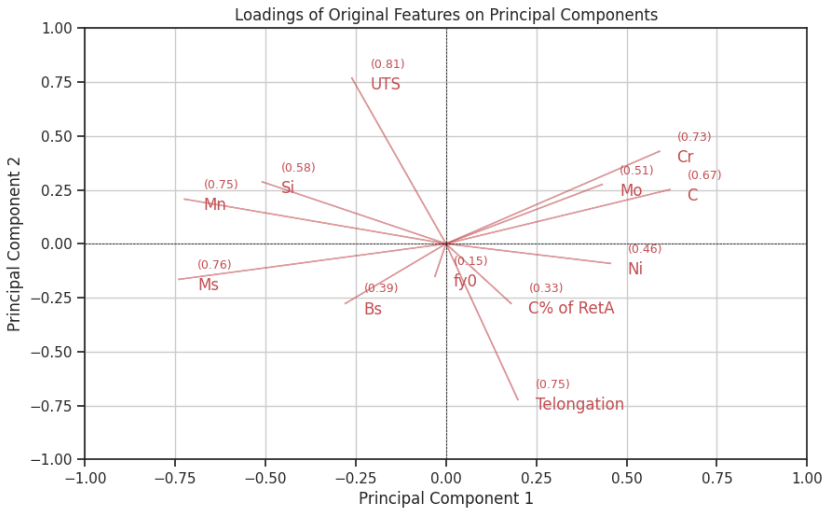

Figure 4.7: Loading of original features on principal components 1 and 2. Nickel is included.

The main goal of clustering is to discover the inherent structure or patterns in the data. By grouping similar data points into clusters, these algorithms aim to maximize the intra-cluster similarity and minimize the inter-cluster similarity. It is important to first pre-process and prepare the data, such as handling missing values, normalizing or standardizing. There are several clustering algorithms available, where K-means is a popular one. It consists of a centroid-based algorithm that partitions the data into K clusters, where K is an arbitrarily selected value. It aims to minimize the sum of squared distances between data points and their respective cluster centroids. This is represented in Figure 4.8, where the two principal components derived earlier, are divided into 5 clusters.

Figure 4.9 defines a simple alternative to group the principal components into different groups. The datapoints are coloured in each subplot with the selected continuous variables, showing therefore different physical meanings. It is also possible to divide them into selected ranges or number of clusters. This helps observe the trends seen in Figure 4.6, where for example carbon and molybdenum display an increasing transition across PC1, or the tensile strength and elongation showing a different behaviour across the PC2.

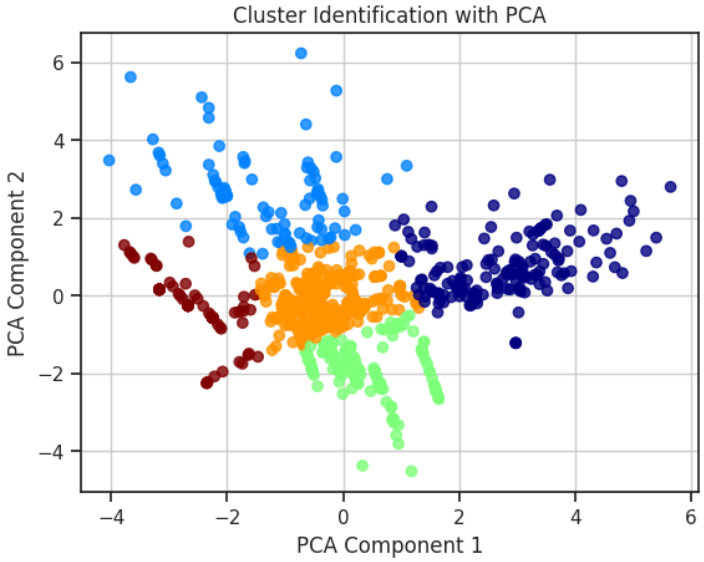

Figure 4.8: Clustering identification of the two main principal components using K-means.

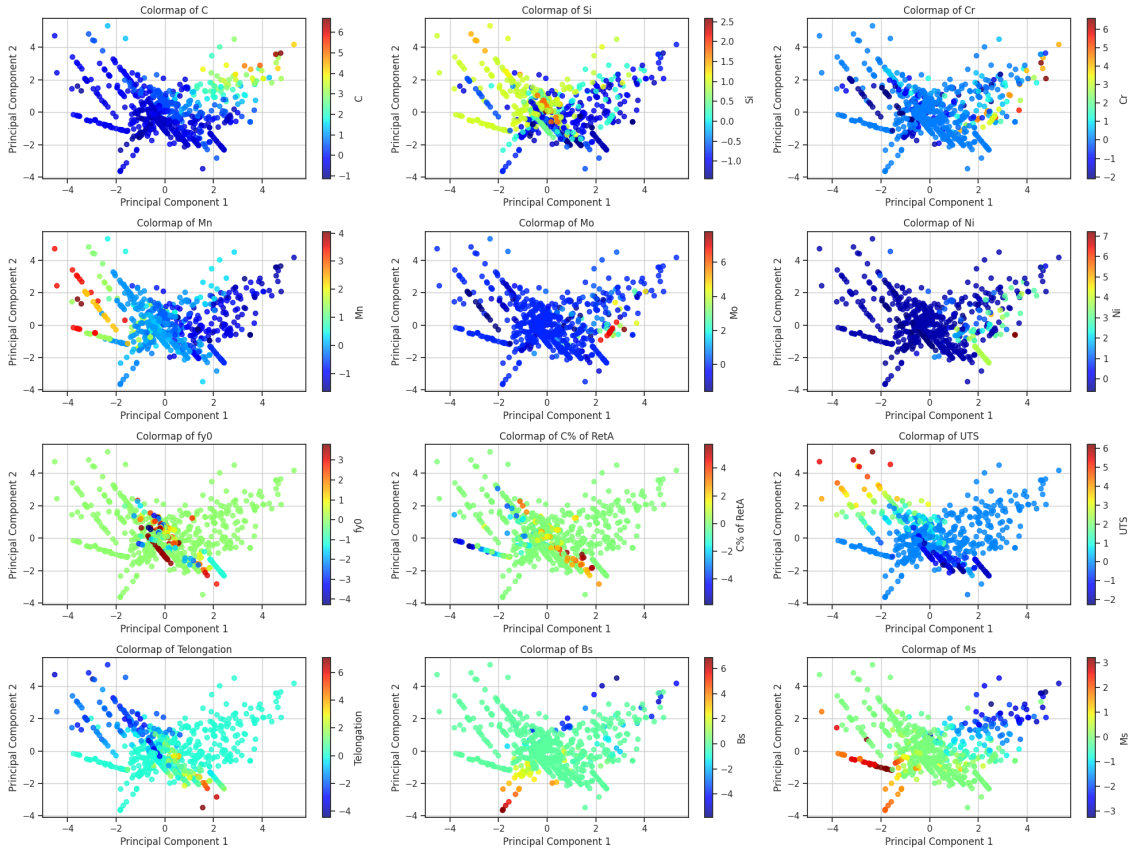

Figure 4.9: Clustering identification using a colorbar.

UMAP

Alternatively to PCA, Uniform Manifold Approximation and Projection (UMAP) is as well a dimensionality reduction technique in data analysis, clustering and visualization. Differently from PCA, UMAP involves non-linear dimension reduction, aiming to map high-dimensional data in typically 2D, while retaining local and global structures. It works particularly well with non-linear relationships in the data. In exploratory data analysis, it can aid in identifying clusters or patterns.

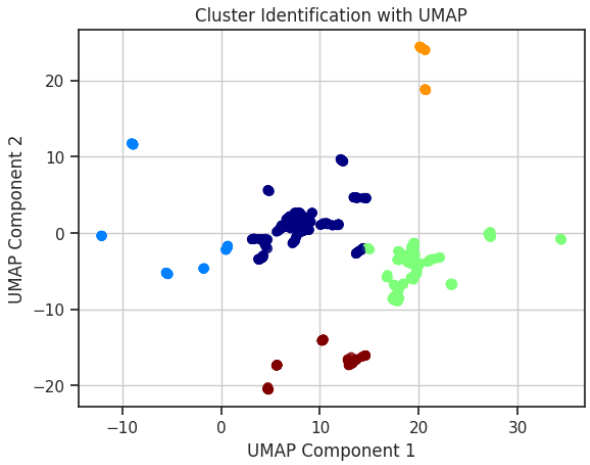

Figure 4.10: Cluster identification using UMAP.

4.2. Meta-analysis discussion

Claim 1

The start temperatures of bainite and martensite transformation reveal an exponential carbon dependency, according to the analysis of published experimental data. Several empirical models have been proposed to represent this carbon dependence. The first empirical equations proposed were linear approximations, as the ones proposed by Steven and Haynes, or Andrews [108]. These models are designed to be accurate for ordinary steels with less than 7 wt.% of alloying elements and a carbon concentration within the range of 0.1-1.9 wt%C. The following figures show the results from the dataset.

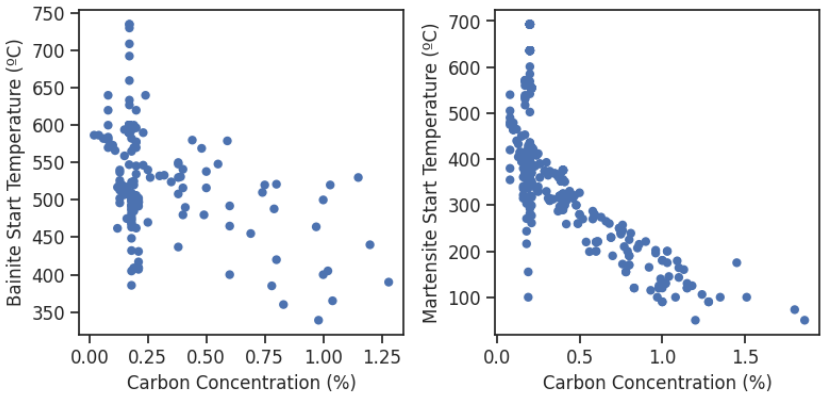

Figure 4.11: Bainite and Martensite start temperatures as a function of carbon concentration.

The B_S and M_S datapoints support that an exponential dependence on the carbon content exists, as represented in Figure 4.11. Based on this obvious trend, it is interesting to evaluate how this data fits in the existing empirical relations that predict B_S and M_S. Nonlinear type equations, such as polynomial and exponential functions, should be compared, to take into consideration the non-linear dependence of carbon.

Claim 2

The following subplots in Figure 4.12 have been represented using the morphological features of the collected data, concerning the content levels of manganese. The fractions of the second phases (retained austenite, martensite), the fraction of bainite, the initial volume fraction of RA, and the carbon concentration of RA change depending on the concentration of Mn present in the steel alloy. Three vertical lines are added, in the theoretically mentioned ideal amounts of manganese, and limit amount where bainite transformation cannot reach completion in an acceptable amount of time. Indeed, it is observed that there are no bainite fraction data points in the zone above 3.6% Mn. This means that in the experiments above this amount, the bainitic phase was not reported, so no data was introduced for this parameter. On the other hand, large values of RA are found at approximately 3% Mn. These results support in some way what is expected: when adding a large amount of manganese, the transformation of austenite is delayed and a large amount of residual austenite remains.

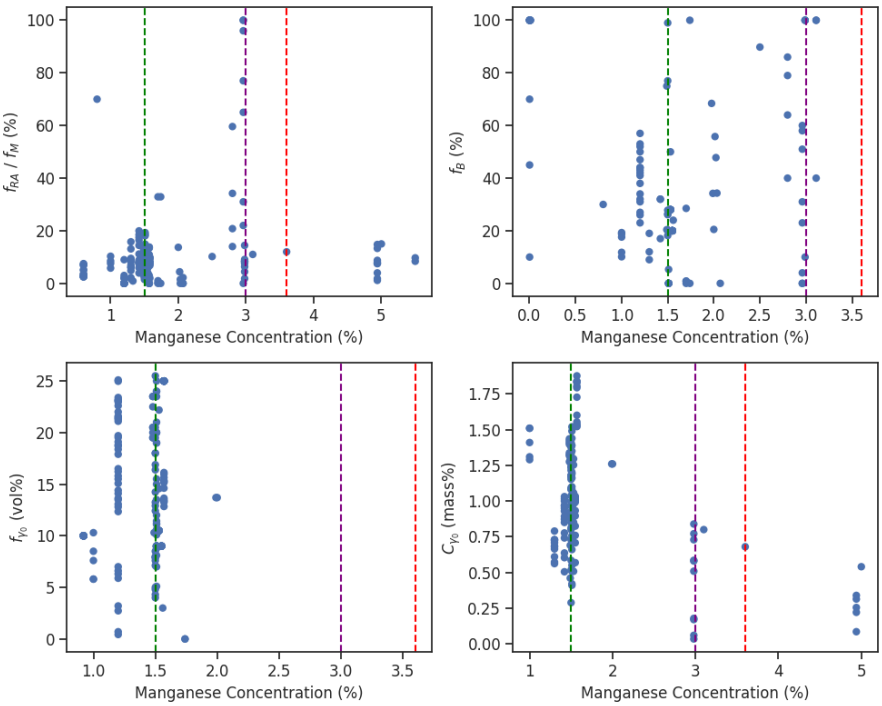

Figure 4.12: Morphological features as a function of the manganese concentration. In green and purple, ideal amounts of manganese. In red, the limited amount of manganese.

Furthermore, in large concentrations, manganese produces carbides together with C, limiting the carbon that diffuses into the RA, as seen in the bottom left plot. This stabilizes the austenite at room temperature, making it difficult for other phases to form.

On the other hand, it is indeed seen that no bainite is transformed above 3.6% Mn, but there is no difference among the values within the range of 0-3% Mn. This might be the case because other alloying elements, heat treatment conditions, and cooling rates can all alter the effect of manganese on the kinetics of phase transformation. The importance of other variables can help understand better the top left subplot. Around 3% Mn is the optimum amount on which more RA is formed, achieving theoretically the largest levels of ductility by the TRIP effect. However, some datapoints still show the same low values from 5-20% RA. By checking process variables, it is observed that these low values coincide with atypical large values of austenization time, or lower isothermal temperatures, which favour the formation of less ductile phases like martensite or lower bainite. In the Appendix A.4 a representation is shown.

On another page, the claim assures that around 1.5% Mn the best strength combination is found, and the maximum strength-ductility combination is achieved at concentrations of 3.0% Mn. These combinations of strength-ductility are achieved when 10-15% RA remains in the matrix. The strength, ductility, toughness and hardness properties for all Mn-containing steels are summarized in Figure 4.13. The strength values increase with the increase of manganese content, supported by the correlation values of 0.42 and 0.52 with YS and UTS respectively. The ductility values instead decrease when manganese is added to the steel, with a correlation value of -0.32 and -0.35 with UEl and TEl respectively. It is around 1.5% Mn where the larger ductility and strength-ductility values are achieved. The larger values of hardness are reached around 2% Mn. At this composition, the microstructure is mainly composed of bainitic ferrite and film-like retained austenite, which favours the hardenability of the steel. Finally, not enough data is available to reach any conclusion about the toughness of the material.

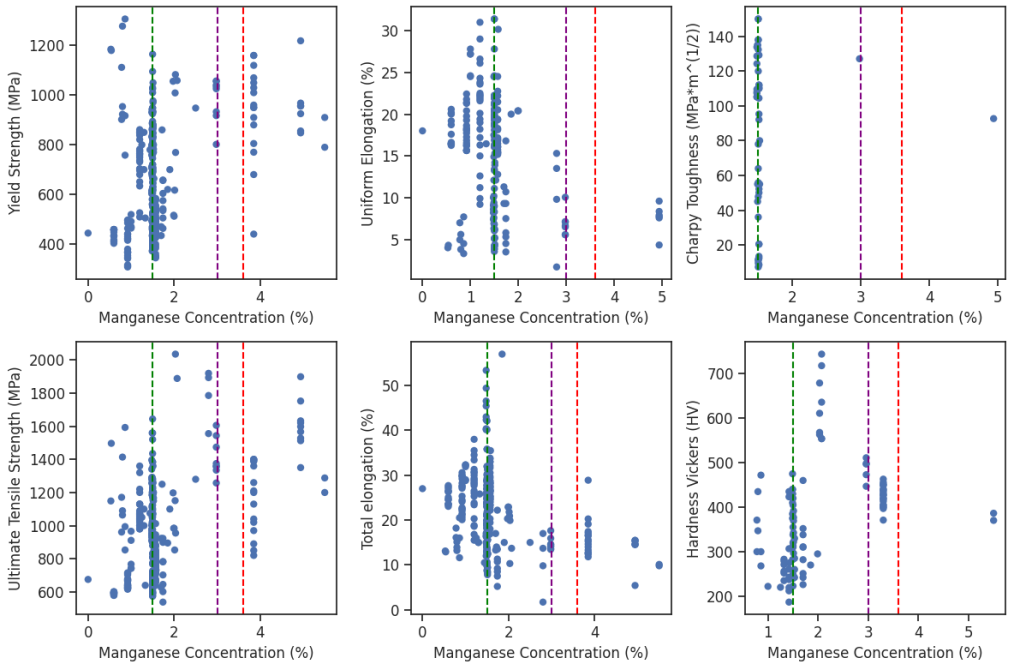

Figure 4.13: Mechanical properties as a function of the manganese concentration.

Claim 3

This section analyses what the literature states on how silicon influences the microstructure and mechanical properties during the bainitic transformation of steels, using the collected data. To begin, the relationship with the B_S temperature is examined in Figure 4.14. It is seen that when 1.5 wt% Si is added, bainite starts growing at temperatures below 550ºC. while at lower additions this happens at temperatures above 500ºC. The top left and right plots are coloured with C and Cr contents respectively to show their influence. As explained in Section 3.2 and already substantiated in claim 1 for carbon, these elements strongly delay the start of bainite formation when present in high amounts. Most of the low values in low-Si steels contain large values of these alloys. If focus is therefore made on the colder datapoints of the illustration, where there is less influence of these elements, a decreasing tendency is seen. To furthermore evidence the tendency, in the Correlation plot 4.2, the value that relates Si and B_S shows a strong inverse relation of -0.50.

To show a more representative analysis, standard TRIP-assisted multiphase steels usually contain 0.1-0.4 wt%C, so in the bottom plot, only these types of steels are accounted for. This plot aims to represent the influence of silicon in low-C steels. As stated, in the lower range of 0-0.2 wt% Si, B_S decreases harshly from 596ºC to 513ºC, while after this amount it only decreases slightly. The red vertical line at 0.2%Si evidences the different behaviour above and below this composition. It is supported that at lower compositions the decrease is harsher, from values around 600ºC to around 500ºC, with a slight decrease after this inflexion point.

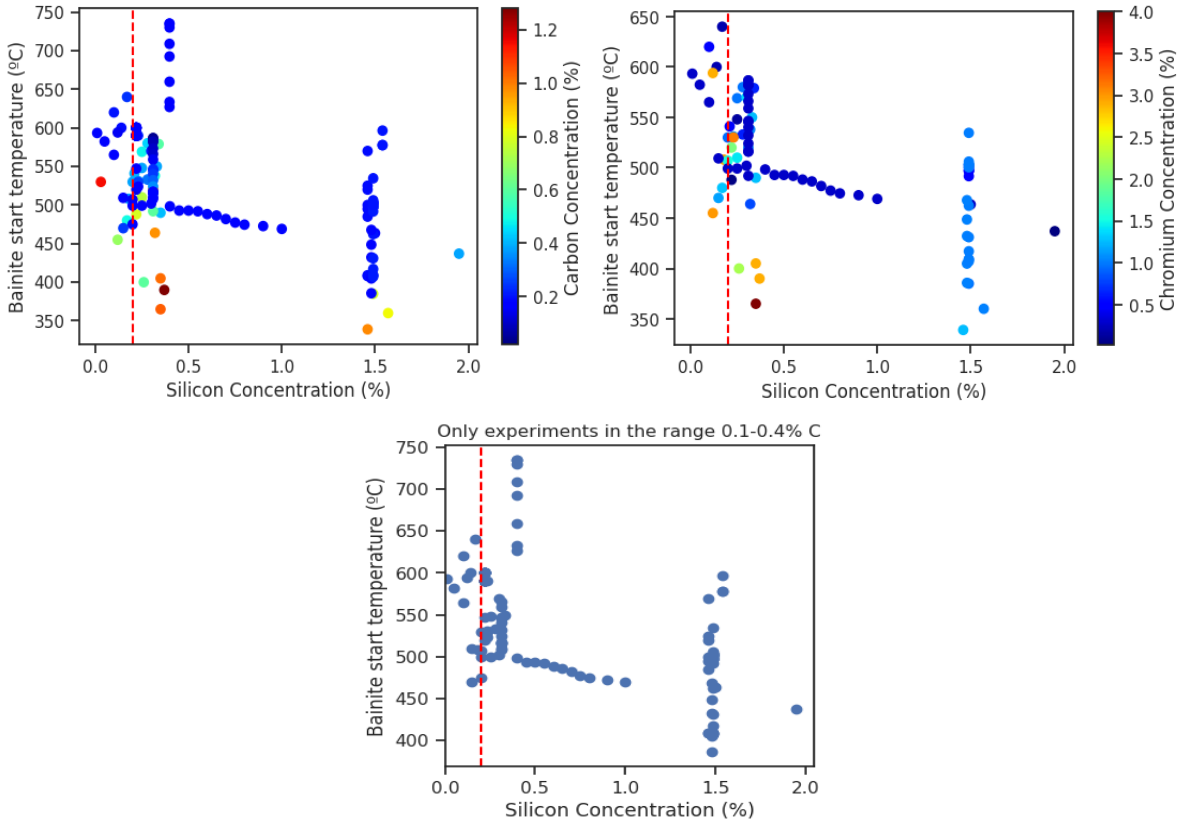

Figure 4.14: Bainite start temperature as a function of silicon concentration. The red line represents the inflexion amount of silicon.

In the following Figure 4.15, analysis of some microstructural parameters is exhibited:

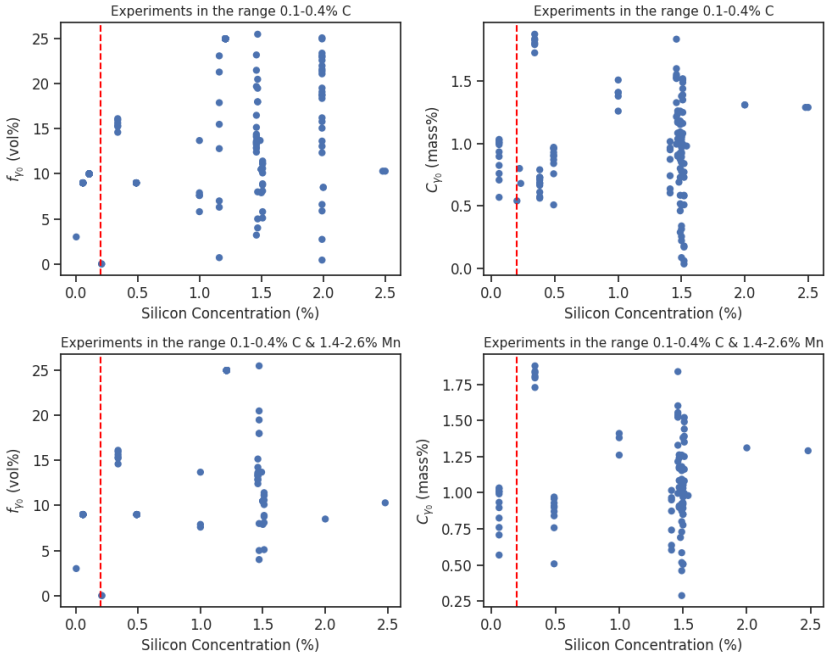

Figure 4.15: Morphological features as a function of the silicon concentration. The red line represents the inflexion amount of silicon.

Adding high quantities of about 1.5% Si should be enough to inhibit cementite precipitation. Furthermore, this stabilizes the residual austenite phase and increases $C_{\gamma 0}$. However, this is not supported by the data collected. Even when only typical values in the range of TRIP steels are represented, meaning low-C and medium to high manganese amounts, the austenite phase does not seem to be (more) enriched in carbon. This can maybe be explained by the quality of the dataset. This claim is true when certain conditions surrounding the process are made [47]. Most important is that Si tends to inhibit carbides through a two-stage bainitic transformation [109] [110], and therefore carbon enrichment occurs. Therefore, it may be the case that part of the data does not represent a two-stage transformation, as most of the experiments contain only one isothermal step.

A similar situation occurs when observing the results of $f_{\gamma 0}$, where no increasing tendency is seen. Coming back to the meta-analysis, different sources in the literature report that cementite precipitation is only totally prevented at approximately 2 wt pct silicon. In our collected data, however, over 90% of the datapoints have quantities of 1.52%Si or below, as shown in the descriptive statistics in chapter 3.1.2. The lack of experiments with larger amounts of silicon can be why these tendencies are not supported by our data. It might be the case that the brittle cementite is not prevented enough.

Next, it is analysed if the strength and ductility rise when the composition of silicon rises to 1-2%. Figure 4.16 represents the ultimate strength and total elongation in the composition range of mechanically aided-TRIP steels. A tendency of increasing UTS with Si is seen, with a correlation value of 0.57 when all types of steel in the dataset are considered. Whilst the tendency with strength is evident, the same cannot be said about the TEl. Similarly to the volume fraction of RA, which transforms into martensite during the mechanical straining, no trend is seen here.

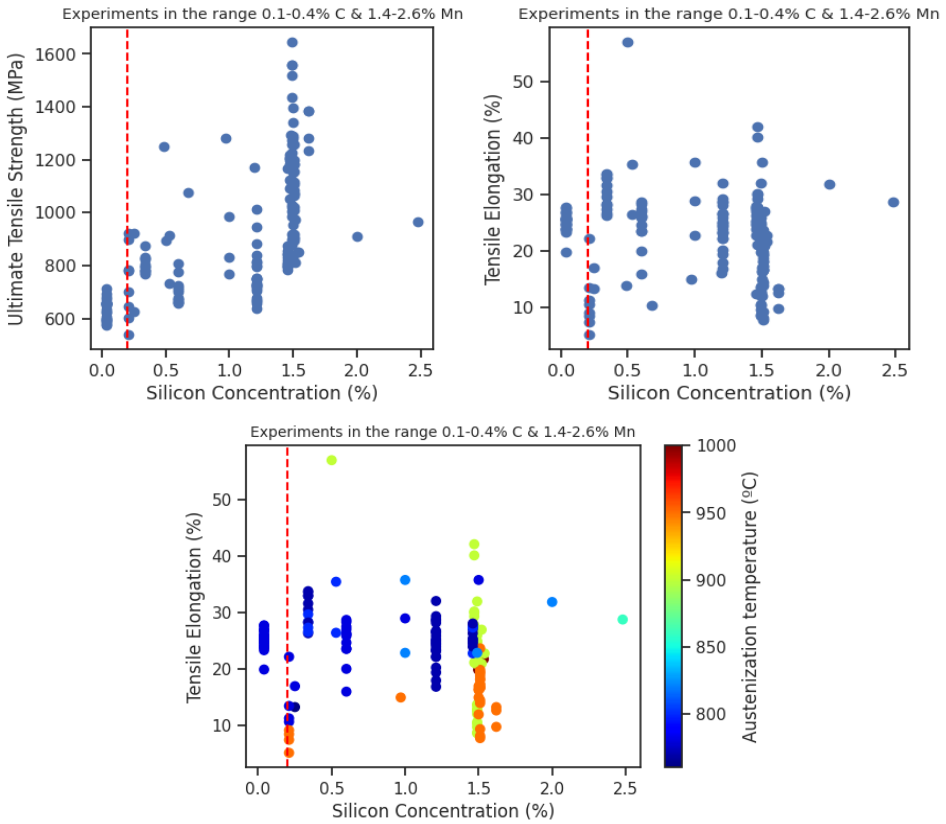

Figure 4.16: Mechanical properties as a function of silicon concentration. In red, the inflexion amount of silicon.

While some studies have proven that the improvement of ductility and strength is related directly to $f_{\gamma 0}$, which increases within others with increasing contents of silicon [111] [112], other investigations

mention that the stability of RA is as important and must be taken into account [48] [113]. The gradual development of the strain-induced transformation during straining attains a larger strength-ductility equilibrium and mainly superior ductility. Several parameters that are normally related to austenite stability are stabilizing elements like carbon or the reduction of austenite grain size. No sufficient information on the grain size and the reduction of grain size is available, therefore it may be a potential reason behind the not-observed improvement of ductility. However, the strength-ductility ratio still does show an increasing pattern as expected.

Finally, it would be useful to have measurable/qualitative morphological information of each experiment. Knowing if the samples present a CFB microstructure or not is crucial to knowing whether to expect improved mechanical properties or not. Additionally, Figure 4.16 shows an example of how other parameters play a role rather than only the silicon content. Within others are the austenization temperature and holding time, isothermal temperature, bainitic holding time, and cooling rates, which are all very important factors influencing the microstructure and therefore ductility of each phase. The complete problem is quite extensive, and only some aspects of it are addressed in the available data. it must be emphasised that all these results are very difficult to interpret, as a general picture with all the parameters cannot be visually represented, and alterations in other factors are happening.

Claim 4

It is stated that aluminium is added in standard TRIP-assisted steels as an alternative to silicon, due to surface finishing and industrial issues. The left subplot 4.17 represent the aluminium concentration against the silicon concentration in the available data. Indeed, this inverse relation demonstrates that when Al is added, Si levels decrease more or less linearly. Several zones are recognised: an initial one where the aluminium contents are negligible, with a repetitive amount of around 0.04% Al, followed by a middle zone where aluminium additions co-exist with amounts of silicon, and a third and last area where a maximum of 1.5% Al is added and silicon values are very small, under 0.5 wt%. The interaction value is -0.61, which is a relatively strong correspondence (perfect linear relation would be -1).

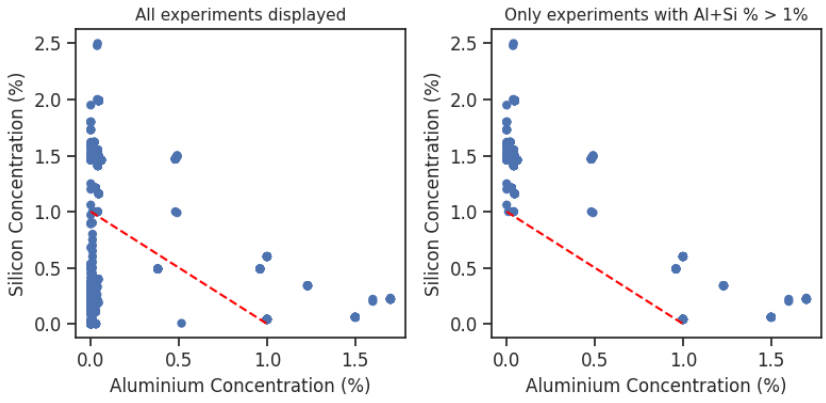

Figure 4.17: Aluminium concentration as a function of silicon concentration. The region of interest is found above the red line.

The red line separates the plot into two regions. Above the red line lies the region of interest, where the datapoints represent steels rich in silicon, aluminium, or both of them, which are the three cases desired to be compared in this analysis. Below the red line are the cases where neither aluminium nor silicon is sufficiently added to the steel, so it does not show any useful information for this comparison. Therefore, these values are taken out of the equation. The hidden values under the line in the right subplot are datapoints of which the sum of the amount of both alloying elements is below 1%.

$f_{\gamma 0}$ and $C_{\gamma 0}$ are represented against the aluminium concentration in Figure 4.18, where only the region of interest is represented.

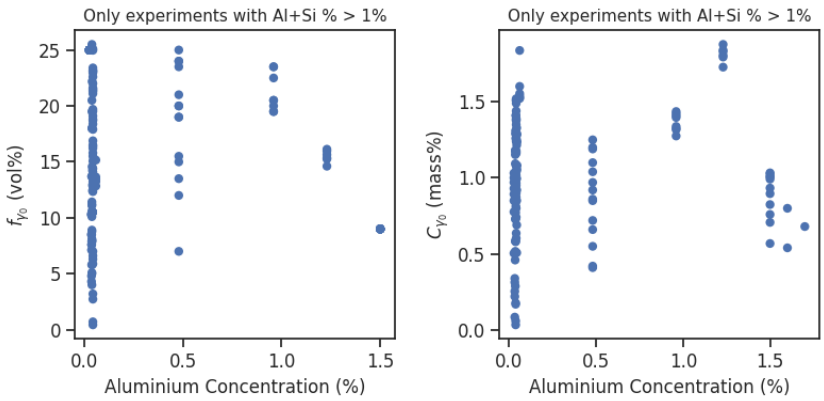

Figure 4.18: Morphological features as a function of aluminium concentration.

With the collected data, it is evident that there are different patterns followed in the three different situations. Starting with $f_{\gamma 0}$, the centre region that combines both elements shows high levels of this parameter. This means that the substitution with aluminium effectively suppresses the cementite phase and acts the same way as silicon. However, in the right sector where silicon is not present, the volume fraction drops remarkably, meaning that silicon acts in some way better as an austenite stabilizer element. How that will influence the mechanical properties will be seen later.

Moving on to the carbon enrichment of austenite retained at ambient temperature, the combination of both elements exhibits remarkable results, with very large amounts of up to 1.75% carbon when 1% and 1.25% aluminium are present. This shows the great ability to stabilize the austenite that these two elements have when combined. Instead, when silicon is not present, there is a significant drop, suggesting that silicon is a crucial element, and alternatively, aluminium is a great balancing supplement for this objective.

At first sight, there seems to be substantive evidence to support the claim made, as the data exhibits consistent patterns that align with the hypothesis that partial substitution of Si by Al increases the volume fraction of RA, and stabilizes this phase by carbon enrichment. According to the current representation of the data, there is robust evidence that these elements work well together. Next, it is seen if the promising results of the partial substitution influence as well with an increase of both the strength and ductility after the mechanically induced deformation process. The following subplots show the main mechanical properties that represent these two properties:

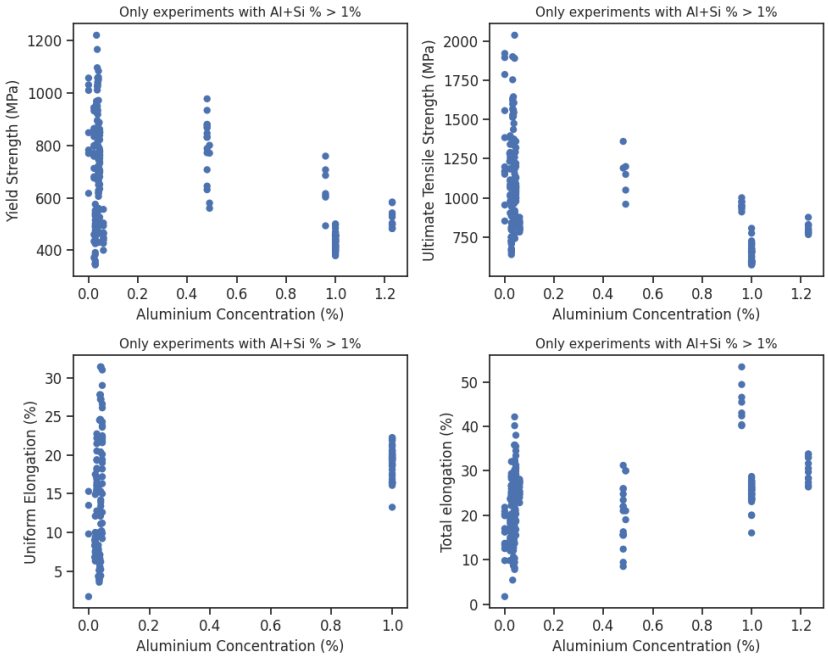

Figure 4.19: Mechanical properties as a function of aluminium concentration.

In terms of strength, we can see in that both the tensile and the yield strength have decreasing tendencies against the Al concentration. When reasonable amounts of Al and Si contents coexist, the strength values are extremely low, with tensile strength values below 1GPa. Even though balanced amounts of these alloying elements correctly stabilize the RA at room temperature, the larger expected values in strength are not seen. Indeed, aluminium is not a strong solid-solution strengthening element, whereas silicon is as proven in Figure 4.16. However, even though strength is expected to decrease when silicon is not present, an increase was expected when partially substituted. On the other hand, the TEl shows no improvement with the inclusion of Al. There is however a peak of very large ductility values just below 1% Al, which is not consistent with the results surrounding it, where ductility is much lower. There is almost no difference in terms of silicon and aluminium, but the carbon content is almost double, leading to this large ductility.

There is currently no substantial evidence to support the claim being made. However, the findings do specify that the strength and ductility values are increased by the TRIP process. With what is available, there is no additional information on how the steel has been treated after the heat treatment process. To draw reliable conclusions, it would be necessary to continue exploring and gathering additional data to further investigate this claim. Rather than discarding the reliability of the claim, the absence of important information makes it necessary to be cautious and sceptical regarding the validity of the claim. On the other hand, it is good to remember that other reasons encourage the addition of Al, rather than only on improved mechanical properties, for example, industrial requirements like the surface quality of the steel, and the processing operation.

Claims 5 & 6

In Appendix A.4 it is demonstrated that the presence of the elements chromium and molybdenum are independent of each other in our dataset. Even though they exhibit similar influence when added individually in steel, the presence or absence of one element influences the other. In analysing this claim, it is aimed to see if it is indeed true that single additions can show better results than when combined. The complementarity between chromium and molybdenum is of great importance for designing advanced steel alloys, highlighting the importance of considering element interactions beyond simple additive effects. As weak stabilizer elements, ductility should not be strongly enhanced, but rather maintained. The following figures show the results from the available database:

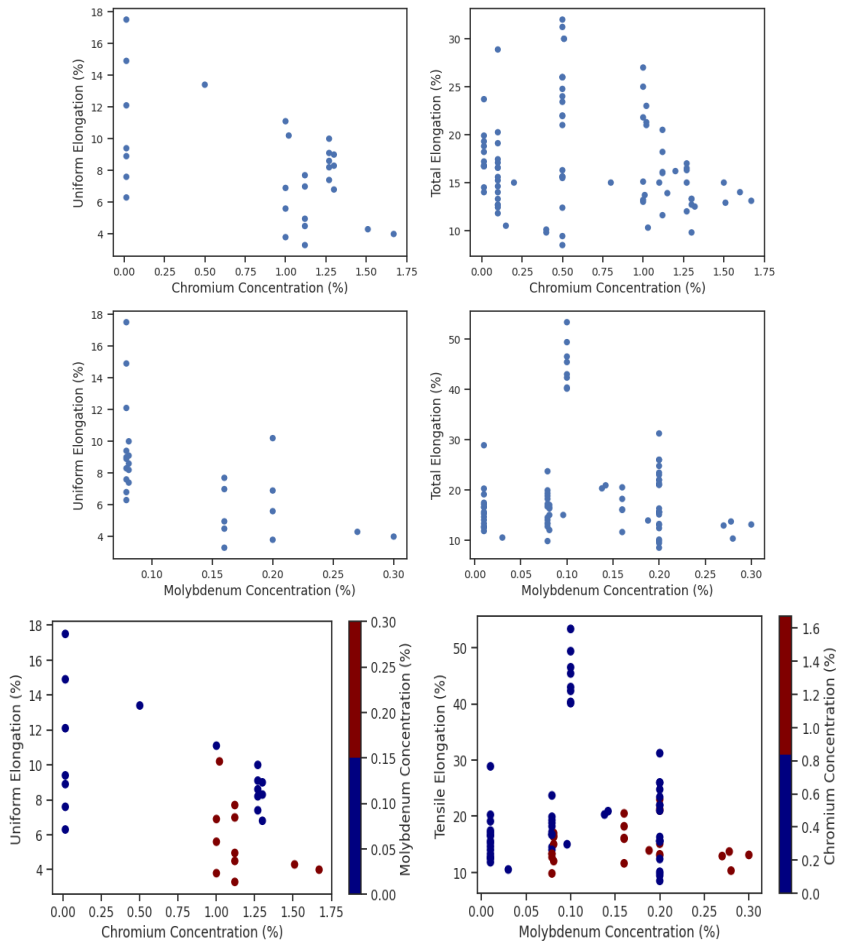

Figure 4.20: Ductility properties as a function of chromium and molybdenum concentration.

As seen in the illustration above, there is a clear decreasing tendency of the UEl when adding Cr and Mo. Therefore, their presence results in a very poor ability of the steel to absorb energy without deforming. On the other hand, it is more difficult to spot any trend in the total elongation. What can be accepted from the observations is that these elements are very weak austenite stabilizers, they are not appropriate if the objective is to retain a high amount of austenite at room temperature.

The bottom plots separate these two properties into lower and higher amounts of either of the chemical elements, to represent a comparison between single and multiple additions. In both cases, it is observed how very low uniform and total elongation values are obtained when a high amount of both is present (red points). It would be easy to think that this implies that single additions can show better results when combined. However, the elongation already decreases with the addition of both components, so it is difficult to evaluate this case because the sum of the individual contributions is already expected to give worse ductility levels. In the tensile elongation instead, where the tendency is not as clear, it is better seen how single additions of Mo exhibit better ductility than when combined with Cr.

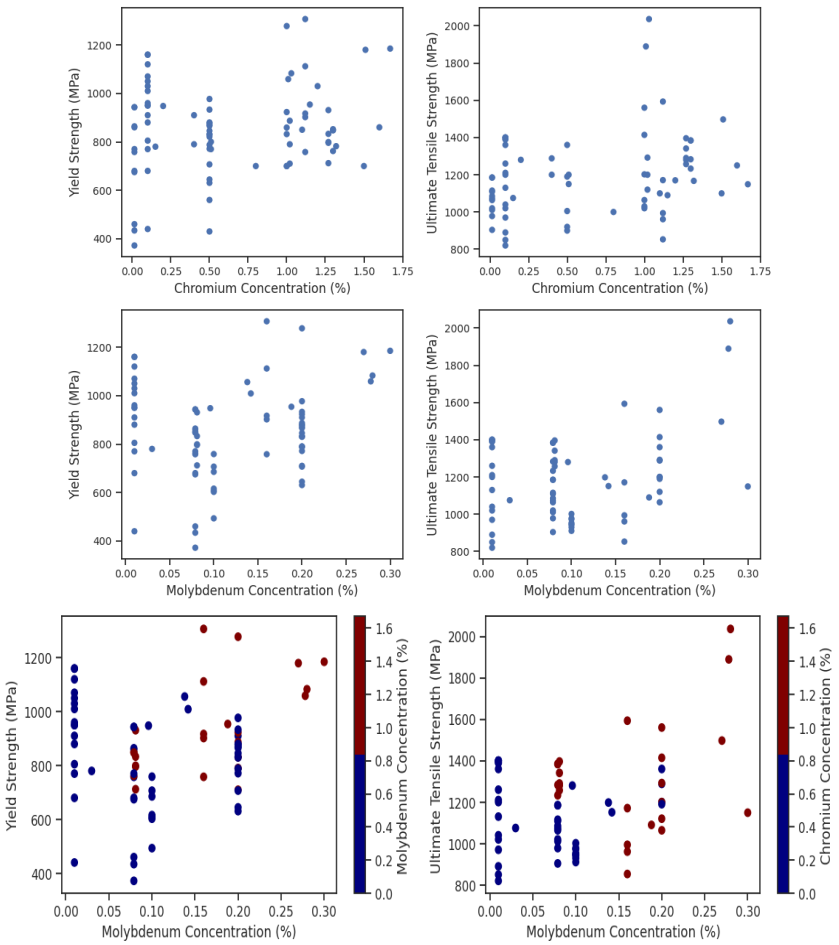

Figure 4.21: Strength properties as a function of chromium and molybdenum concentration.

Strength values exhibit a slightly increasing tendency, where some individual data points featuring high amounts of the chemical compounds accentuate larger strength. When comparing single against multiple additions, this time there is a different behaviour than what is observed with the ductility. Multiple additions show higher values of yield strength, and it is more adventurous to accept this as a trend in the case of the total strength, even though the greatest values contain high concentrations of both Cr and Mo. What is more apparent is that single additions do not show superior results in terms of strength. Following, it is well supported by a large number of experiments that the addition of at least 1% Cr in the designed steel increases notably the hardness. In addition, when accompanied by molybdenum (Figure 4.22, bottom), the hardness levels increase further. Hardness also increases with the addition of molybdenum. The increased hardenability is due to the formation of hard, stable carbides, which strengthen the matrix. However, some experiments with high Mo levels show very low HV. Additions of 0.4 wt% Mo lead to adverse effects, as excessive carbide precipitation can occur which may coarsen the microstructure and reduce the total hardness of the steel, as finer microstructures generally exhibit better mechanical properties.

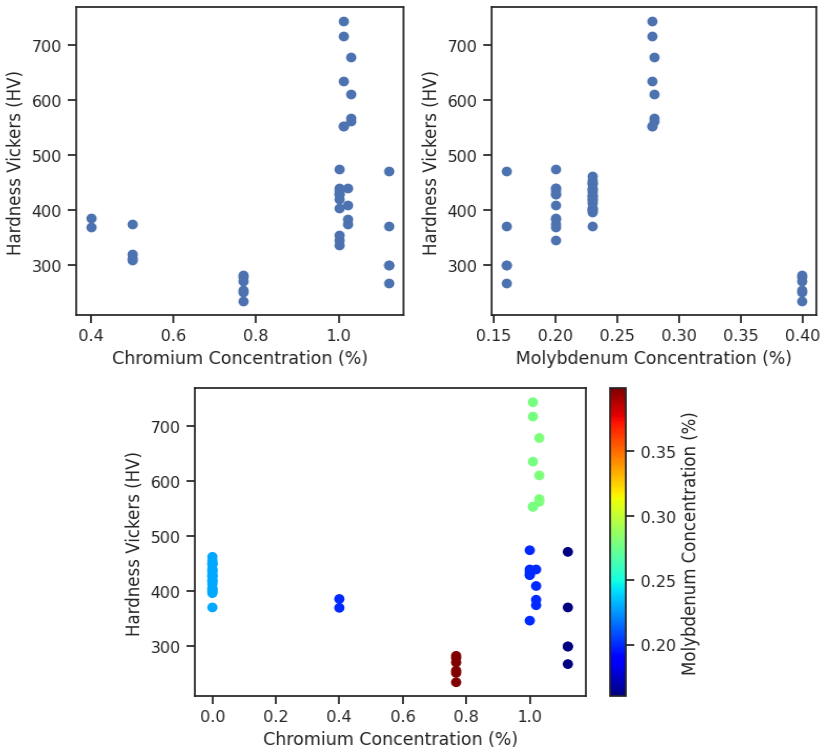

Figure 4.22: Hardness Vickers as a function of molybdenum and chromium concentration.

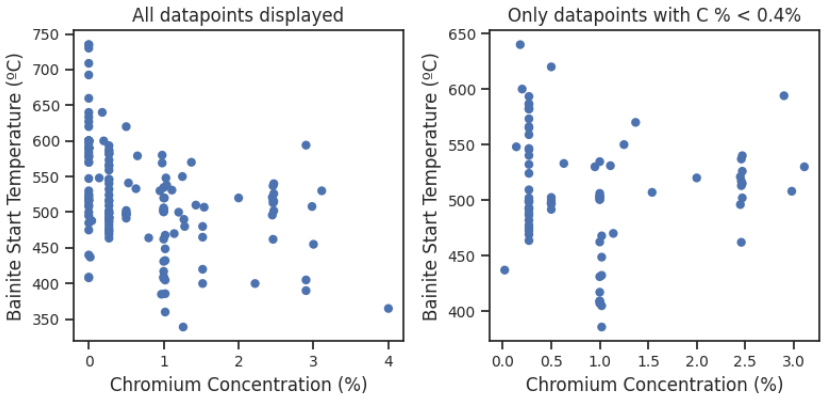

Figure 4.23: Bainite start temperature as a function of chromium concentration.

According to literature, the addition of chromium should delay the start of bainite formation, due to the bay of incomplete transformation that occurs at temperatures between 450ºC to 550ºC. At first sight, this claim can be accepted when observing the right plot in Figure 4.23. However, it is possible to study this while excluding the powerful influence of carbon, demonstrated in claim 1, by removing from the plot all the experiments with carbon levels above 0.4%C. This time, the bay of ICT is not seen in the right subplot. The literature [101] does mention that this happens in Fe-C-Cr steels, however, this is not the situation here. The presence of other chemical compounds can be the differential factor that hinders the partial transformation of austenite to bainite.

Claim 7

Figure 4.24 represents the content of Nb against the ferrite transformation start temperature and the final phase fraction of ferrite. By observing the representation of the data, it is important to note

that the available dataset might not incorporate a sufficient number of data points to validate the claim being made. When merging all the experiments that include data on Nb content, F_S, and f_α, the results show a clear decrease of the ferrite fraction while increasing the niobium, with an increase of F_S. The information on microstructural parameters like phase fractions is normally not given in quantitative results, leading to a lack of information to perform this comparison. Only 7% of the dataset contains a numeric value of this parameter. While the present data can give a useful insight into the microstructural influence of Nb, the small number of datapoints leaves room for unpredictable results. A larger and more diverse dataset would be required to securely investigate the claim.

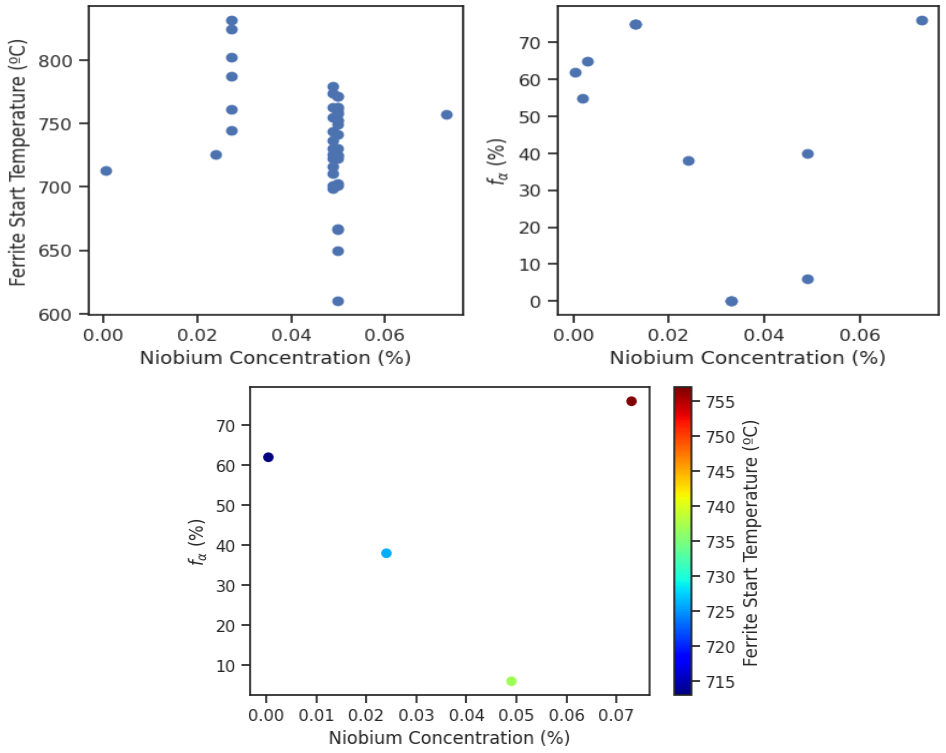

Figure 4.24: Ferrite start temperature and ferrite fraction as a function of niobium concentration.

Claim 8

For the experiments collected in this project, a maximum level of elongation and strength-elongation is said to occur at complex additions of 0.05% Nb and 0.5% Al. Figure 4.25 depicts the variation of the mentioned chemical elements with the mechanical properties:

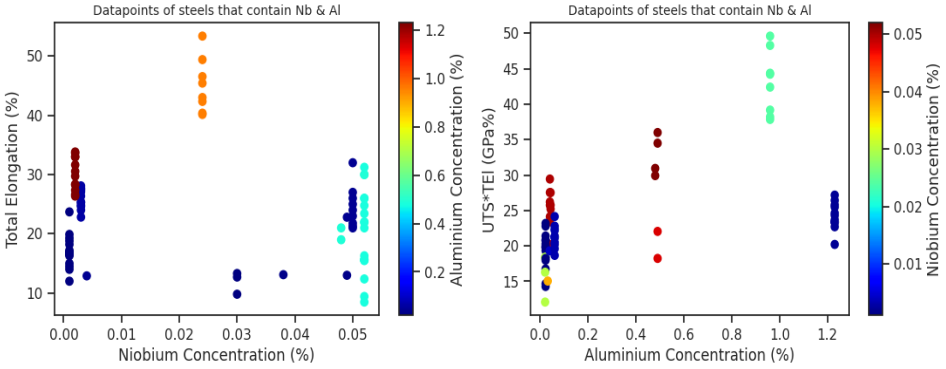

Figure 4.25: Total elongation and Ultimate strength as a function of silicon and niobium concentration.

It is said that this proportion increases the TEl and the strength-elongation combination, however, the analysis does not support this, but a maximum level of ductility is seen instead when Al levels are double than mentioned in the experiment. The relationship between alloy composition and mechanical properties is complex, and there could be situations where the combined presence of Al and Nb does not necessarily result in a proportional increase in tensile elongation.

Again, other variables are required to explain why the maximum is not at this composition. The literature explicitly mentions that the steel analyzed is 0.2%C, 1.5%Si, and 1.5%Mn. Instead, the datapoints at the interest region have 0.35-0.4 %C, which is not the steel type desired for the analysis. Therefore, it is not possible to reach any conclusion regarding the affirmation of this dataset. In alloy design and metallurgical engineering, a delicate balance between multiple factors is important, and if one of them differs largely, the behaviour of other elements can change in unexpected ways. In any case, the strength-elongation lies within good levels for this type of steel.

Claim 9

The strength relationship of each experiment with Mo and Nb levels is outlined in Figure 4.26. It is seen that adding molybdenum has a positive tendency in the strength of the steel. With varying levels of the alloy composition and other process parameters, it is at high levels of Mo where the maximum values of strength are found, reaching UTS and YS values of up to 2000 and 1200 MPa respectively. This happens because molybdenum favours bainitic transformation.

Additionally, there is a zone of extremely low UTS values when Nb is not present as a micro-alloy. Instead, a wider range with acceptable and high strength values is obtained when adding 0.2-0.5 %Nb. Therefore, it can be agreed that a finer microstructure is being transformed when micro-additions of Nb are added.

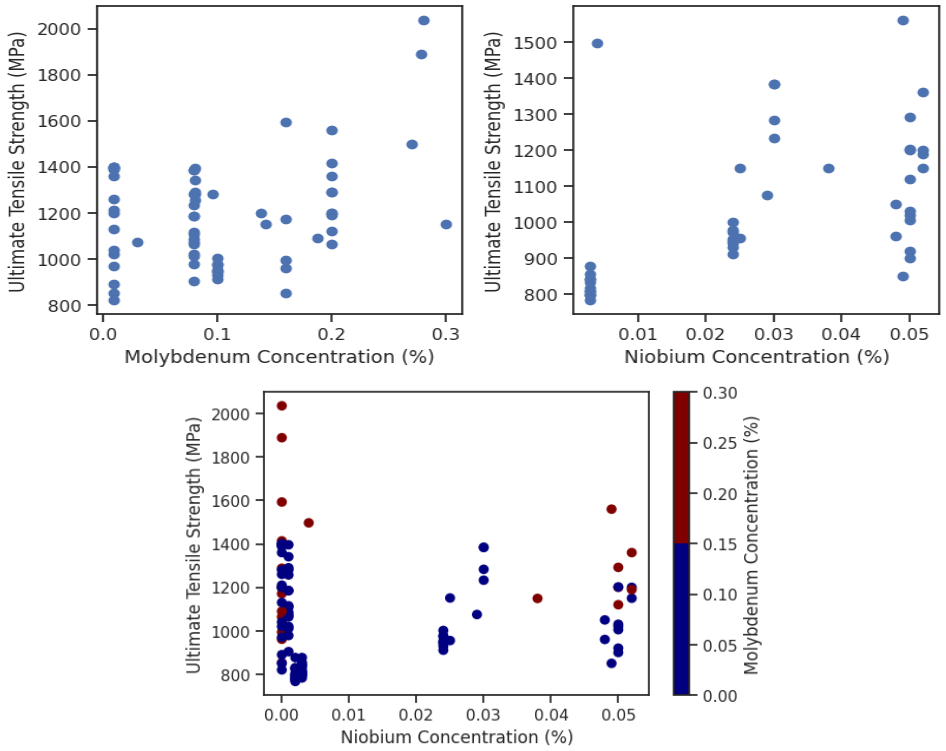

Figure 4.26: UTS as a function of molybdenum and niobium concentration.

Lastly, the bottom subplot exhibits the experiments where the three parameters are available, aiming to visually represent a comparison between single and complex additions of Nb and Mo. Even

though it is true that both alloying elements improve strength separately, it is not the multiple addition that results in the best strength levels. There are two zones separated, where the larger values of strength correspond to larger levels of Mo. It is the single addition of molybdenum when the optimum strength levels are achieved. This occurs because the Nb addition weakens the promoting function of Mo on bainite transformation. Therefore, it is safe to accept this claim and can be concluded that Nb addition can be avoided in Mo-containing steels if the application requires a high strength of the steel.

5

Prediction modelling

In the fast-growing world of data science and predictive analysis, the quality and suitability of the data used for modelling have been recognized as critical factors in the accuracy and reliability of predictive outputs. The question of whether the collected data is adequate for an accurate prediction of certain attributes is of great importance. This investigation is motivated by the observation that, while a large amount of data is easily available, its intrinsic characteristics are crucial to determine its suitability for predictive modelling.

Predicting qualities or properties is valuable in many fields, enabling educated decision-making and helping in risk assessment. Still, the fact of having a large dataset does not ensure its suitability for a successful prediction, as different factors as biases, noise, and shortage of fundamental features, can lead to misleading predictions. As a result, the concern on how to determine if the data gathered is favourable for successful predictive modelling arises.

Exploring the predictive potential of data requires an understanding of the environment in which the data has been collected, data preprocessing, exploratory data analysis, and finally rigorous validation procedures. This section explores the task of determining if the obtained data is suitable for predicting specific properties in the transformation behaviour of bainite. Combining a mix of theoretical principles and practical approaches, it ought to understand better the important role that data plays in defining the accuracy and usefulness of the predicted model.

The features chosen to be predicted are the B_S and M_S temperatures, which are dependent mainly on the alloying elements. Accurate knowledge of these start temperatures is important for the development of AHSS, as they help ensure that the bainitic transformation will occur in a certain temperature range, or it can serve in choosing the quench temperature below the M_S temperature. Many empirical equations have been proposed in the past, which Steven and Haynes and Andrews [108] are the most known and used. Alloying elements influence the Gibbs free energy difference between the ferritic and austenitic parent phases, and the stability of the latter strongly influences both the B_S and M_S temperatures. Moreover, it is known that the B_S temperature in the TTT diagram for certain steel may be different than the one deduced from the CCT diagram, implying that it also depends on the cooling rate.

Empirical formula

The empirical models that have been developed in the past are simple and sufficiently precise for a range of carbon contents and other additions of alloying elements. The analysis of the data in the previous chapter can give a better understanding of the carbon dependence for further development of more sophisticated empirical models.

A linear model is the most basic, where the outcome is linearly associated with the other factors. There are six empirical formulas for the calculation of B_S and four for M_S. The following shows models

5.1 and 5.2. Models A.2 - A.9 are shown in the Appendix A.5.1.

$$B_S(°C) = 830 - 270C - 90Mn - 37Ni - 70Cr - 83Mo \tag{5.1}$$
$$M_S(°C) = 539 - 423C - 30Mn - 11Si - 18Ni - 12Cr - 7Mo \tag{5.2}$$

In regression analysis, there are many ways to create a model. Ordinary Least Squares (OLS) is a statistical method that searches for the best-fitting relation between features. In essence, OLS looks for a linear equation that minimizes the sum of the squares differences (residuals) between the values of the dependent variable and those that are predicted by the linear model.

Model performance evaluation metrics

When there are multiple models fitted to a dataset, different criteria for model selection can be used, with each having its particular limitations. In this study, to quantitatively describe the prediction performance of the model, root mean square error (RMSE), mean absolute error (MAE), and regression coefficient (R^2) are applied to comprehensively evaluate the model prediction effect. (Eqs. 5.3-5.5). These quality metrics assess the predictive power of the ML models.

$$RMSE = \sqrt{\frac{1}{N}\sum_{i=1}^{N}(Y_i - \hat{Y}_i)^2} \tag{5.3}$$

$$MAE = \frac{1}{N}\sum_{i=1}^{N}|Y_i - \hat{Y}_i| \tag{5.4}$$

$$R^2 = 1 - \frac{\sum_{i=1}^{N}(Y_i - \hat{Y}_i)^2}{\sum_{i=1}^{N}(Y_i - \bar{Y})^2} \tag{5.5}$$

where N represents the number of data points, Y_i and $\hat{Y}_i$ represent the observed and predicted values, and $\bar{Y}$ is the mean of the observed values. The smaller RMSE and MAE values indicate higher prediction accuracy of the model, and the R_2 converges to 1, implying a better match between the prediction values and the experimental values.

Outliers detection and treatment

Based on the dataset, the outliers of B_S and M_S are calculated and removed. Figure 5.1 (left) shows the box plot calculation results of B_S outliers, where upper and lower are 683.49 ºC and 403.02 ºC respectively. Eight outliers exist beyond the limits. There are not many data of B_S beyond these limits according to experimental publications, therefore it seems reasonable to eliminate these values that may influence negatively on the model prediction. On the right side of the figure, the dispersion of carbon with the outliers for B_S (red pentagrams) is represented. Similarly, other elements are shown in the Appendix A.5.2 (A.6, A.7). The same procedure is followed with M_S, shown in Figure 5.2.

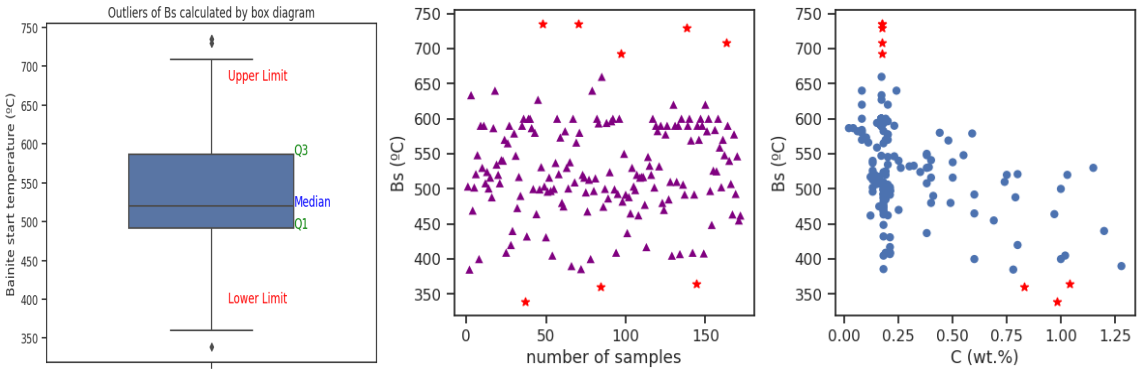

Figure 5.1: (Left) Outliers of B_S calculated by box diagram. (Centre) B_S data distribution. (Right) C-B_S dispersion with B_S outliers highlighted.

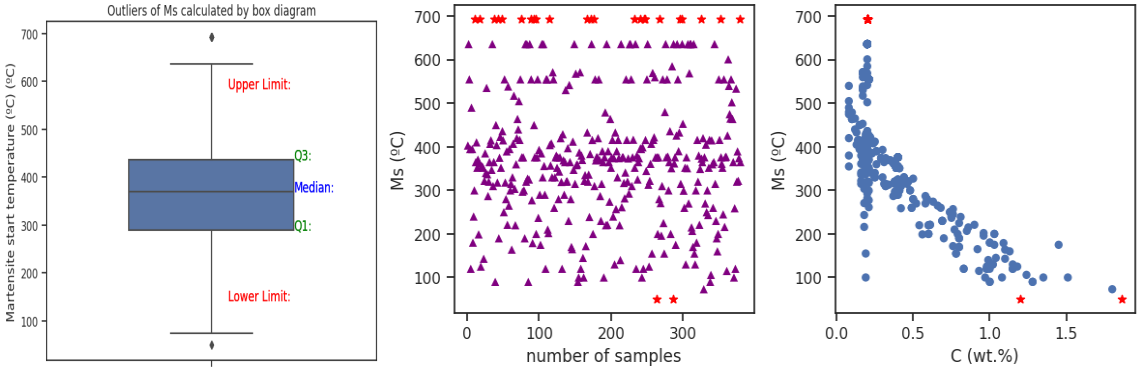

Figure 5.2: (Left) Outliers of M_S calculated by box diagram. (Centre) M_S data distribution. (Right) C-M_S dispersion with M_S outliers highlighted.

As shown clearly in Fig. 5.1c, the decrease in B_S temperature is inversely proportional to the increase in carbon concentration, within the range of 0-1.25 wt%C. This happens because increasing the carbon concentration in austenite would give rise to a decrease in the carbon concentration within the austenite particles before transformation. Correspondingly, the C % gradient is the effective driving force for bainite growth, therefore reducing this driving force will surely increase the time required for the diffusion of carbon atoms from the interface and thus inevitably reduce the bainite growth kinetics [114]. Moreover, more carbon leads to a decrease in the Gibbs energy difference between bainite and austenite, triggering the bainite nucleation [115].

5.1. Results and discussion

5.1.1. Comparison of empirical relations with data

The following representation shows the prediction results of empirical Eqs. A.2-A.6. The ideal fit between the calculated value and the observed value is included as a dashed line.

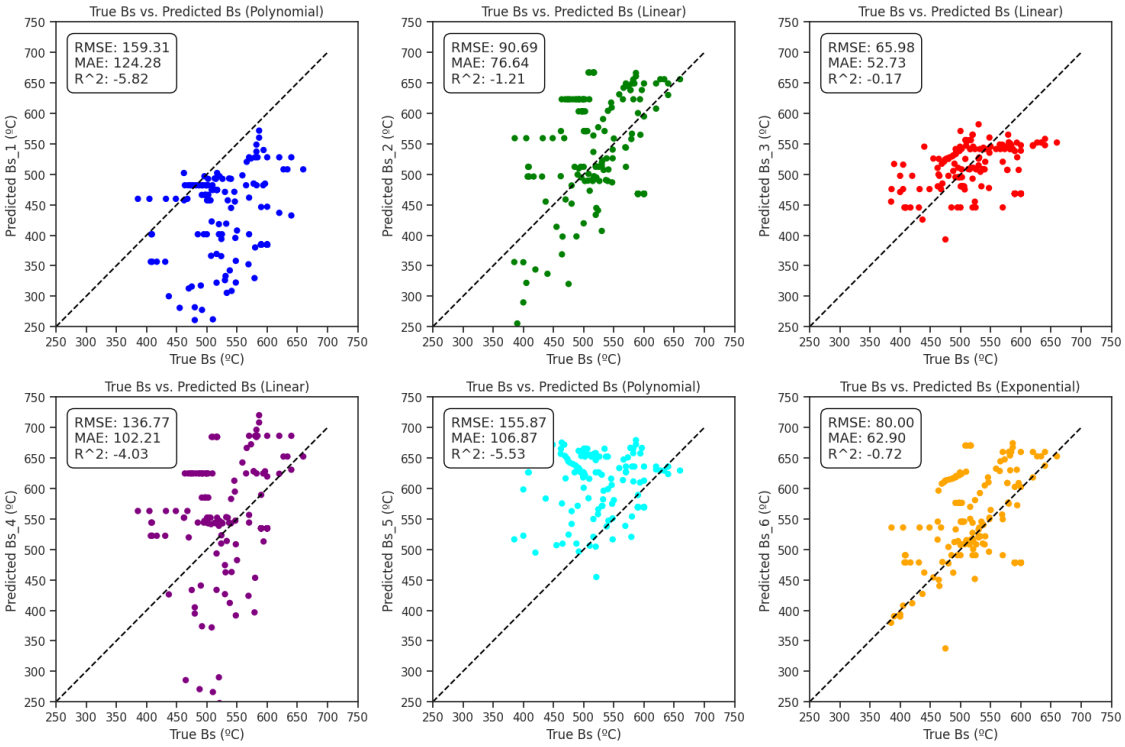

Figure 5.3: Fitting between the B_S experimental value and the B_S predicted by the empirical equations.

The results show that the models do not have a positive prediction accuracy. The R^2 values are negative, indicating that the models are a poor fit for the data. Negative R-squared means that the models fit the collected data worse than a horizontal line.

In the 6 empirical equations fitted above, there is only one (A.3) that does not include the carbon content in the prediction parameters and is precisely the one that gets closer to a positive fit (R^2=-0.17), Followed by the model that accounts for an exponential carbon dependence (R^2=-0.72). The worst four models account for a linear relationship of carbon, which may suggest that the non-linear relationship of carbon should be accounted for, as these offer a better fitting. However, confounding factors or the overfitting of data can also influence the carbon-B_S interaction.

Figure 5.4 shows how extraordinarily well the exponential model A.6 predicts the B_S temperature. The datapoints above 0.5%C fall all practically in the ideal fit line, therefore predicting this parameter with great accuracy. The opposite occurs in all the other models where high-carbon steels are very poorly predicted. The comparison of models indicates that the composition dependence of the B_S temperature is best described assuming an exponential dependence on the carbon content.

The M_S data are plotted in Figure 5.5. The polynomial model A.7 offers the best prediction of martensite transformation (R^2=0.45). However, in steels with carbon content higher than 0.8%, the predicted values are much larger than the experimental ones. Instead, at very low carbon composition it reveals a slight improvement of the prediction, making it most probably the differential factor to show an overall better prediction, as the large majority of the datapoints are in the low-C range. In comparison, the linear models 5.2, A.8 work much better at larger carbon amounts. Even if the accuracy is not great, the consistency best describes these steels. The exponential carbon model A.9, again, predicts with great accuracy M_S in high-carbon steels.

Overall, the models work pretty well in high-carbon steels. The deviation is much lower, suggesting that the error on the fitting is much lower in high-carbon steels. The fact that there are many more datapoints in the low-carbon range as well contributes to a reduced error. The polynomial model should be avoided for high-carbon steels, as it predicts temperatures much larger than the real one.

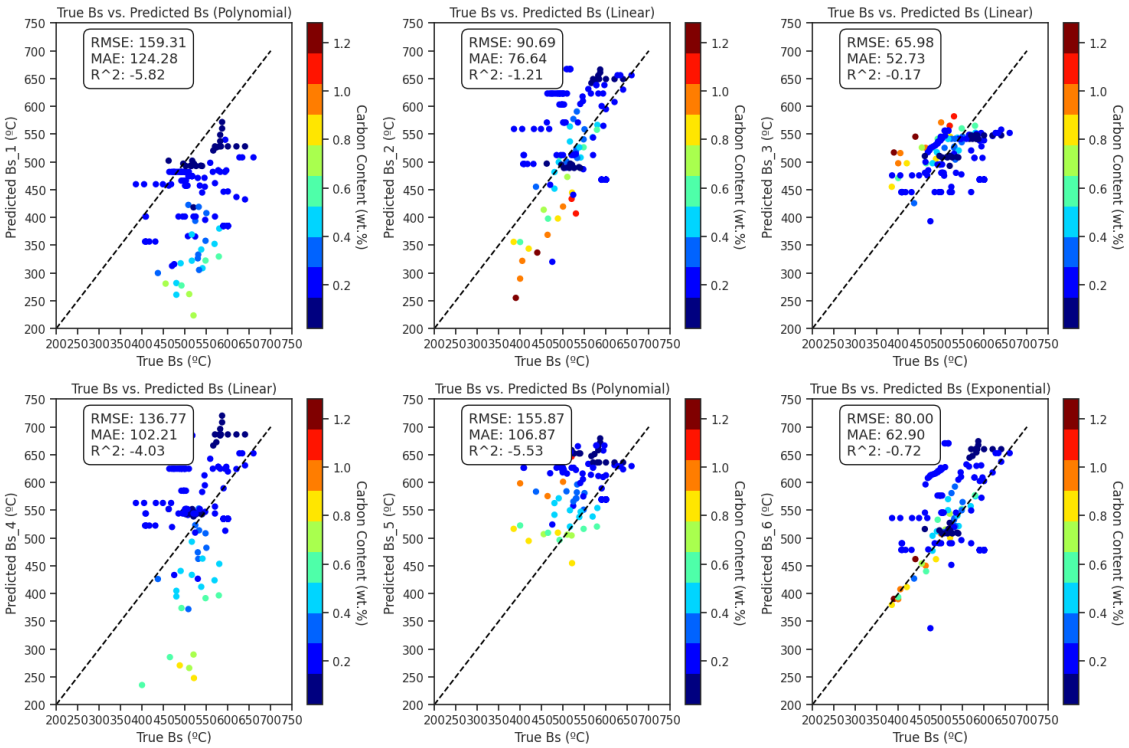

Figure 5.4: Bs fitting with empirical models as a function of carbon content.

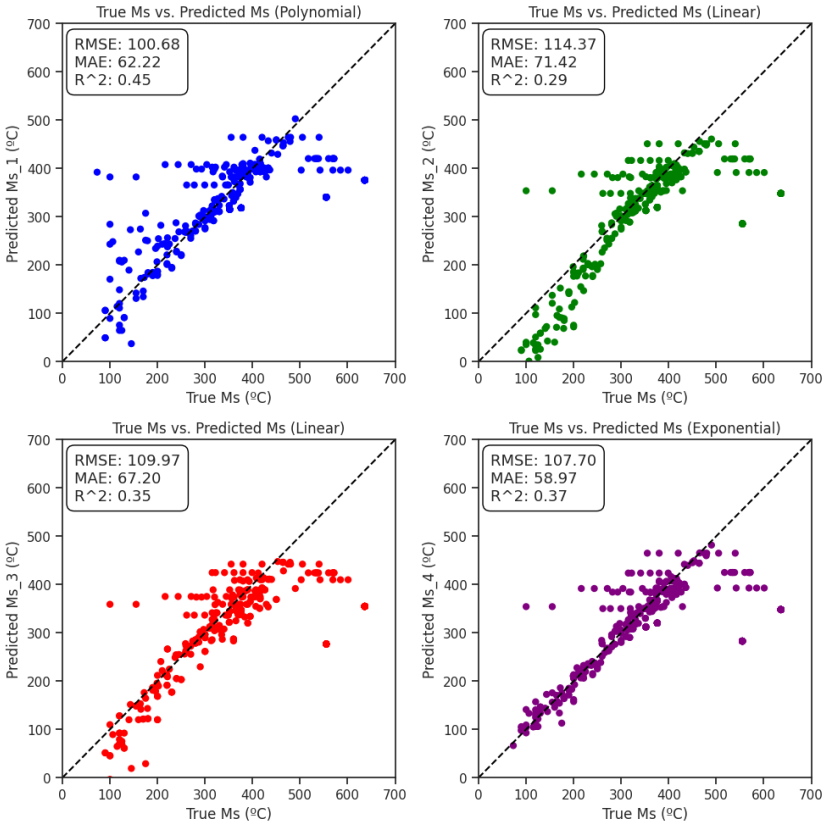

Figure 5.5: Fitting between the M_S experimental value and the M_S predicted by the empirical equations

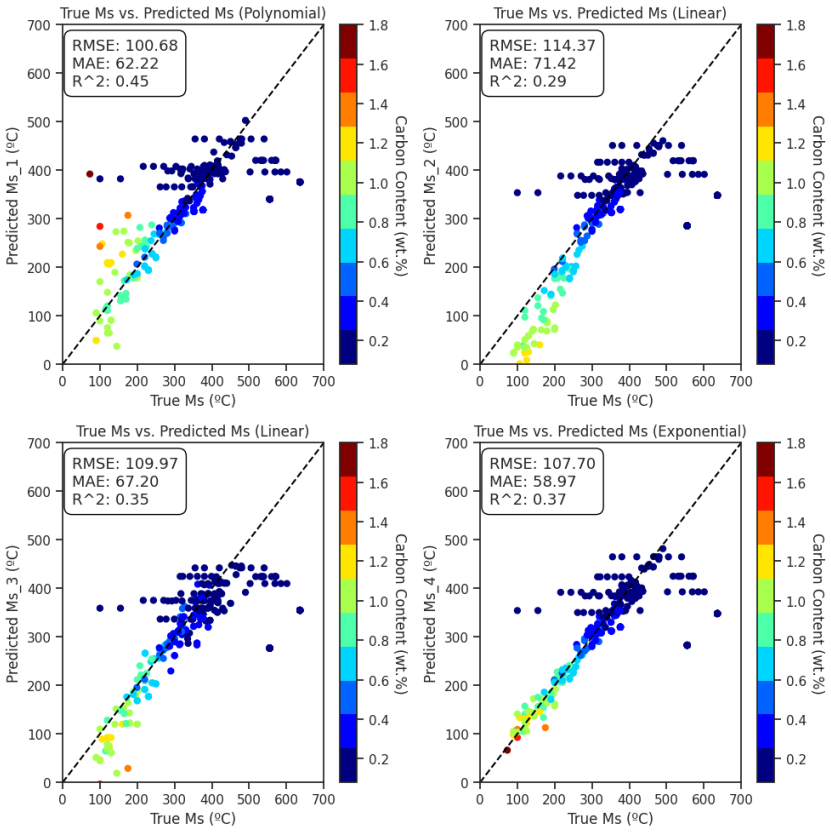

Figure 5.6: M_S fitting with empirical models as a function of carbon content

There is a noticeable difference in the predictions of B_S and M_S. This is expected, as the bainitic transformation is a more complex process. Martensite is more sensitive to factors like alloy composition, making it easier to predict based on known parameters. The kinetics of martensite transformation occur rapidly, instead bainitic transformation is a more complex diffusional transformation that involves multiple types of nucleation and growth stages. It is also composition-sensitive but can be influenced by a wider range of alloying elements and their interactions.

In contrast with the complexity of bainite transformation, more experimental data has been produced to predict M_S, facilitating the creation of more accurate predictive models. B_S requires of more advanced modelling and a better understanding of the alloy system and heat treatment conditions. This is mainly due to the existence of multiple types of bainite, such as UB and LB. Different morphologies make a need to account for different nucleation and growth mechanisms. UB normally nucleates at austenite grain boundaries, while LB can also develop within the austenite grains. As mentioned earlier in this section, the cooling rate and isothermal conditions influence significantly the type of bainite that forms, and not in all the experiments collected is the cooling rate recorded, which also contributes to a worse prediction. The overall complexity of bainitic transformation complicates the prediction of B_S in comparison to the more straightforward prediction of martensite.

Even with a simpler transformation process, the empirical relations used from the literature show poor fits on our dataset. A proper understatement of the development of the proposed models is required to reason this. Firstly, the models for both M_S and B_S have been developed under a defined set of conditions, with specific input conditions, whereas the collected data comes from different types of experiments. The collected data cover several real-world scenarios, like a wide range of cooling rates, alloy compositions or heat treatment history. The processing of the steel has a large impact on the microstructure and therefore on the transformation behaviour, such as hot rolling, recrystallization, or other thermal treatments. The austenite grain size D^{γ} has a strong influence, mainly in M_S. It has

been well established that the M_S can decrease about 15 ºC due to a decrease in D^γ from about 50 to 5 μm [116] [117] [118] [119].

Furthermore, the exponential models that predict M_S A.9 and B_S A.6 are restricted to the composition ranges of 0.1-1.4 wt%C, 0-3 wt%Mn, 0-2 wt%Si, 0-4 wt%Cr, 0-5 wt%Ni and 0-0.8 wt%Mo. Moreover, they do not contain significant additions of Cu, Nb, V, Co, or Al, within others [120]. The models developed by Steven Haynes and Andrews 5.1, 5.2 are developed with a dataset of around 60 steels with C contained in the range 0.1-0.55 wt%. Both polynomial models A.2, A.7 have shown a poor fit at high carbon contents, as they have most probably been developed and validated using data of steels with a rather small carbon range (0.1-0.5 %C). For higher carbon contents, the quadratic term becomes predominant, which explains the high M_S values obtained in the high-C range in a model A.7.

5.1.2. Prediction modelling

The results of models based on the entire dataset

To construct a model, six approaches have been considered, to estimate what model better fits the data. Data regression analysis is applied in different ways, to determine how big of an impact the main chemical elements have on the variables of interest, in this case, M_S and B_S. Not only the model is useful for making predictions, but also for analyzing the behaviour of the data and finding important variables. Similarly to empirical models from the literature, the starting approaches are a linear model, a polynomial model, an exponential model, and a new combined model where only carbon is accounted to have an exponential influence on the temperatures. The models are used to predict B_S and M_S with the arbitrarily selected most influential chemical elements, which for this analysis will still be carbon, manganese, silicon, chromium, nickel and molybdenum.

In addition, two more approaches are investigated. The fitting of the empirical equations in the dataset has suggested that a clear distinction between low- and high-carbon needs to be made. Therefore, a distinction is made, where 0.4 wt%C separates the dataset into two zones. In the high-C zone, it has been seen that a linear approach predicts with reasonably good accuracy the corresponding temperatures. Instead, for low-carbon steels the fully-exponential and only carbon-exponential are created. These are shown in Figures 5.7-5.8. In Appendix A.5.3 these representations are plotted as a function of the carbon content.

The models that work best are, in decreasing order, polynomial, exponential, linear, and the combined model. The polynomial model fitted to the data exhibits a surprising R^2 value of 0.92 but is more likely to have overfitting issues when working with unseen data. On the other hand, the linear models can experience underfitting issues, due to the non-linearity. This can be understood better by the new models that split into low- and high-carbon. In steels with C% $\geq$ 0.4%, the linear models display R^2 values of 0.94 and 0.92 for B_S and M_S respectively. In high-carbon steels, the model can be fitted extraordinarily well by a linear model, which exemplifies the non-existence of non-linearity in these compositions. On the other hand, the fact that at lower compositions the prediction still shows very poor results demonstrates that the challenge is at low compositions rather than higher ones. Splitting the dataset into two different models does not improve the prediction. The least squares fit of the B_S data and the M_S data to a linear model display the following equations:

$$B_S(°C) = 618.35 - 91.01C - 2.24Mn - 67.99Si - 23.38Cr - 18.28Ni - 28.38Mo \quad (5.6)$$

$$M_S(°C) = 459.74 - 284.86C + 18.75Mn + 7.24Si - 11.72Cr - 13.65Ni - 101.68Mo \quad (5.7)$$

These differ greatly from the empirical formulations in published literature. This is expected, as already explained because the types of steels and the processes that these have been subjected to differ greatly from the experiments that the published models have experienced, which are under a certain set of conditions. The most significant difference in the B_S equation developed is the impact of the manganese content on the predicted B_S, with a really small coefficient of 2.24.

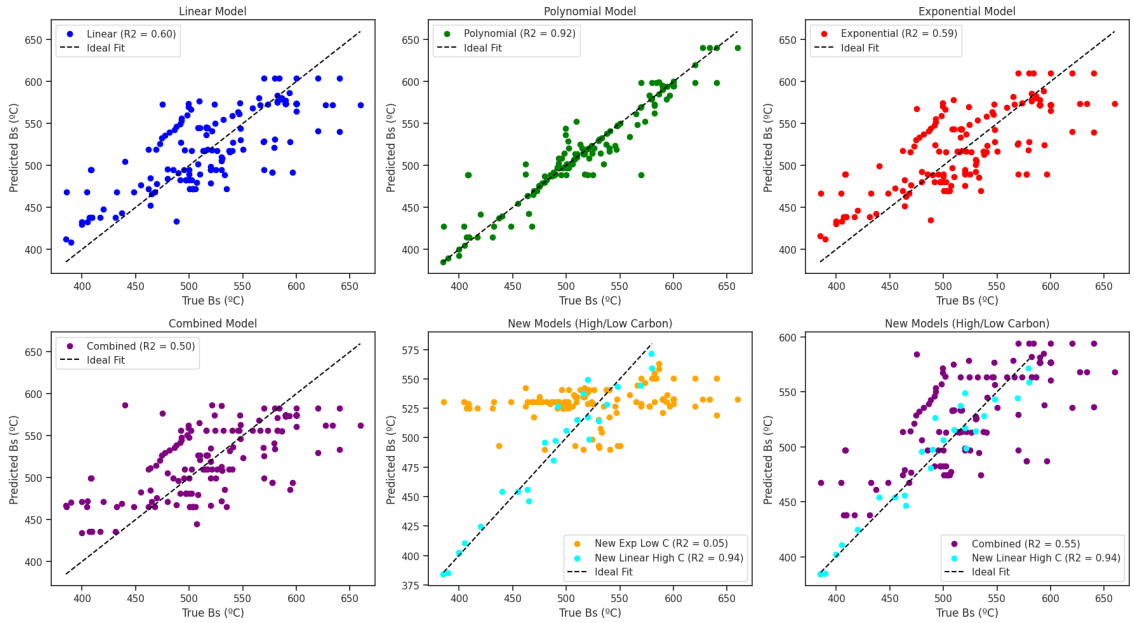

Figure 5.7: Correlation between experimental B_S temperatures and values predicted by regression analysis of several modelling approaches.

However, in ML it is critical to make sure that the fitting of the model to the data is balanced. The potential of ML is that it does not need to understand the feature-dependent variable relationships beforehand, but it discovers them automatically. In the simple case of linear regression, the development of the model and evaluation of the accuracy are in general performed on the entire dataset. This works well in simple linear regression but is susceptible to overfitting in a nonlinear ML model. A nonlinear ML model can, in principle, learn every single point in the dataset, but this model would most likely not work well on unseen data. Therefore, the accuracy of ML models must be evaluated based on unseen data. For more information on overfitting/underfitting models, refer to Appendix A.5.4.

The results of models tested by unseen data

In the models created earlier, all the data points are used for training, therefore the models will most likely not work well with unseen data. They are useful to gain insights into how the different models respond to the data, but new models must be developed to be evaluated in unseen data.

A simple way to do this is to build the model using a random subset of the data and then use the remaining subset for the evaluation of the accuracy of the model. This approach is called the train-test split approach or cross-validation. In addition, to improve the predicted accuracy, the random forest algorithm (RF) [121] is used as a dominant ML method, based on the idea of integration learning. Appendix A.5.5 gives a brief explanation of how the random forest model works.

To compare and choose the best model as the actual prediction model, machine learning requires the use of several models [122]. Therefore, in addition to RF and the proposed models, GBDT (Gradient Boosting Decision Tree) is used for comparison. GBDT constructs iteratively a sequence of decision trees, where each tree corrects the errors of its predecessor, being these the data points that were incorrectly predicted by the ensemble so far. The new trees are therefore designed to minimize the residual errors, improving the predictive accuracy of the model, which is the basics of the approach of the boosting method [123]. Boosting is effective in generating accurate predictions close to the experimental data, but it can be more susceptible to overfitting, which will be explained further. In ML they are therefore particularly well suited for situations where high predictive accuracy is essential.

Additionally to the train-test split, to obtain a more accurate and representative estimate, K-fold cross-validation is a machine learning technique that serves as a robust method to evaluate the perfor-

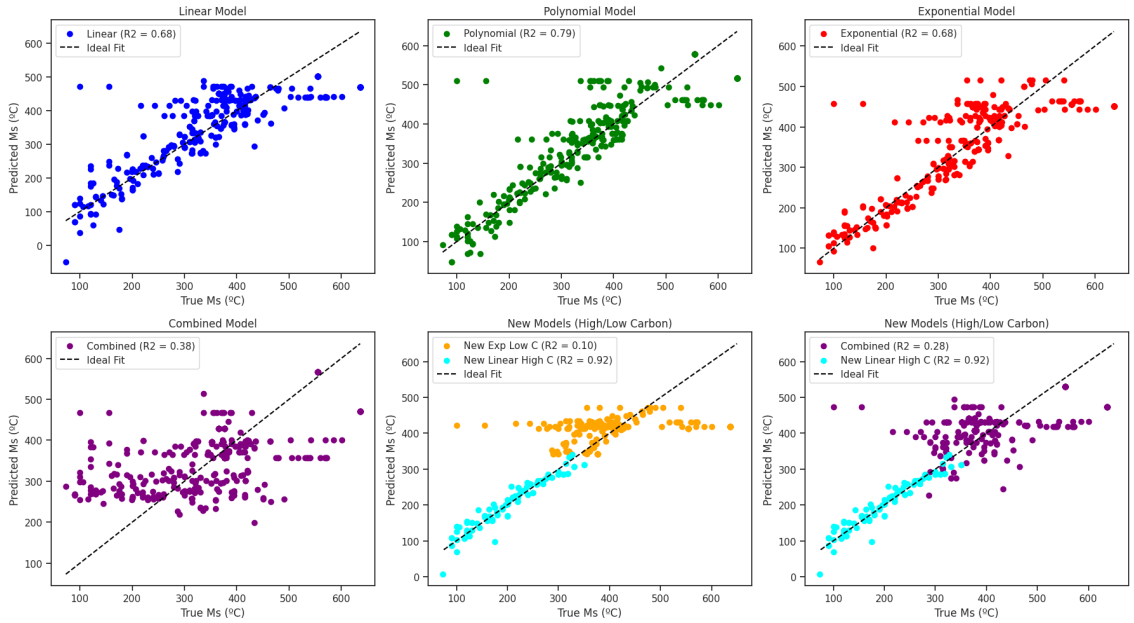

Figure 5.8: Correlation between experimental M_S temperatures and values predicted by regression analysis of several modelling approaches.

mance of all the predictive models. It divides the dataset into 'K' (typically 5) equal-sized "folds". The model is then trained and tested 'K' times, always using a different fold as the test set while the others are used for training. This way it ensures that every experiment is used for both training and testing. The outcome is a more representative estimate of the models performance compared to a single train-test split. By averaging the results of multiple evaluations, K-fold cross-validation reduces the impact of the randomness inherent in a single train-test split.

The prediction results of the different algorithms used for modelling, after 5 splits and with a train-to-test ratio of 4:1, are listed in Table 5.1. RF and GBDT algorithms use 100 estimators. The results show that the B_S model has the highest prediction accuracy of 67.95% when modelled with the RF algorithm, followed by the GBDT algorithm prediction rate of 67.22%. Similarly, the best M_S models are the GBDT with 92.77% accuracy followed closely by RF with 92.27%. The excellent coefficient of determination indicates that the martensite transformation start temperature can be accurately predicted by the effective ensemble algorithms based on the existing data. It can be seen that the ensemble methods consistently perform better than the regression models based on all the different quality metrics. Through the results in Table 5.1, it is also seen that the prediction accuracy has big differences with regression models.

The R^2 value provides a measure of the goodness of fit, while RMSE and MAE offer information on the accuracy and magnitude of errors in the predictions. Except for the polynomial model, all the other models exhibit lower errors when predicting B_S. Instead, the R^2 is better when predicting M_S, except with the combined model where both fits are poorly predicted. The large difference in R^2 value can be accounted for several reasons. The B_S data might have a higher variability or noise. R^2 measures the proportion of variance in Bs that is explained by the chosen independent variables. Therefore, other data variables that can influence Bs are unaccounted for, which can lead to a lower R^2 value. This is the case of the cooling rate, which is known to influence the transformation start of bainite. Some of the experiments collected are from TTT diagrams, and not CCT diagrams, and therefore do not account for the cooling rate which turns out to be a key factor as well.

It should be noted that a basic requirement in ML modelling is that the training datasets need to be relatively large, allowing for sufficient partitioning into training and testing sets. A small training dataset can result in inaccurate predictions and unstable and biased models. The models are evaluated with

Table 5.1: Transformation temperatures model results according to R^2, RMSE and MAE

Algorithms	R^2	RMSE	MAE
Bs			
Linear model	0.5434	40.33	32.44
Polynomial model	-2.4528	106.82	60.05
Exponential model	0.5373	40.61	33.03
Combined model	0.4224	44.95	35.56
RF	0.6795	32.63	21.51
GBDT	0.6722	33.85	22.20
Ms			
Linear model	0.6618	77.86	57.83
Polynomial model	0.7806	61.97	40.10
Exponential model	0.6597	78.42	56.05
Combined model	0.3351	109.28	86.00
RF	0.9227	36.61	21.73
GBDT	0.9277	35.21	20.67

355 M_S datapoints, from which 284 are used for training and 71 for testing in each fold. A lower number of B_S observations are used, 164, of which 132 are used in training and 32 in testing. A smaller sample size often leads to a less precise estimate of the model performance, therefore impacting the R^2 value. On the other hand, the smaller sample size also leads to a lower magnitude of error, the reason behind the lower RMSE and MAE values in the models predicting the bainite start temperature.

Randomness is not an issue in the results, as the algorithm of K-fold cross-validation makes sure that all the datapoints are used at least once for training and testing. It is therefore interesting to see if these results are consistent across the different folds. Figure 5.9 displays the prediction results of B_S using the six models, where the five folds are represented separately. A similar representation is displayed in Figure 5.10 for the martensite start temperature.

Furthermore, Appendix A.5.6 displays a more extended visualization of the results, where each fold in every model is also displayed as a function of the six chemical components.

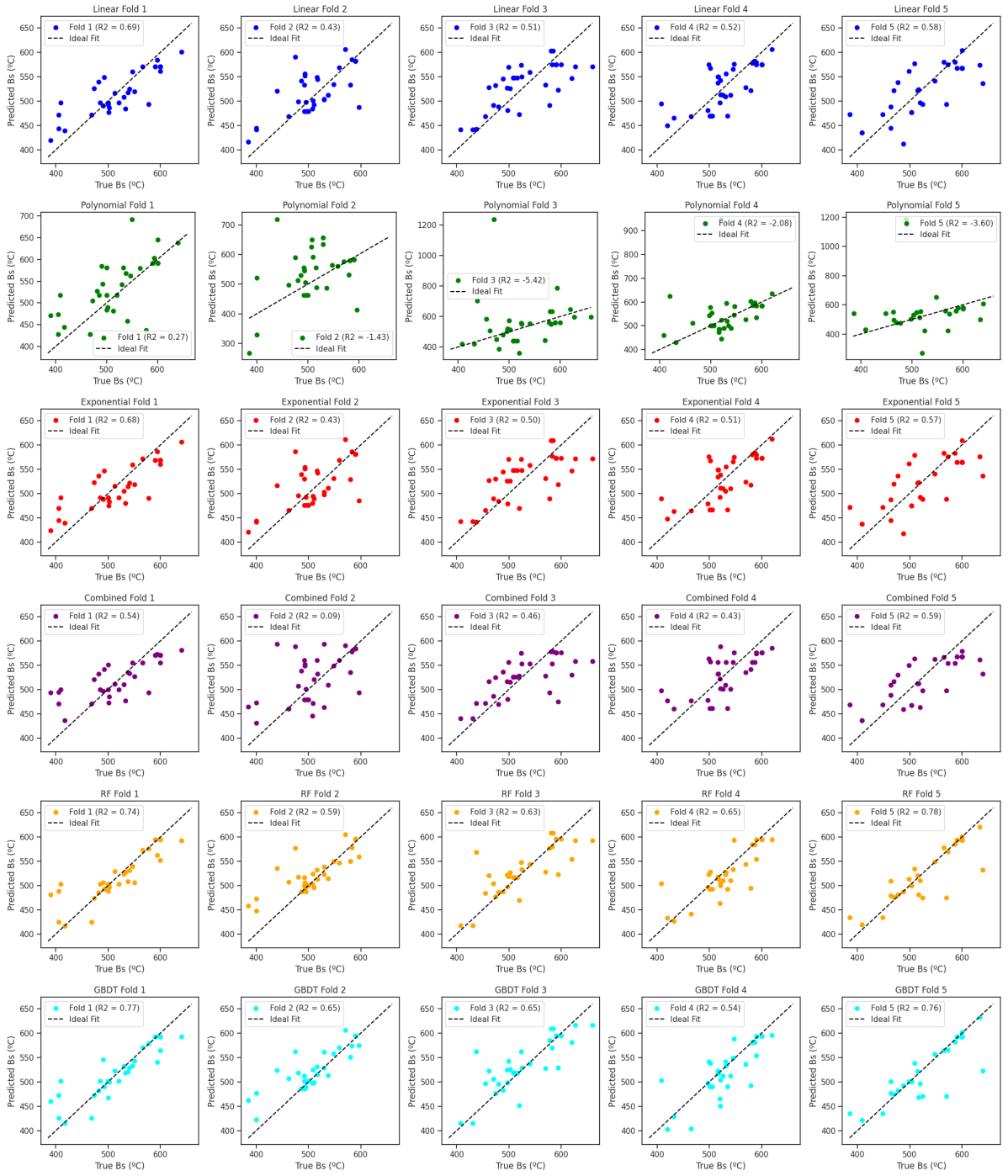

Figure 5.9: Prediction of B_S temperature using K-means cross-validation. The subplots include linear, polynomial, exponential, combined, RF and GBDT models.

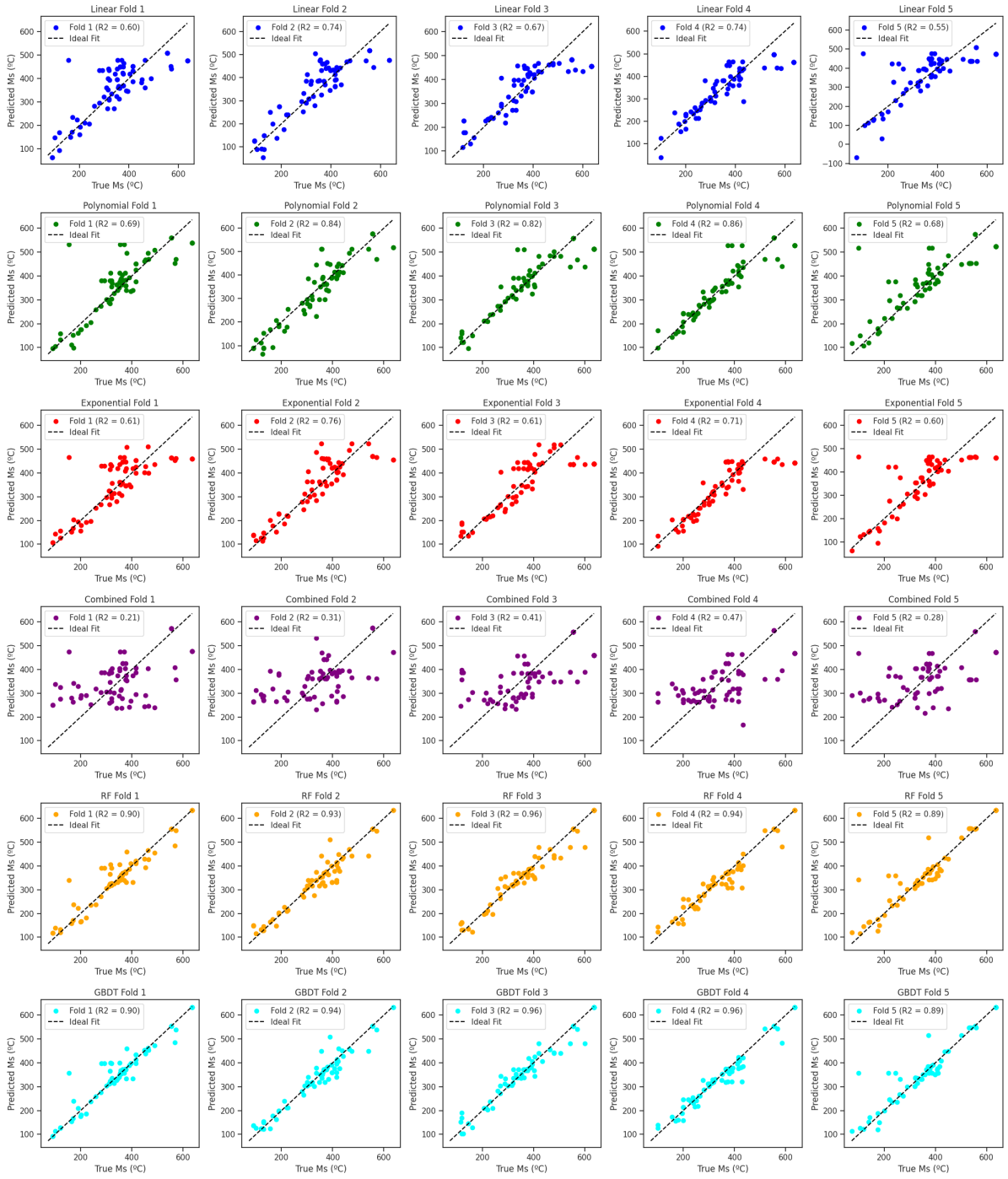

Figure 5.10: Prediction of M_S temperature using K-means cross-validation. The subplots include linear, polynomial, exponential, combined, RF and GBDT models.

The polynomial model employed for predicting the B_S temperature exhibits signs of overfitting, as evidenced by its suboptimal performance on new data. During the training phase, the model may have become overly complex, capturing mainly noise and random fluctuations in the data rather than detecting patterns. This has resulted in a lack of generalization to unseen data. Besides this model, the other ones are pretty predictive. The R^2 values across different folds exhibit some fluctuations, which can be expected and attributed to the limited number of data points available for training and evaluation. Despite the challenges that a small dataset size creates, the models are still able to learn underlying patterns in the data. By looking at the fitting, the models appear to be capturing meaningful patterns, showing some signs of learning that suggest that it is predicting on the right track.

Following, the modelling of the M_S temperature shows a similar behaviour, with better accuracy in the prediction. The polynomial and exponential models of M_S exhibit excellent prediction in high-C steels, with less precision in low-C steels. The RD and GBDT algorithms show outstanding results, which are both highly precise and consistent. However, the variance in some datapoints is pretty high across the six models. By closer examining them when representing the results as a function of the chemical components (A.18-A.23), it can be seen that in fact, it is always the same 2 datapoints that worsen the prediction. These experiments are in particular from steels with approximately 0.2%C and 3%Mn. They can be identified very well in Figure 5.11, as these two datapoints already stand out and do not follow the general pattern that the other experiments have.

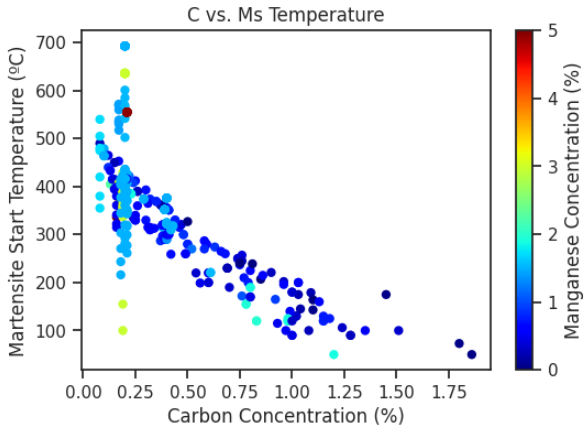

Figure 5.11: Martensite start temperature as a function of carbon and manganese content.

The variance between folds that these two experiments create is a clear indication that the dataset size is not enough. In situations where the data is robust and abundant, the presence of outliers typically has no impact on the model accuracy. However, in this dataset, the sensitivity to data fluctuations of just a couple of observations suggests that the model is highly dependent on the available data, making it susceptible to variations. This is a clear indication that the data is not good enough by itself to create a predictive model. Addressing this challenge would involve efforts to augment the dataset.

Besides the dataset size, it would be very interesting to study other parameters rather than only the chemical composition. The kinetics of phase transformation are influenced by other factors, such as the grain size or process parameters. In this project, the data is collected from experiments with different processing routes. A crucial factor in the kinetics of phase transformation during the cooling of steel alloys is the amount of dynamic recrystallization (DRX). DRX refers to the process by which grains nucleate and grow within a material while it is being deformed at elevated temperatures. The first effect of DRX is grain refining, which produces smaller, more equiaxed grains. This fine-grain structure has a significant impact on mechanical properties like strength, toughness, and hardness. Furthermore, the evolution of the microstructure is significantly influenced by the degree of DRX. The phase transitions that occur during subsequent cooling, which affect both mechanical and thermal properties, can be considerably influenced by a finer and more homogeneous microstructure. Additionally, DRX introduces a large number of nucleation sites for phase transformations, affecting the B_S and M_S temperatures. As a result of the different microstructure and particular crystallographic orientations, the kinetics of phase transformations also change, which affects how quickly various phases form and transform.

The experiments used during the collection of data involve samples that have been previously hot rolled, while others are simply cooled without hot deformation. Therefore, in the case of this dataset where experiments come from varying degrees of hot deformation and dynamic recrystallization, accounting for the amount of DRX is crucial. This supports the idea that a more detailed analysis of the hot rolling parameters would potentially be able to explain the obtained results during the modelling of the two-phase transformation temperatures.

6

Conclusions and Future Research

In this research, I have explored experimental data of different heat treatments yielding bainitic phase transformation in steel. The project has been separated into three main chapters, that follow the initial literature study. Firstly, data has been collected from different sources. This did come with a fair share of challenges. First of all, the data itself had to be obtained from public literature. Getting all data in a single form for comparison, editing and interpretation was a long process. The main issue in this process was to obtain comparable, quantitative data from experiments that were all different from each other, and that were provided in different formats, units and names. After pre-processing, the data file included 930 observations and 79 features.

Following, it was interesting to explore the potential that data collection from the literature has. A list of metallurgic accepted claims was elaborated. The aim was to investigate whether it is valid or not to reach judgments by simply collecting data across many experiments. Besides, this process would provide useful insight into the quality of the data, allowing us to learn if it is representative of the transformation process. If the data would not be representative, using the data to further develop models would not be valid. Furthermore, principal component analysis and clustering techniques have been used to understand the behaviour of the parameters and to identify the main patterns and the most important features.

The following conclusions can be drawn in the comparison between the collected data and published literature:

- The bainite and martensite temperatures have an exponential carbon dependence, and therefore nonlinear models are required to model them.
- Comparison between isothermal and two-stage bainitic transformations is not adequate, as they have different microstructural outcomes. It would be useful to have qualitative morphological information on each experiment, to understand the microstructure of the samples and how this influences on the mechanical properties.
- Aluminium effectively suppresses the cementite phase as silicon does but acts as a worse austenite stabilizer element. Silicon is a crucial element in preventing the cementite phase, and aluminium is only a great balancing supplement for this purpose. There are no mechanical properties or advantages when partially substituting silicon with aluminium.
- Molybdenum and chromium are not appropriate elements if the objective is to retain a high amount of austenite at room temperature. As strong carbide-forming elements, the strength values are enhanced by their formation of strong carbides. however, multiple additions of both elements do not display larger strength values. They provide an increased hardenability, due to the formation of hard, stable carbides. However, excessive carbide precipitation coarsens the microstructure and reduces the total hardness of the steel.

- Niobium, as a strong stabilizer element, decreases the fraction of ferrite. However, when an excessive amount of niobium is added, it combines with carbon and forms NbC, which acts as a nucleation site for ferrite formation and dramatically increases the fraction of this phase.
- Niobium can be avoided in molybdenum-containing steels if the application requires a high strength of the steel because the addition of Nb weakens the promotion function of Mo on bainite transformation.

The bainite (B_S) and martensite (M_S) start temperatures are critical parameters when designing high-performance steels and their heat treatments. It has been investigated the usage of ML to predict the B_S and M_S of steels based solely on their chemical composition. Their outliers have been evaluated and removed from the prediction model. A list of empirical equations from existing literature has been used to evaluate how the collected data performs with existing models. The results show that the B_S empirical relations fit poorly to the collected data. The polynomial model that predicts M_S works well with low-C steels while the same occurs with the exponential model in high-C steels.

Finally, machine learning modelling is performed using different regression techniques and supervised learning ensemble methods. Train-test split series are used to evaluate the models, and is found that the ensemble methods outperform the regression techniques. Cross-validation is used to support the consistency of each model. The RF and GBDT models provide excellent martensite start temperature predictions on the validation dataset with R^2 values of 0.92 and 0.93, RMSE of 37 and 35, and MAE of 22 and 21 respectively. For the B_S temperature, the prediction using RF and GBDT have an R^2 of 0.68 and 0.67, RMSE of 33 and 34, and MAE of 22 and 22.

The complexity of bainite transformation in comparison with the simpler transformation mechanism of martensite is a principal reason why M_S shows more accurate predictions. In addition, the larger number of experiments for M_S also adds up to larger R^2, RMSE and MAE values. The models appear to be capturing meaningful patterns, showing signs of learning suggesting that the prediction is in the correct direction. However, the impact that outliers have on the modelling results indicates that the data is not good enough by itself to create a predictive model. Finally, missing parameters during the modelling, like the amount of dynamic recrystallization or other parameters influencing the kinetics of bainite transformation, would be necessary to create a more developed model.

6.1. Future Research

As we navigate the limits of research in an increasingly digitized era, the classic idea of experimental work stands against a new environment where the combination of literature and data-driven approaches seems promising. In the past, research predominantly relied on experimental work; however, this exclusive dependence is no longer necessary. In this modern era, the combination of literature-driven insights and the vast array of experiments available online offer a new way to investigate.

A deep transformation is underway, marked by the influence of machine learning and artificial intelligence. These technologies, reliant on large amounts of data, appear in a paradigm where the creation of impactful models depends on the strategic use of data. Researchers find themselves with two ways to go - opting to generate data through sophisticated software simulations or using real-world datasets to fuel their investigations. The following paragraphs dig into a notable concern that has surfaced during this study, which has followed the second approach to create a model: the inconsistency in reported data across research papers. As a community, we face a collective challenge: the absence of a standardized format for presenting data, leading to potential gaps and difficulties in reproducibility.

I believe it is time for the research community to consider adopting a unified approach to data reporting. A suggested way for improvement involves establishing standardized formats for data representation, promoting reproducibility, and facilitating integration into emerging digital frameworks. The adoption of such criteria could significantly improve the accessibility and utility of research results.

Consider the usefulness of reporting data in widely recognized formats such as JSON (JavaScript Object Notation) files or employing databases that support computer systems in making use of infor-

mation. These formats are not only machine-readable but also lend themselves well to automated algorithms, a crucial aspect of the current digital landscape. By doing so, researchers can contribute not only to the knowledge within their papers but also to future investigation within the same field and a further away domain of data analytics. To encourage the general adoption of these standards, collaborative efforts within the academic community are needed. Journals, institutions and researchers can all incorporate and promote guidelines for data reporting of their findings, and not only sharing their findings but as well the dataset in these standardized formats.

These guidelines should be created through a collaborative process that includes proposals from experts across different fields. Conferences, workshops, and open forums might be used as discussion and revision forums for these guidelines. Online repositories or databases that are created particularly to host datasets in standardized formats would also help to build a community resource that encourages a culture of availability and repeatability. As a recap, the era of digitization presents us with an opportunity to reconsider and reshape how we publish and share our research data. By collectively welcoming standardized reporting formats, we can enhance the reproducibility of studies and promote future investigation.

Concerning the final ML predictor models created, the ensemble methods have proven that can be potentially great methods when predicting transformation temperatures, even though in this project they are not good enough by itself to create a predictive model. The model is agile, and can easily incorporate additional features as long as a more extensive database is developed. Future research could therefore incorporate features that are known to influence the kinetics of phase transformation, as can be morphological parameters such as the austenite grain size, or process parameters like the amount of dynamic recrystallization. Some parameters are more difficult to record, like the later that involves measurements at very high temperatures or with several deformation steps.

With a more extensive dataset, the importance of individual feature variables should be calculated. With many features available to be used in the prediction model, it is desirable to find the feature variables that are highly correlated with the target value and to guarantee the prediction accuracy by selecting as few features as possible. Therefore, calculating and ranking the importance of each feature should be done.

References

[1] A. Morita. *Aluminium alloys for automobile applications*. 6 vol. Proc. of ICAA, 1998.

[2] J Galán et al. “Advanced high strength steels for automotive industry”. In: *Revista de metalurgia* 48.2 (2012), p. 118.

[3] EJ Pavlina and CJ Van Tyne. “Correlation of yield strength and tensile strength with hardness for steels”. In: *Journal of materials engineering and performance* 17.6 (2008), pp. 888–893.

[4] Minghui Cai and Hongshuang Di. “Advanced High Strength Steels and Their Processes”. In: *Rolling of Advanced High Strength Steels: Theory, Simulation and Practice,* (2017), pp. 1–25.

[5] Kate Hickey. *3rd Generation Steels*. Sept. 2021. URL: https://ahssinsights.org/metallurgy/steel-grades/3rd-generation-steels/.

[6] Tadao Murata et al. “Characteristics of 1180 MPa grade cold-rolled steel sheets with excellent formability”. In: *Kobelco Technol. Rev* 45 (2017), pp. 17–20.

[7] Katharina Hausmann. “TRIP-assisted Thin Sheet Steel with a Bainitic and/or Martensitic Matrix”. PhD thesis. Technische Universität München, 2015.

[8] Rosalia Rementeria and Francisca G Caballero. “Cold Rolling and Annealing of Advanced High Strength Steels”. In: *Rolling of Advanced High Strength Steels*. CRC Press, 2017, pp. 482–521.

[9] DT Han et al. “The determining role of pre-annealing on Mn partitioning behavior in medium-Mn-TRIP steel: experimental and numerical simulation”. In: *Journal of Materials Science* 55.10 (2020), pp. 4437–4452.

[10] Z. Nishiyama. *Martensitic transformation: Introduction to martensite and Martensitic transformation*. last edited and published in 2012. Burlington: Elsevier Science, 1978.

[11] The Hand Book on Mechanical Maintenance. *I-T Diagram and Cooling Curves*. URL: https://practicalmaintenance.net/?p=1345.

[12] A. Kumar Gulapura. “Thermodynamic modelling of martensite start temperature in commercial steels”. PhD thesis. KTH ROYAL INSTITUTE OF TECHNOLOGY, 2017.

[13] G. Kurdjumow and G. Sachs. “Uber den Mechanismus der Stahlhartung”. In: *Zeitschrift fur Physik* 64.5-6 (May 1930), pp. 325–343. DOI: 10.1007/bf01397346. URL: http://dx.doi.org/10.1007/bf01397346.

[14] Z Nishiyama. “X-ray investigation of the mechanism of the transformation from face centered cubic lattice to body centered cubic”. In: *Sci. Rep. Tohoku Univ.* 23 (Jan. 1934), pp. 637–.

[15] E. C. Bain. “The nature of martensite”. In: (1924).

[16] D. S. Lieberman M. S. Wechsler and T. A. Read. “On the theory of formation of Martensite”. In: (197, 1953, 1503).

[17] J.S Bowles and J.K Mackenzie. “The crystallography of martensite transformations I”. In: *Acta Metallurgica* 2.1 (Jan. 1954), pp. 129–137. DOI: 10.1016/0001-6160(54)90102-9. URL: http://dx.doi.org/10.1016/0001-6160(54)90102-9.

[18] C.M. Wayman. “Crystallographic theories of martensitic transformations”. In: *Journal of the Less Common Metals* 28.1 (July 1972), pp. 97–105. DOI: 10.1016/0022-5088(72)90172-5. URL: http://dx.doi.org/10.1016/0022-5088(72)90172-5.

[19] Fady Archie et al. *Damage nucleation in DP-steels: experimental characterization of the contributing microstructural parameters*. Tech. rep. Fachgruppe für Materialwissenschaft und Werkstofftechnik, 2018.

[20] P. M. Kelly. “”Crystallography of martensite transformations in steels,” in Phase transformations in steels Volume 2: Diffusionless transformations, high strength steels, modelling and advanced analytical techniques”. In: *Applied Physics Letters* 2 (2012), pp. 3–33.

[21] I. R. Aseguinolaza et al. “Transformation volume strain in Ni-Mn-Ga thin films”. In: *Applied Physics Letters* 101.24 (Dec. 2012), p. 241912. DOI: 10.1063/1.4772005. URL: http://dx.doi.org/10.1063/1.4772005.

[22] A.L. Roitburd. “Martensitic Transformation as a Typical Phase Transformation in Solids”. In: *Solid State Physics* (1978), pp. 317–390. DOI: 10.1016/s0081-1947(08)60471-3. URL: http://dx.doi.org/10.1016/s0081-1947(08)60471-3.

[23] Troiano. A. R. Greninger. A. B. “On the theory of formation of Martensite”. In: (1949, 185, pp 590).

[24] Ming-Xing Zhang and Patrick M. Kelly. “Crystallographic features of phase transformations in solids”. In: *Progress in Materials Science* 54.8 (Nov. 2009), pp. 1101–1170. DOI: 10.1016/j.pmatsci.2009.06.001. URL: http://dx.doi.org/10.1016/j.pmatsci.2009.06.001.

[25] H.K.D.H. Bhadeshia. “A rationalisation of shear transformations in steels”. In: *Acta Metallurgica* 29.6 (June 1981), pp. 1117–1130. DOI: 10.1016/0001-6160(81)90063-8. URL: http://dx.doi.org/10.1016/0001-6160(81)90063-8.

[26] M. Hillert, L. Höglund, and J. Ågren. “Role of carbon and alloying elements in the formation of bainitic ferrite”. In: *Metallurgical and Materials Transactions A* 35.12 (Dec. 2004), pp. 3693–3700. DOI: 10.1007/s11661-004-0275-5. URL: http://dx.doi.org/10.1007/s11661-004-0275-5.

[27] E. S. Davenport and E. C. Bain. “Transformation of austenite at constant subcritical temperatures”. In: *Metallurgical and Materials Transactions B* 1.12 (Dec. 1970), pp. 3503–3530. DOI: 10.1007/bf03037892. URL: http://dx.doi.org/10.1007/bf03037892.

[28] LCD Fielding. “The bainite controversy”. In: *Materials Science and Technology* 29.4 (2013), pp. 383–399.

[29] G.R Purdy and M Hillert. “Overview no. 38: On the nature of the bainite transformation in steels”. In: *Acta Metallurgica* 32.6 (June 1984), pp. 823–828. DOI: 10.1016/0001-6160(84)90018-x. URL: http://dx.doi.org/10.1016/0001-6160(84)90018-x.

[30] M Hillert. “The growth of ferrite, bainite and martensite”. In: *Report, Swedish Inst. Metal Res. Stockholm* (1960), pp. 113–58.

[31] Co Laird and HI Aaronson. “The dislocation structures of the broad faces of widmanstätten γ plates in an Al-15% Ag alloy”. In: *Acta Metallurgica* 15.1 (1967), pp. 73–103.

[32] M. Takahashi and H. K. D. H. Bhadeshia. “Model for transition from upper to lower bainite”. In: *Materials Science and Technology* 6.7 (July 1990), pp. 592–603. DOI: 10.1179/mst.1990.6.7.592. URL: http://dx.doi.org/10.1179/mst.1990.6.7.592.

[33] Haijiang Hu et al. “Effect of temperature, carbon content and crystallography on the lengthening kinetics of bainitic ferrite laths”. In: *Materials Characterization* 187 (May 2022), p. 111860. DOI: 10.1016/j.matchar.2022.111860. URL: http://dx.doi.org/10.1016/j.matchar.2022.111860.

[34] R. F. Hehemann, K. R. Kinsman, and H. I. Aaronson. “A debate on the bainite reaction”. In: *Metallurgical Transactions* 3.5 (May 1972), pp. 1077–1094. DOI: 10.1007/bf02642439. URL: http://dx.doi.org/10.1007/bf02642439.

[35] Clarence Zener. “Kinetics of the decomposition of austenite”. In: *Trans. Aime* 167 (1946), pp. 550–595.

[36] Annika Borgenstam, Mats Hillert, and John Ågren. “Metallographic evidence of carbon diffusion in the growth of bainite”. In: *Acta Materialia* 57.11 (June 2009), pp. 3242–3252. DOI: 10.1016/j.actamat.2009.03.026. URL: http://dx.doi.org/10.1016/j.actamat.2009.03.026.

[37] W. T. Reynolds et al. “An investigation of the generality of incomplete transformation to bainite in Fe-C-X alloys”. In: *Metallurgical Transactions A* 21.6 (June 1990), pp. 1479–1491. DOI: 10.1007/bf02672563. URL: http://dx.doi.org/10.1007/bf02672563.

[38] M. Takahashi and H. K. D. H. Bhadeshia. “A Model for the Microstructure of Some Advanced Bainitic Steels”. In: *Materials Transactions, JIM* 32.8 (1991), pp. 689–696. DOI: 10.2320/matertrans1989.32.689. URL: http://dx.doi.org/10.2320/matertrans1989.32.689.

[39] SJ Matas and RF Hehemann. “The structure of bainite in hypoeutectoid steels”. In: *Transactions of the Metallurgical Society of AIME* 221.1 (1961), pp. 179–185.

[40] P.J. Jacques. “Transformation-induced plasticity for high strength formable steels”. In: *Current Opinion in Solid State and Materials Science* 8.3-4 (June 2004), pp. 259–265. DOI: 10.1016/j.cossms.2004.09.006. URL: http://dx.doi.org/10.1016/j.cossms.2004.09.006.

[41] P. J. Jacques et al. “The Developments of Cold-rolled TRIP-assisted Multiphase Steels. Low Silicon TRIP-assisted Multiphase Steels.” In: *ISIJ International* 41.9 (2001), pp. 1061–1067. DOI: 10.2355/isijinternational.41.1061. URL: http://dx.doi.org/10.2355/isijinternational.41.1061.

[42] X. Vanden Eynde, J. P. Servais, and M. Lamberigts. “Investigation into the surface selective oxidation of dual-phase steels by XPS, SAM and SIMS”. In: *Surface and Interface Analysis* 35.12 (2003), pp. 1004–1014. DOI: 10.1002/sia.1639. URL: http://dx.doi.org/10.1002/sia.1639.

[43] P. J. Jacques et al. “The Developments of Cold-rolled TRIP-assisted Multiphase Steels. Al-alloyed TRIP-assisted Multiphase Steels.” In: *ISIJ International* 41.9 (2001), pp. 1068–1074. DOI: 10.2355/isijinternational.41.1068. URL: http://dx.doi.org/10.2355/isijinternational.41.1068.

[44] Etienne Girault et al. “Comparison of the effects of silicon and aluminium on the tensile behaviour of multiphase TRIP-assisted steels”. In: *Scripta Materialia* 44.6 (Apr. 2001), pp. 885–892. DOI: 10.1016/s1359-6462(00)00697-7. URL: http://dx.doi.org/10.1016/s1359-6462(00)00697-7.

[45] M. De Meyer, D. Vanderschueren, and B. C. De Cooman. “The Influence of the Substitution of Si by Al on the Properties of Cold Rolled C-Mn-Si TRIP Steels.” In: *ISIJ International* 39.8 (1999), pp. 813–822. DOI: 10.2355/isijinternational.39.813. URL: http://dx.doi.org/10.2355/isijinternational.39.813.

[46] Sandra Traint et al. “Influence of silicon, aluminium, phosphorus and copper on the phase transformations of low alloyed TRIP-steels”. In: *Steel Research* 73.6-7 (June 2002), pp. 259–266. DOI: 10.1002/srin.200200206. URL: http://dx.doi.org/10.1002/srin.200200206.

[47] H. C. Chen, H. Era, and M. Shimizu. “Effect of phosphorus on the formation of retained austenite and mechanical properties in Si-containing low-carbon steel sheet”. In: *Metallurgical Transactions A* 20.3 (Mar. 1989), pp. 437–445. DOI: 10.1007/bf02653923. URL: http://dx.doi.org/10.1007/bf02653923.

[48] Yasuharu Sakuma, David K. Matlock, and George Krauss. “Intercritically annealed and isothermally transformed 0.15 Pct C steels containing 1.2 Pct Si-1.5 Pct Mn and 4 Pct Ni: Part I. transformation, microstructure, and room-temperature mechanical properties”. In: *Metallurgical Transactions A* 23.4 (Apr. 1992), pp. 1221–1232. DOI: 10.1007/bf02665053. URL: http://dx.doi.org/10.1007/bf02665053.

[49] P. J. Jacques. “Experimental investigation of the influence of the austenite grain size on the mechanism and kinetics of the bainite transformation in steels”. In: *Journal de Physique IV (Proceedings)* 112 (Oct. 2003), pp. 297–300. DOI: 10.1051/jp4:2003887. URL: http://dx.doi.org/10.1051/jp4:2003887.

[50] Stéphane Godet et al. “Critical Assessment of the Bainite Transformation of Finely Grained and Deformed Austenite”. In: *Materials Science Forum* 426 (Aug. 2003), pp. 1433–1438. DOI: 10.4028/www.scientific.net/msf.426-432.1433. URL: http://dx.doi.org/10.4028/www.scientific.net/msf.426-432.1433.

[51] P. Jacques et al. “On the sources of work hardening in multiphase steels assisted by transformation-induced plasticity”. In: *Philosophical Magazine A* 81.7 (July 2001), pp. 1789–1812. DOI: 10.1080/01418610108216637. URL: http://dx.doi.org/10.1080/01418610108216637.

[52] Q. Furnémont et al. “Critical Assessment of the Micromechanical Behaviour of Dual Phase and Trip-Assisted Multiphase Steels”. In: *Canadian Metallurgical Quarterly* 43.1 (Jan. 2004), pp. 35–42. DOI: 10.1179/cmq.2004.43.1.35. URL: http://dx.doi.org/10.1179/cmq.2004.43.1.35.

[53] P. J. Jacques, F. Delannay, and J. Ladrière. “On the influence of interactions between phases on the mechanical stability of retained austenite in transformation-induced plasticity multiphase steels”. In: *Metallurgical and Materials Transactions A* 32.11 (Nov. 2001), pp. 2759–2768. DOI: 10.1007/s11661-001-1027-4. URL: http://dx.doi.org/10.1007/s11661-001-1027-4.

[54] Akihiko NAGASAKA et al. “Effects of warm forming on stretch-flangeability of a TRIP-aided dual-phase sheet steel”. In: *Tetsu-to-Hagané* 83.5 (1997), pp. 335–340.

[55] K Hausmann et al. “Trip-aided bainitic-ferritic sheet steel: A critical assessment of alloy design and heat treatment”. In: *MS&T’13* (2013), pp. 209–218.

[56] T. Sourmail et al. “The Influence of Vanadium on Ferrite and Bainite Formation in a Medium Carbon Steel”. In: *Metallurgical and Materials Transactions A* 48.9 (July 2017), pp. 3985–3996. DOI: 10.1007/s11661-017-4188-5. URL: http://dx.doi.org/10.1007/s11661-017-4188-5.

[57] Koh-ichi Sugimoto et al. “Ductility of 0.1-0.6 C-1.5 Si-1.5 Mn ultra high-strength TRIP-aided sheet steels with bainitic ferrite matrix”. In: *ISIJ international* 44.9 (2004), pp. 1608–1614.

[58] F.G. Caballero et al. “Design of cold rolled and continuous annealed carbide-free bainitic steels for automotive application”. In: *Materials amp; Design* 49 (Aug. 2013), pp. 667–680. DOI: 10.1016/j.matdes.2013.02.046. URL: http://dx.doi.org/10.1016/j.matdes.2013.02.046.

[59] H-D Wu et al. “Incomplete bainite transformation in Fe-Si-C alloys”. In: *Acta Materialia* 133 (2017), pp. 1–9.

[60] WT Reynolds et al. “The incomplete transformation phenomenon in Fe-C-Mo alloys”. In: *Metallurgical Transactions A* 21 (1990), pp. 1433–1463.

[61] Goro Miyamoto, Kentaro Yokoyama, and Tadashi Furuhara. “Quantitative analysis of Mo solute drag effect on ferrite and bainite transformations in Fe-0.4 C-0.5 Mo alloy”. In: *Acta Materialia* 177 (2019), pp. 187–197.

[62] F.-C. An et al. “Incompleteness of bainite transformation in quenched and tempered steel under continuous cooling conditions”. In: *Journal of Materials Research and Technology* 9.4 (July 2020), pp. 8985–8996. DOI: 10.1016/j.jmrt.2020.06.039. URL: http://dx.doi.org/10.1016/j.jmrt.2020.06.039.

[63] C Gupta et al. “A study of bainite transformation in a new CrMoV steel under continuous cooling conditions”. In: *Scripta materialia* 53.5 (2005), pp. 559–564.

[64] S Reisinger et al. “Strain energy contributions on the bainitic phase transformation in a CrMoV steel during continuous cooling”. In: *Materials & Design* 155 (2018), pp. 475–484.

[65] N Takayama, G Miyamoto, and T Furuhara. “Chemistry and three-dimensional morphology of martensite-austenite constituent in the bainite structure of low-carbon low-alloy steels”. In: *Acta Materialia* 145 (2018), pp. 154–164.

[66] ZX Qiao et al. “Incompleted bainitic transformation characteristics in an isochronally annealed 30CrNi3MoV steel”. In: *Journal of alloys and compounds* 478.1-2 (2009), pp. 334–340.

[67] HI Aaronson and HA Domian. “Partition of alloying elements between austenite and proeutectoid ferrite or bainite”. In: *AIME MET SOC TRANS* 236.5 (1966), pp. 781–796.

[68] M Enomoto and HI Aaronson. “Nucleation kinetics of proeutectoid ferrite at austenite grain boundaries in Fe-CX alloys”. In: *Metallurgical Transactions A* 17 (1986), pp. 1385–1397.

[69] GJ Shiflet and HI Aaronson. “Growth and overall transformation kinetics above the bay temperature in Fe-C-Mo alloys”. In: *Metallurgical Transactions A* 21 (1990), pp. 1413–1432.

[70] FG Caballero et al. “Very strong low temperature bainite”. In: *Materials science and technology* 18.3 (2002), pp. 279–284.

[71] Carlos GARCIA-MATEO and FG Caballero. “Ultra-high-strength bainitic steels”. In: *ISIJ international* 45.11 (2005), pp. 1736–1740.

[72] Carlos Garcia-Mateo, Caballero FG, and Bhadeshia HKDH. “Development of hard bainite”. In: *ISIJ international* 43.8 (2003), pp. 1238–1243.

[73] FG Caballero and HKDH Bhadeshia. “Very strong bainite”. In: *Current opinion in solid state and materials science* 8.3-4 (2004), pp. 251–257.

[74] F. Caballero. *Design of Novel Bainitic Steels: Moving from UltraFine to Nanoscale Structures*. Mar. 2014. URL: https://link.springer.com/article/10.1007/s11837-014-0908-0?error=cookies_not_supported&code=f5afb862-2260-4869-814b-96b65d0a7779.

[75] Carlos Garcia-Mateo et al. “Nanostructured steel industrialisation: plausible reality”. In: *Materials Science and Technology* 30.9 (May 2014), pp. 1071–1078. DOI: 10.1179/1743284713y.0000000428. URL: https://www.tandfonline.com/doi/pdf/10.1179/1743284713Y.0000000428?needAccess=true.

[76] FG Caballero et al. “Design of novel high strength bainitic steels: Part 1”. In: *Materials Science and Technology* 17.5 (2001), pp. 512–516.

[77] Carl Kusche et al. “Large-area, high-resolution characterisation and classification of damage mechanisms in dual-phase steel using deep learning”. In: *PLOS ONE* 14.5 (May 2019), e0216493. DOI: 10.1371/journal.pone.0216493. URL: http://dx.doi.org/10.1371/journal.pone.0216493.

[78] Xiaoya Huang et al. “A combined machine learning model for the prediction of time-temperature-transformation diagrams of high-alloy steels”. In: *Journal of Alloys and Compounds* 823 (2020), p. 153694.

[79] Physics Stack Exchange. *Is cooling really exponential?* URL: https://physics.stackexchange.com/questions/100775/is-cooling-really-exponential.

[80] John E. Hunter and Frank L. Schmidt. *Methods of Meta-Analysis: Correcting error and bias in research findings*. Jan. 2015. DOI: 10.4135/9781483398105. URL: https://doi.org/10.4135/9781483398105.

[81] National Center for Biotechnology Information. *Meta-analysis in medical research*. Dec. 2010. URL: https://pubmed.ncbi.nlm.nih.gov/21487488/.

[82] Christopher Hansen, Holger Steinmetz, and Joern Block. “How to conduct a meta-analysis in eight steps: a practical guide”. In: *Management review quarterly* 72.1 (Nov. 2021), pp. 1–19. DOI: 10.1007/s11301-021-00247-4. URL: https://doi.org/10.1007/s11301-021-00247-4.

[83] Michael B. Harari et al. “Literature searches in systematic reviews and meta-analyses: A review, evaluation, and recommendations”. In: *Journal of Vocational Behavior* 118 (Apr. 2020), p. 103377. DOI: 10.1016/j.jvb.2020.103377. URL: https://doi.org/10.1016/j.jvb.2020.103377.

[84] Michael Gusenbauer and Neal R. Haddaway. “Which academic search systems are suitable for systematic reviews or meta□analyses? Evaluating retrieval qualities of Google Scholar, PubMed, and 26 other resources”. In: *Research Synthesis Methods* 11.2 (Jan. 2020), pp. 181–217. DOI: 10.1002/jrsm.1378. URL: https://doi.org/10.1002/jrsm.1378.

[85] Sascha Kraus, Matthias Breier, and Sonia Dasí-Rodríguez. “The art of crafting a systematic literature review in entrepreneurship research”. In: *International Entrepreneurship and Management Journal* 16.3 (Feb. 2020), pp. 1023–1042. DOI: 10.1007/s11365-020-00635-4. URL: https://doi.org/10.1007/s11365-020-00635-4.

[86] S.M.C. Van Bohemen. “Bainite and martensite start temperature calculated with exponential carbon dependence”. In: *Materials Science and Technology* 28.4 (Apr. 2012), pp. 487–495. DOI: 10.1179/1743284711y.0000000097. URL: https://doi.org/10.1179/1743284711y.0000000097.

[87] W Steven. “The Temperature of Martensite and Bainite in Low-alloy Steels”. In: *Journal of the Iron and Steel Institute* 183 (1956), pp. 349–359.

[88] Mateusz Morawiec et al. “Effect of Mn on the chemical driving force and bainite transformation kinetics in medium-manganese alloys”. In: *Journal of Thermal Analysis and Calorimetry* 148.4 (Oct. 2022), pp. 1567–1576. DOI: 10.1007/s10973-022-11664-2. URL: https://doi.org/10.1007/s10973-022-11664-2.

[89] Mateusz Morawiec et al. “Dilatometric study of the phase transformations under conditions of recrystallized and non-recrystallized austenite in 3Mn–1.5Al steel”. In: *Journal of Thermal Analysis and Calorimetry* 147.2 (Dec. 2020), pp. 1115–1124. DOI: 10.1007/s10973-020-10409-3. URL: https://doi.org/10.1007/s10973-020-10409-3.

[90] Jer-Ren Yang et al. “Mechanical Stabilization of Austenite against Bainitic Reaction in Fe-Mn-Si-C Bainitic Steel”. In: *Materials Transactions Jim* 37.4 (Jan. 1996), pp. 579–585. DOI: 10.2320/matertrans1989.37.579. URL: https://doi.org/10.2320/matertrans1989.37.579.

[91] Yuki Toji, Hiroshi Matsuda, and Dierk Raabe. “Effect of Si on the acceleration of bainite transformation by pre-existing martensite”. In: *Acta Materialia* 116 (Sept. 2016), pp. 250–262. DOI: 10.1016/j.actamat.2016.06.044. URL: https://doi.org/10.1016/j.actamat.2016.06.044.

[92] Jiali Zhao et al. “Transformation behavior and microstructure feature of large strain ausformed low-temperature bainite in a medium C - Si rich alloy steel”. In: *Materials Science and Engineering A-structural Materials Properties Microstructure and Processing* 682 (Jan. 2017), pp. 527–534. DOI: 10.1016/j.msea.2016.11.073. URL: https://doi.org/10.1016/j.msea.2016.11.073.

[93] Yangni Liu et al. “The effect of element characteristics on bainite transformation start temperature using a machine learning approach”. In: *Journal of Materials Science* 58.1 (Jan. 2023), pp. 443–456. DOI: 10.1007/s10853-022-08035-5. URL: https://doi.org/10.1007/s10853-022-08035-5.

[94] Bruno Buchmayr. “Critical Assessment 22: bainitic forging steels”. In: *Materials Science and Technology* 32.6 (Apr. 2016), pp. 517–522. DOI: 10.1080/02670836.2015.1114272. URL: https://doi.org/10.1080/02670836.2015.1114272.

[95] Harshad Kumar Dharamshi Hansraj Bhadeshia and JW Christian. “Bainite in steels”. In: *Metallurgical transactions A* 21 (1990), pp. 767–797.

[96] HKDH Bhadeshia and DV Edmonds. “The bainite transformation in a silicon steel”. In: *Metallurgical Transactions A* 10 (1979), pp. 895–907.

[97] S Traint et al. “Mechanical properties and phase transformations of an aluminum alloyed TRIP-steel”. In: *MECHANICAL WORKING AND STEEL PROCESSING CONFERENCE PROCEEDINGS*. Vol. 39. 2001, pp. 449–468.

[98] R Langeborg, O Sandberg, and W Roberts. “Fundamentals of Microalloying Forging Steels”. In: *Krauss, G., Banerji, SK, Eds* (1986), pp. 39–54.

[99] Björn Uhrenius. “Hardenability Concepts with Applications to Steel”. In: *TMS-AIME, Warrendale, PA* 28 (1978).

[100] JS Kirkaldy. *Hardenability Concepts with Applications to Steel: Symposium, 1977, Chicago: Proceedings*. Metallurgical Society of AIME, 1978.

[101] W. Reynolds. *An investigation of the generality of incomplete transformation to bainite in Fe-C-X alloys*. June 1990. URL: https://link.springer.com/article/10.1007/BF02672563?error=cookies_not_supported&code=a855856c-fd91-4ae4-b40a-f04d3dda5879.

[102] Christoph Alexander Keul, Vera Wirths, and Wolfgang Bleck. “New bainitic steels for forgings”. In: *Archives of Civil and Mechanical Engineering* 12.2 (June 2012), pp. 119–125. DOI: 10.1016/j.acme.2012.04.012. URL: https://doi.org/10.1016/j.acme.2012.04.012.

[103] Koh Ichi Sugimoto et al. “Effects of Cr and Mo on mechanical properties of Hot-Forged Medium Carbon TRIP-Aided bainitic ferrite steels”. In: *Metals* 9.10 (Sept. 2019), p. 1066. DOI: 10.3390/met9101066. URL: https://doi.org/10.3390/met9101066.

[104] Emmanuel De Moor. *Advanced High-Strength Sheet Steels for automotive applications*. Dec. 2020, pp. 113–151. DOI: 10.1007/978-3-030-53825-5\{_}4. URL: https://doi.org/10.1007/978-3-030-53825-5_4.

[105] Koh-Ichi Sugimoto, Muneo Murata, and Sung-Moo Song. “Formability of Al–Nb Bearing Ultra High-strength TRIP-aided Sheet Steels with Bainitic Ferrite and/or Martensite Matrix”. In: *Isij International* 50.1 (Jan. 2010), pp. 162–168. DOI: 10.2355/isijinternational.50.162. URL: https://doi.org/10.2355/isijinternational.50.162.

[106] Sangeeta Khare, Kyooyoung Lee, and H. K. D. H. Bhadeshia. “Relative effects of Mo and B on ferrite and bainite kinetics in strong steels”. In: *International Journal of Materials Research* 100.11 (Nov. 2009), pp. 1513–1520. DOI: 10.3139/146.110222. URL: https://doi.org/10.3139/146.110222.

[107] Henry Hu et al. “The effects of Nb and Mo addition on transformation and properties in low carbon bainitic steels”. In: *Materials Design* 84 (Nov. 2015), pp. 95–99. DOI: 10.1016/j.matdes.2015.06.133. URL: https://doi.org/10.1016/j.matdes.2015.06.133.

[108] KW Andrews. “Empirical formulae for the calculation of some transformation temperatures”. In: *J. Iron Steel Inst.* (1965), pp. 721–727.

[109] HKDH Bhadeshia and DV Edmonds. “The bainite transformation in a silicon steel”. In: *Metallurgical Transactions A* 10 (1979), pp. 895–907.

[110] HKDH Bhadeshia and DV Edmonds. “Bainite in silicon steels: New composition–property approach Part 1”. In: *Metal Science* 17.9 (1983), pp. 411–419.

[111] Ichiro Tsukatani, Shun’ichi Hashimoto, and Tsuyoshi Inoue. “Effects of silicon and manganese addition on mechanical properties of high-strength hot-rolled sheet steel containing retained austenite”. In: *ISIJ International* 31.9 (1991), pp. 992–1000.

[112] Osamu Matsumura et al. “Effect of retained austenite on formability of high strength sheet steels”. In: *ISIJ international* 32.10 (1992), pp. 1110–1116.

[113] Atsushi Itami, Manabu Takahashi, and Kosaku Ushioda. “Plastic stability of retained austenite in the cold-rolled 0.14% C-1.9% Si-1.7% Mn sheet steel”. In: *Isij International* 35.9 (1995), pp. 1121–1127.

[114] Francisca G. Caballero et al. “Atomic scale observations of bainite transformation in a high carbon high silicon steel”. In: *Acta Materialia* 55.1 (Jan. 2007), pp. 381–390. DOI: 10.1016/j.actamat.2006.08.033. URL: https://doi.org/10.1016/j.actamat.2006.08.033.

[115] John G. Speer et al. “Partitioning of carbon from supersaturated plates of ferrite, with application to steel processing and fundamentals of the bainite transformation”. In: *Current Opinion in Solid State Materials Science* 8.3-4 (June 2004), pp. 219–237. DOI: 10.1016/j.cossms.2004.09.003. URL: https://doi.org/10.1016/j.cossms.2004.09.003.

[116] PJ Brofman and GS Ansell. “On the effect of fine grain size on the M s temperature in Fe-27Ni-0.025 C alloys”. In: *Metallurgical transactions A* 14 (1983), pp. 1929–1931.

[117] A García-Junceda et al. “Dependence of martensite start temperature on fine austenite grain size”. In: *Scripta Materialia* 58.2 (2008), pp. 134–137.

[118] SMC Van Bohemen and J Sietsma. “Martensite formation in partially and fully austenitic plain carbon steels”. In: *Metallurgical and Materials Transactions A* 40 (2009), pp. 1059–1068.

[119] Singon Kang, Suchul Yoon, and Seok-Jae Lee. “Prediction of Bainite Start Temperature in Alloy Steels with Different Grain Sizes”. In: *Isij International* 54.4 (Jan. 2014), pp. 997–999. DOI: 10.2355/isijinternational.54.997. URL: https://doi.org/10.2355/isijinternational.54.997.

[120] John G. Speer et al. “Partitioning of carbon from supersaturated plates of ferrite, with application to steel processing and fundamentals of the bainite transformation”. In: *Current Opinion in Solid State Materials Science* 8.3-4 (June 2004), pp. 219–237. DOI: 10.1016/j.cossms.2004.09.003. URL: https://doi.org/10.1016/j.cossms.2004.09.003.

[121] Yuanjie Zhi et al. “Prediction and knowledge mining of outdoor atmospheric corrosion rates of low alloy steels based on the random Forests approach”. In: *Metals* 9.3 (Mar. 2019), p. 383. DOI: 10.3390/met9030383. URL: https://doi.org/10.3390/met9030383.

[122] Shin-Hyung Song. “Random Forest Approach in Modeling the Flow Stress of 304 Stainless Steel during Deformation at 700 °C–900 °C”. In: *Materials* 14.7 (Apr. 2021), p. 1812. DOI: 10.3390/ma14071812. URL: https://doi.org/10.3390/ma14071812.

[123] Leo Breiman. “Bagging predictors”. In: *Machine learning* 24 (1996), pp. 123–140.

[124] Ankit Rohatgi. *Webplotdigitizer: Version 4.6*. 2022. URL: https://automeris.io/WebPlotDigitizer.

[125] Hervé Abdi and Lynne J Williams. “Principal component analysis”. In: *Wiley interdisciplinary reviews: computational statistics* 2.4 (2010), pp. 433–459.

[126] Samson Abramsky. *Principles of Data Mining*. 2007.

[127] Ian T Jolliffe. *Principal component analysis for special types of data*. Springer, 2002.

[128] Leo Breiman. “Random forests”. In: *Machine learning* 45 (2001), pp. 5–32.

[129] Angshuman Paul et al. “Calculation of phase fraction in steel microstructure images using random forest classifier”. In: *Iet Image Processing* 12.8 (Aug. 2018), pp. 1370–1377. DOI: 10.1049/iet-ipr.2017.1154. URL: https://doi.org/10.1049/iet-ipr.2017.1154.

[130] Angshuman Paul et al. “Calculation of phase fraction in steel microstructure images using random forest classifier”. In: *Iet Image Processing* 12.8 (Aug. 2018), pp. 1370–1377. DOI: 10.1049/iet-ipr.2017.1154. URL: https://doi.org/10.1049/iet-ipr.2017.1154.

A

Appendix

A.1. Data Collection

As pictured in the diagram in Figure A.1, data collection and pre-processing are the initial and most significant steps in the ML pipeline. Without data, machine learning does not exist. Data allows us to build predictive models using trends. Recorded data from past experiments is what emerges patterns that can be predicted over time.

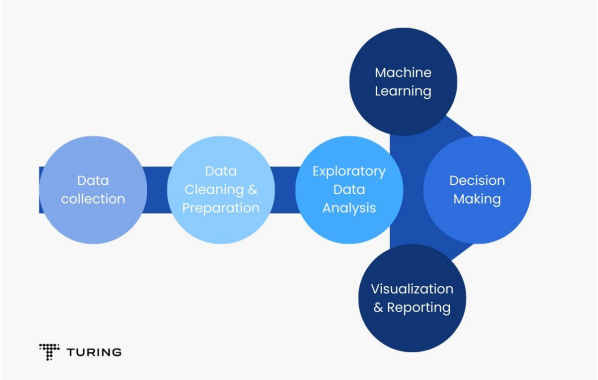

Figure A.1: Basic workflow for machine learning simulation.

The dataset used in this study is created using various resources, mainly based on experimental data from available literature. This includes a wide scope of studies, ranging from experiments that study the effects of chemical components on the driving force for bainite formation, to dilatometric studies of phase transformations or the effects of cooling rate on the microstructure and mechanical properties.

In addition, some studies determining CCT diagrams via thermal analysis have also been used, which offer valuable insights into steel behaviour under varying temperature conditions for a given composition. Since CCT diagrams are graphic illustrations, a semi-automated approach has been employed to facilitate the assimilation of graphical data. The WebPlotDigitizer tool helped make the procedure quite simple, converting visual representations into a structured dataset of time-temperature data points. This digitization not only simplified the extraction but also enhanced the precision of the dataset [124]. Where the time was expressed in logarithmic form, the cooling rate (CR) can be transformed according to Eq. A.1.

$$CR = \frac{Ac3 - T}{t} \tag{A.1}$$

When the data has been collected, different types of problems can be encountered, which are handled during the cleaning of the data. Some common examples involved in data cleaning are the fixing of structural errors, the handling of missing data, the removal of unwanted observations or variables, and the managing of unwanted outliers.

A.2. Correlation matrix

A correlation matrix provides a different visual representation of the relationships between selected variables in a dataset. It gives an in-depth overview of the pairwise correlations between each factor, underlining their strength and direction. Computing the correlation coefficients is very straightforward. After the data treatment is successfully performed, the correlation coefficients are computed and automatically arranged in a matrix structure, with each variable in rows and columns.

For a better visualization of the data, it is again possible to select which variables to represent on the x-axis and which in the y-axis. Then, the *seaborn* library has a module to visualize a correlation matrix, the heatmap. Each cell in the matrix is assigned a colour that represents the strength (colour intensity) and direction of the correlation, with a gradient from colder colours (blue) for negative correlations, to warmer colours (red) for positive. It is possible to leave empty (in white) a cell if there are not enough observations involving the two variables. It is set to require at least 10 observations involving the feature and the target parameter for the correlation to show a minimal representative meaning.

Below, the correlation matrix of the dataset is shown, where in the case that the literature does not explicitly expose the value of a chemical compound, this is treated numerically as 0.

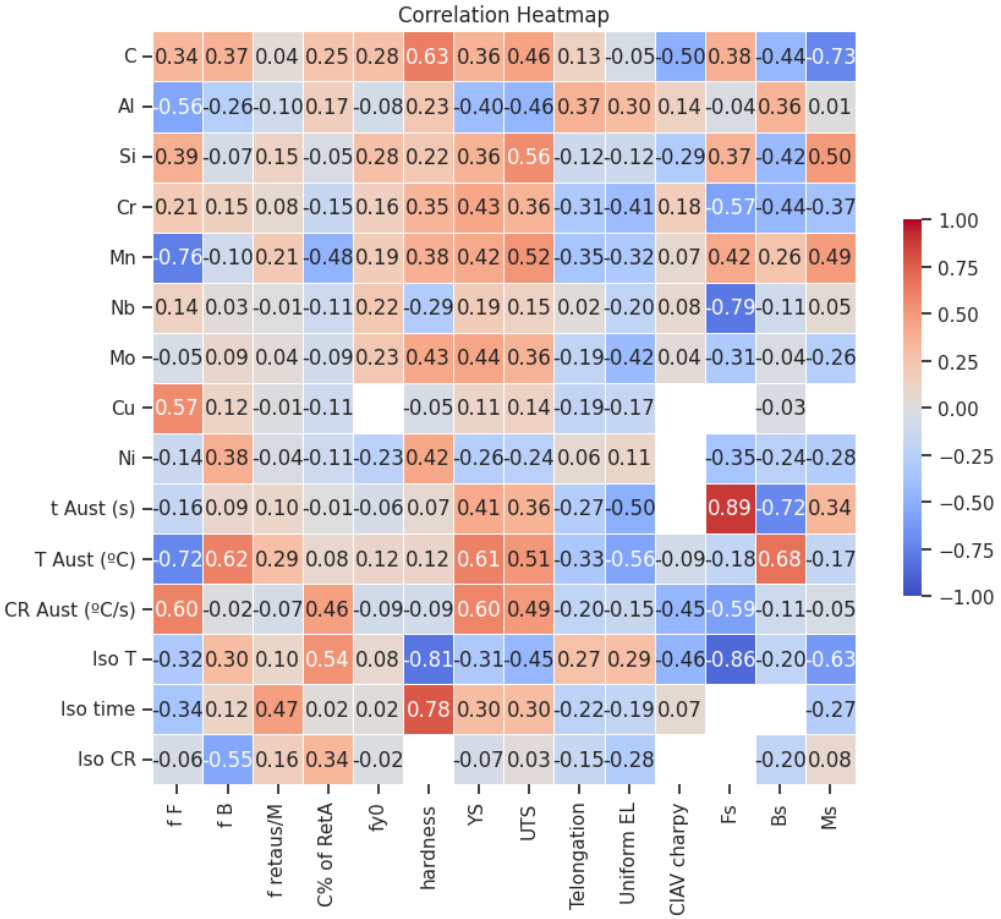

Figure A.2: Correlation Matrix of the dataset, where missing values of chemical elements are considered as zero.

A.3. Principal Component Analysis

Principal Component Analysis is a multivariate approach. Its major goal is to decrease the size of the dataset while keeping the vital elements of the information. To do this, the dataset is represented by a smaller number of new abstract variables that are linear combinations of the original variables. As a result, PCA reduces the size of the data while still extracting the most crucial information from it. The PCA is subject to the assumption that the parameters in the dataset have linear relationships. It changes into a new axis that corresponds with the highest variances. However, because these are linear axes, they will not be able to capture non-linear behaviours successfully.

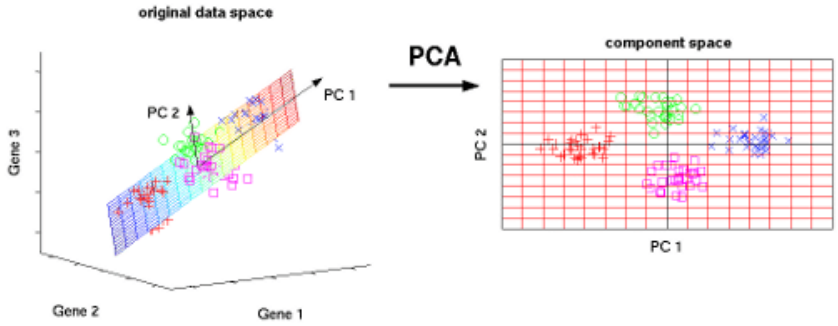

Figure A.3: PCA. PC1 axis is the first principal direction along which the samples show the largest variation. The PC2 axis is the second most important direction, and it is orthogonal to the PC1 axis.

This section primarily draws from H. Abdi and L. Williams' 2010 work, "Principal Component Analysis." [125]. 5 steps are performed in PCA:

1. Covariance Matrix Computation The first step is to compute the covariance matrix, which provides insights into the relationships between the various parameters in the dataset. The variance and co-variance between all pairs of variables in the dataset are calculated in the covariance matrix, which measures how they vary together, either positively or negatively.

2. Scaling and Standardization The next stage in PCA is to standardize the dataset. To do this, the data is then transformed so that each feature has a mean of 0 and a standard deviation of 1 because PCA is sensitive to the relative scales of the variables, therefore standardization is required. With this step, it is guaranteed that all parameters contribute equally to the analysis, and the importance of parameters is equalized.

3. Eigendecomposition In this step, we perform eigendecomposition on the covariance matrix to find its eigenvalues and eigenvectors. The principal components are represented by the eigenvectors, and the variance explained by each principle component is measured by the associated eigenvalues. Here, the dataset is transformed into a new coordinate system defined by the principal components.

4. Principal Component Selection The goal of this step is to select the eigenvectors associated with the greatest eigenvalues since they represent the most significant variation in the data. The principal components are ordered based on their eigenvalues, indicating the amount of variance they explain. Typically, a cumulative explained variance plot is used to determine the number of principal components to retain.

5. Dimensionality Reduction The last step of PCA is to project the original data onto the selected principal components to obtain the lower-dimensional representation. This is made simply by multiplying the normalized data by the matrix of selected eigenvectors, where the resulting transformed dataset has reduced dimensions. Each observation is represented by a set of new variables called the principal components. The dimensionality reduction allows for a simplified representation of the data while

preserving the most important patterns and variability.

Missing data can become a problem when applying PCA and can be handled in several ways. In continuous variables, the two most typical solutions are filling in the average value or the one that occurs most frequently [126]. For example, if a value occurs 70% of the time it may be wise to use that value for the missing data. However, if the data is more evenly distributed, and more uniform, the average value seems to fit better. These are easy options, however, the drawback is that they reduce the variance of the variables and therefore impact the results of the PCA. Empty values are handled before the standardization step so that they are filled with the original coordinate system and original mean or median values. This way, they are taken into account in the rotation of the coordinate system.

By following these steps, PCA provides a way to summarize complex datasets by capturing the most relevant information and reducing the dimensionality, which can be beneficial for data exploration, visualization, and subsequent analysis tasks. It is then time to select the desired number of components, as not all variables provide important information about the dataset. In the cumulative percentage of total variation, the eigenvalues are sorted in descending order. Then you sum up the eigenvalues from the first PC up to a certain component and divide it by the total sum of all eigenvalues. The cumulative representation helps to decide how many principal components to retain for analysis. One decides what percentage one wants to keep of the total variation, and then the number of PCs will be the smallest number with which the chosen percentage is exceeded. As PCA is a dimensionality reduction technique, it is desired to make as small as possible the selection of PCs that together capture a significant amount of variance in the dataset.

An alternative way of doing this is with the Scree-plot, as proposed in the book ‘Principal Component Analysis’ by Ian Jolliffe [127]. All eigenvalues are ordered by size, and in the scree-plot, a point is assigned as the ”elbow”, which divides the data into a steep and a flat slope. The principal components before the elbow are taken into account. However, this is not objective as different people can assign a different point as the elbow.

A.4. Meta-analysis discussion

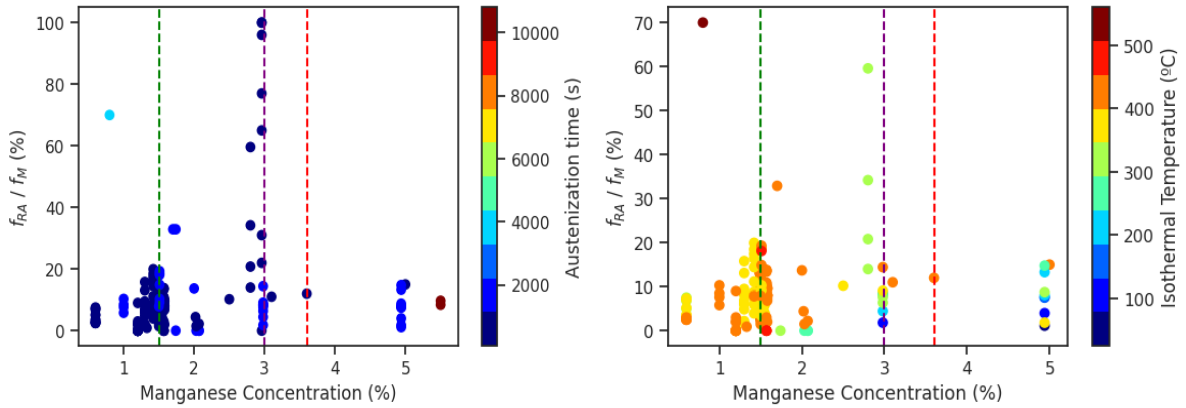

Figure A.4: Process parameters as a function of the manganese concentration.

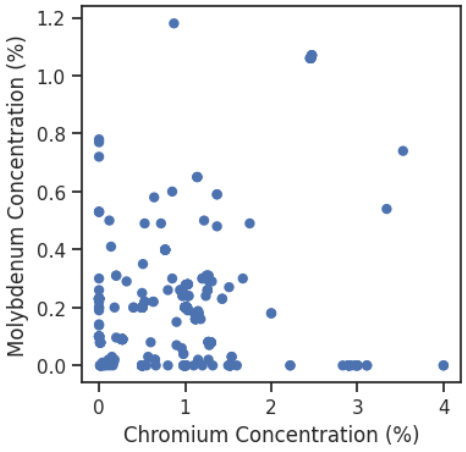

Figure A.5: Chromium concentration vs molybdenum concentration.

A.5. Prediction modelling

A.5.1. Empirical formula

In addition to the empirical equations Eqs. 5.1,5.2, the remaining empirical equations A.2-A.9 are as follows:

$$\begin{aligned} B_S(°C) = {} & 720 - 585.63C + 126.6C^2 - 66.34Ni + 6.06Ni^2 \\ & - 0.232Ni^3 - 31.66Cr + 2.17Cr^2 - 91.68Mn + 7.82Mn^2 \\ & - 0.3378Mn^3 - 42.37Mo \end{aligned} \tag{A.2}$$

$$B_S(°C) = 630 - 45Mn - 40V - 35Si - 30Cr - 24Mo - 20Ni \tag{A.3}$$

$$B_S(°C) = 844 - 597C - 63Mn - 16Ni - 78Cr \tag{A.4}$$

$$B_S(°C) = 711 - 362C + 262C^2 - 28Mn + 44Si \tag{A.5}$$

$$B_S(°C) = 839 - 86Mn - 23Si - 67Cr - 33Ni - 75Mo - 270(1 - \mathsf{exp}(-1.33C)) \tag{A.6}$$

$$M_S(°C) = 512 - 453C + 217C^2 - 17Ni + 15Cr - 72CMn - 68CCr - 7.5Si - 9.5Mo \tag{A.7}$$

$$M_S(°C) = 538 - 350C - 38Mn - 19Ni - 37Cr - 27Mo \tag{A.8}$$

$$M_S(°C) = 565 - 31Mn - 13Si - 10Cr - 18Ni - 12Mo - 600(1 - \mathsf{exp}(-0.96C)) \tag{A.9}$$

A.5.2. Outliers detection

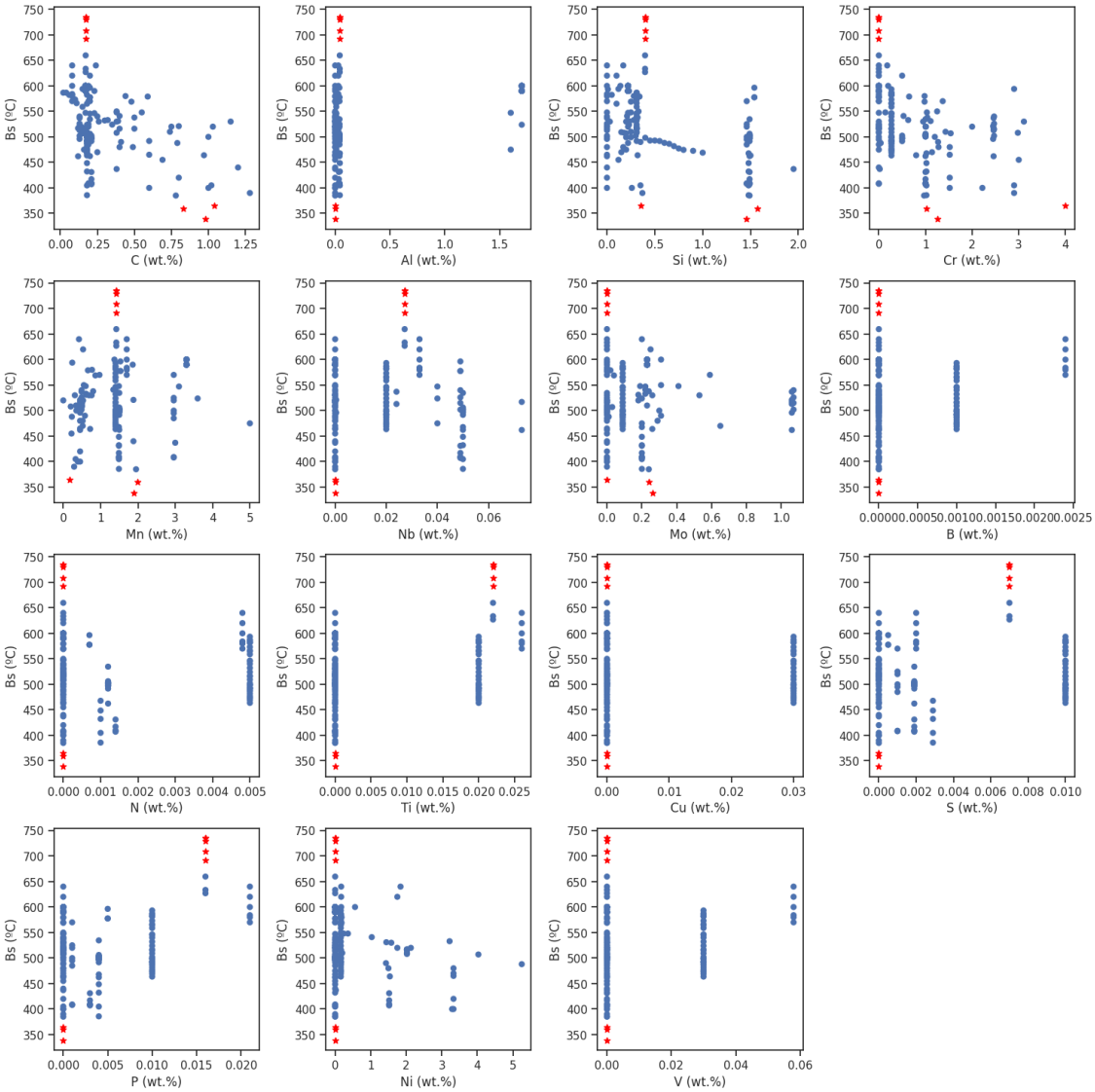

Figure A.6: Bs temperature outliers highlighted in dispersion against chemical elements.

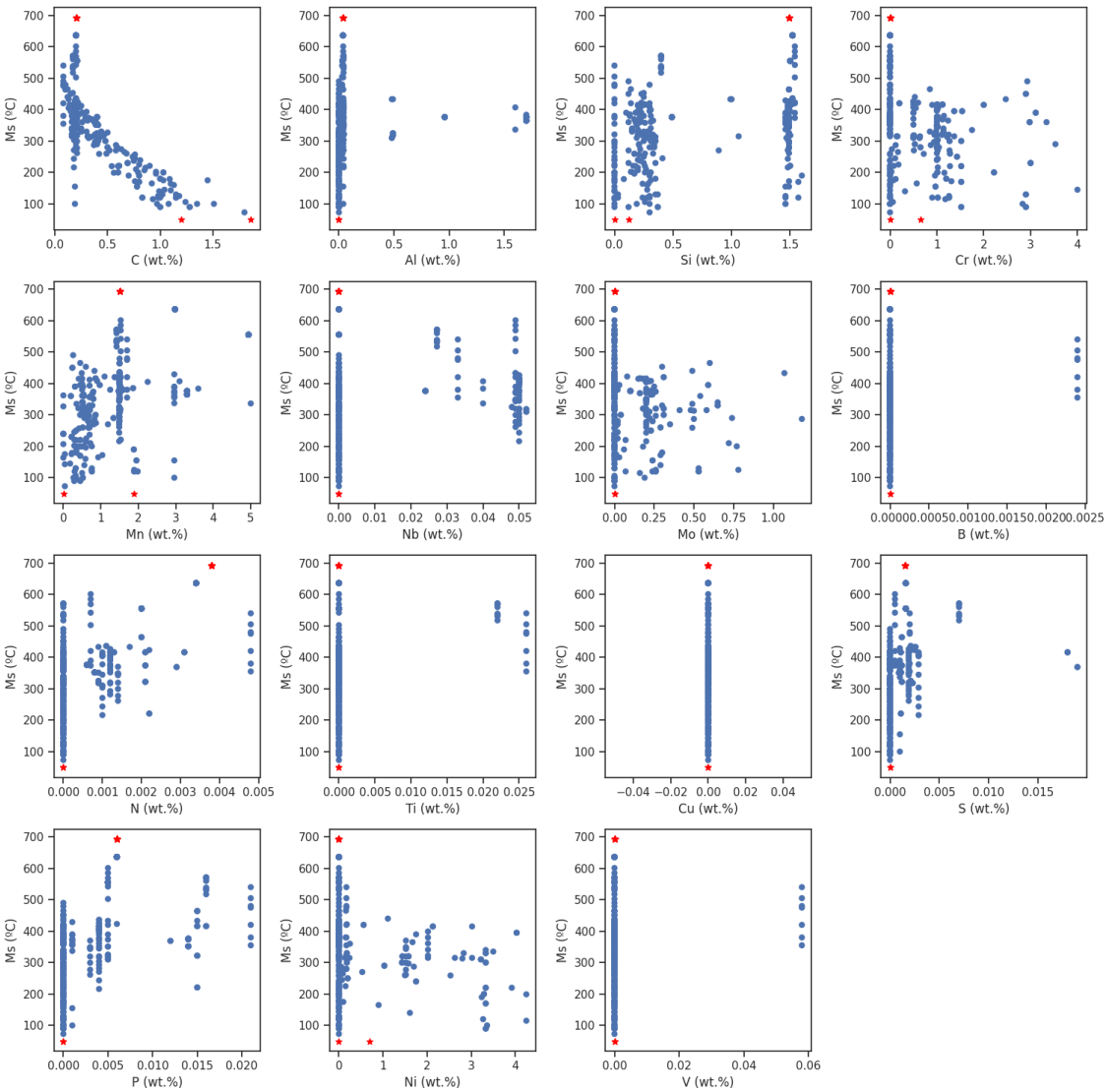

Figure A.7: Ms temperature outliers highlighted in dispersion against chemical elements.

A.5.3. Regression fitting

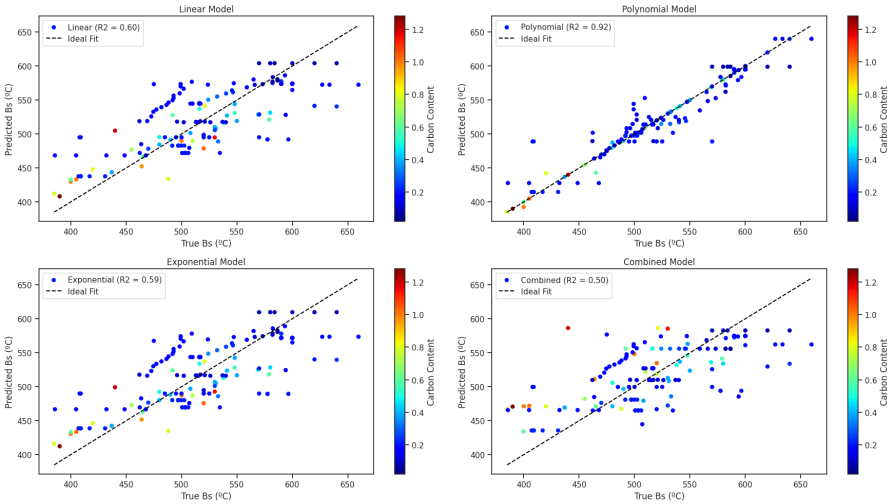

Figure A.8: Bs fitting with regression models as a function of carbon content.

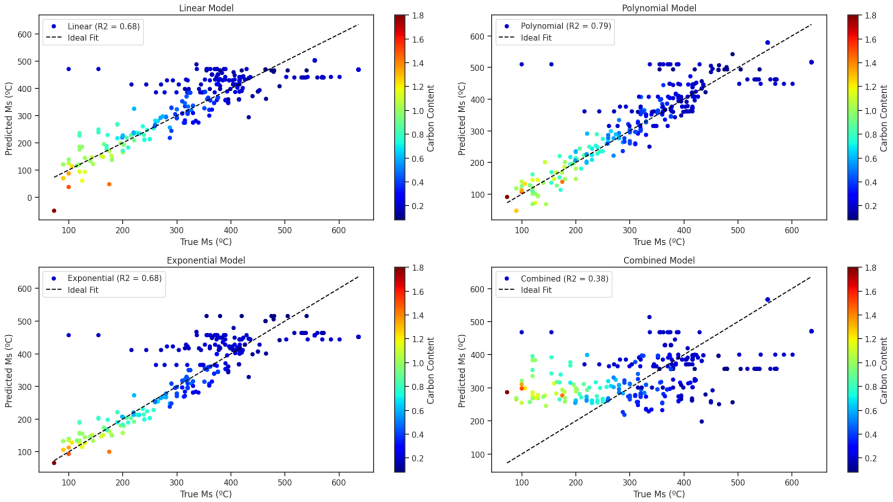

Figure A.9: Ms fitting with regression models as a function of carbon content.

A.5.4. Overfitting and underfitting in machine learning algorithms

A balanced fitting as well as models that underfit and overfit the data is illustrated in Figure A.10. The underfitting model exemplifies a linear model fitted to a nonlinear dataset. The overfitting model fits more-or-less all datapoints during training, but the predictability is likely poor for unseen data. The balanced model should be able to predict unseen data well.

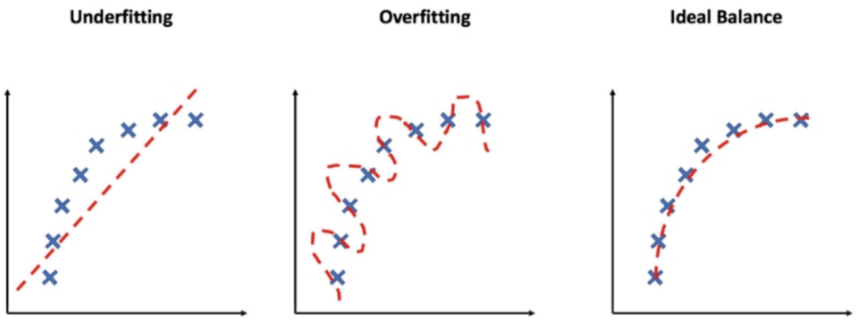

Figure A.10: Illustration of statistical fitting of data: underfitting, overfitting, and a balanced fitting.

A.5.5. Random Forest

The random forest algorithm is an ensemble machine learning approach that mixes the predictions of a large number of decision trees, where each one is trained using a random subset of training data and a random subset of features. The individual trees work together to create a forest that makes predictions. To understand it with the illustration in Figure A.11, the training sets (labelled by 'Decision Tree-N') are generated and a decision tree is generated for each training set (green and blue points). Then, it randomly selects some features for splitting and finds the optimal solution (green dots). It uses the bagging method, where the learning is performed simultaneously and then the outcome is averaged [128]. This way it obtains information on the samples and the corresponding features which avoid overfitting [129]. Following, the results of all trees ('Result-N') are evaluated together, and the final prediction is calculated via either voting or averaging ('Majority Voting / Averaging') [130]. Besides reducing overfitting and handling regression problems, the bagging process in RF helps reduce the variance of the model, which is an important issue in individual trees. By averaging or voting over multiple trees RF improves the predictive performance, making it a robust and widely-used ensemble method in ML.

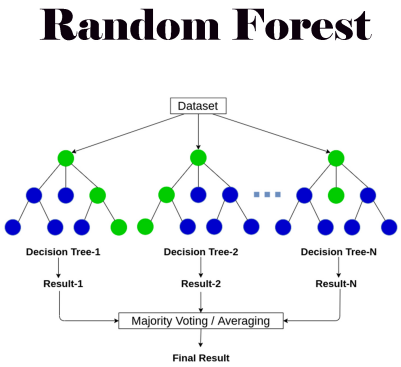

Figure A.11: Structure diagram of Random Forest algorithm.

A.5.6. B_S and M_S prediction results

In the following figures, the results of the five folds that predict the bainite start temperature (A.12-A.17) and martensite start temperature (A.18-A.23) are shown. The models used are linear, polynomial, exponential, combined, RF and GBDT. For every model, the folds are displayed as a function of the chosen six chemical components: C, Mn, Si, Cr, Ni, Mo.

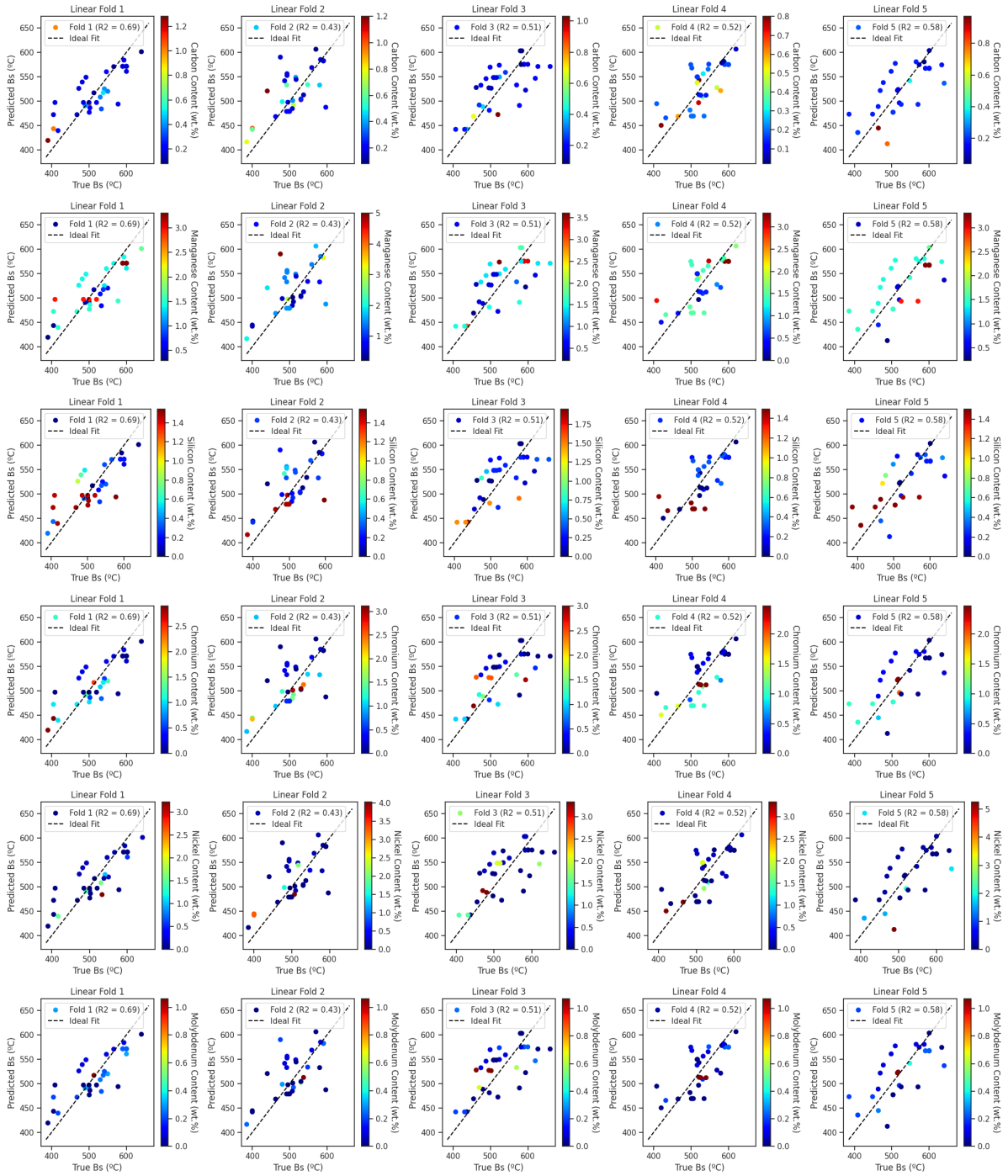

Figure A.12: B_S Predicted with the linear model. The folds are shown as a function of the different chemical components.

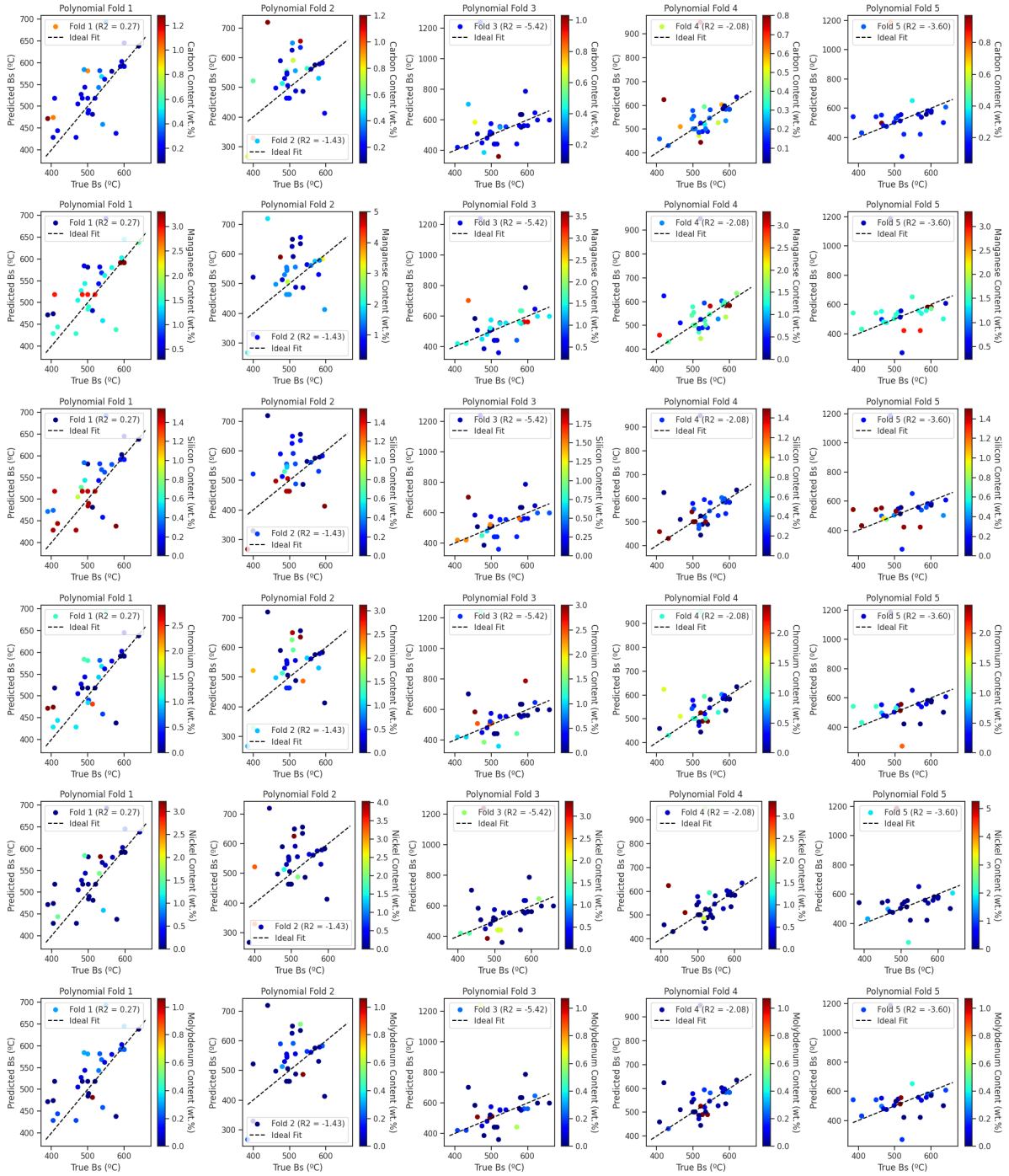

Figure A.13: B_S Predicted with the polynomial model. The folds are shown as a function of the different chemical components.

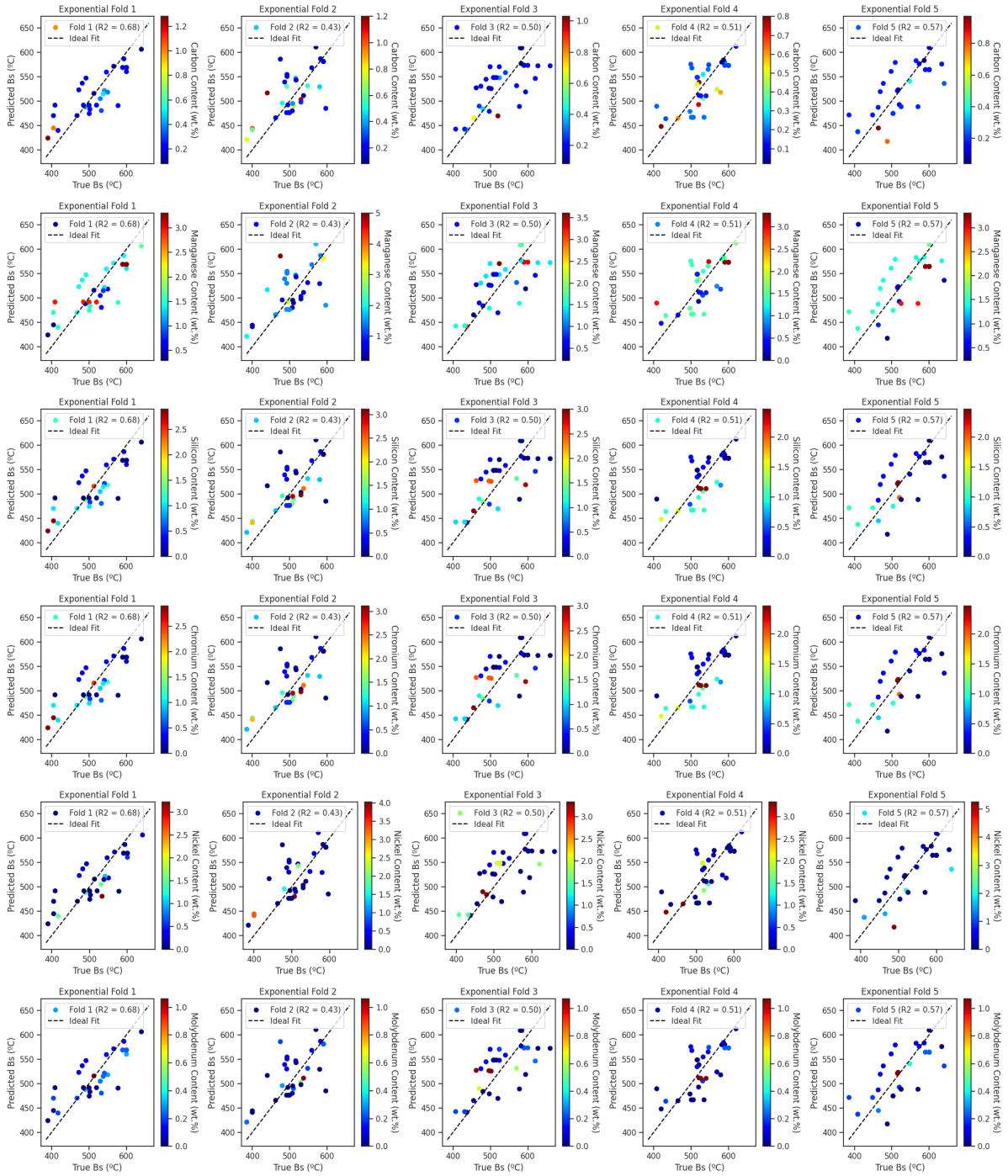

Figure A.14: B_S Predicted with the exponential model. The folds are shown as a function of the different chemical components.

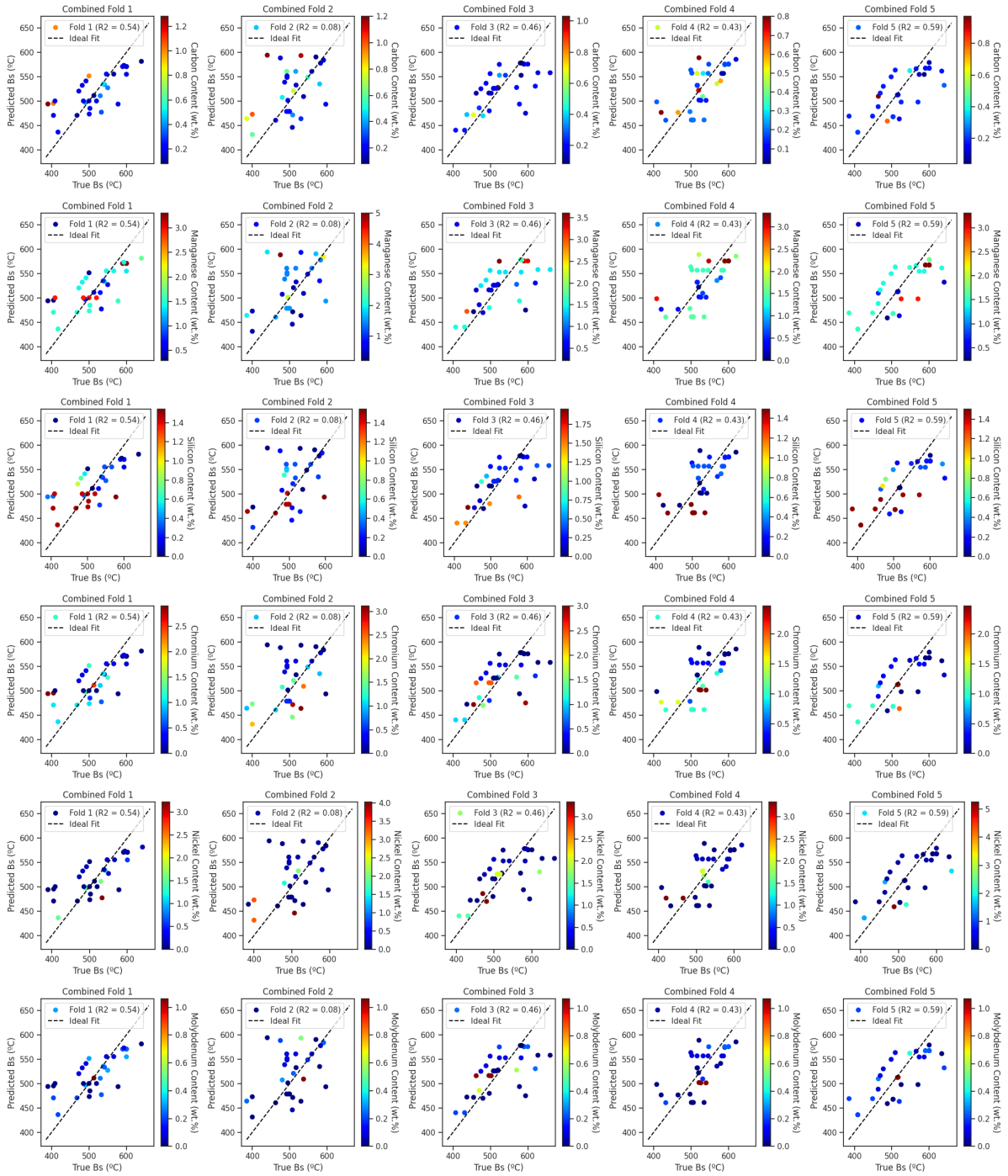

Figure A.15: B_S Predicted with the combined model. The folds are shown as a function of the different chemical components.

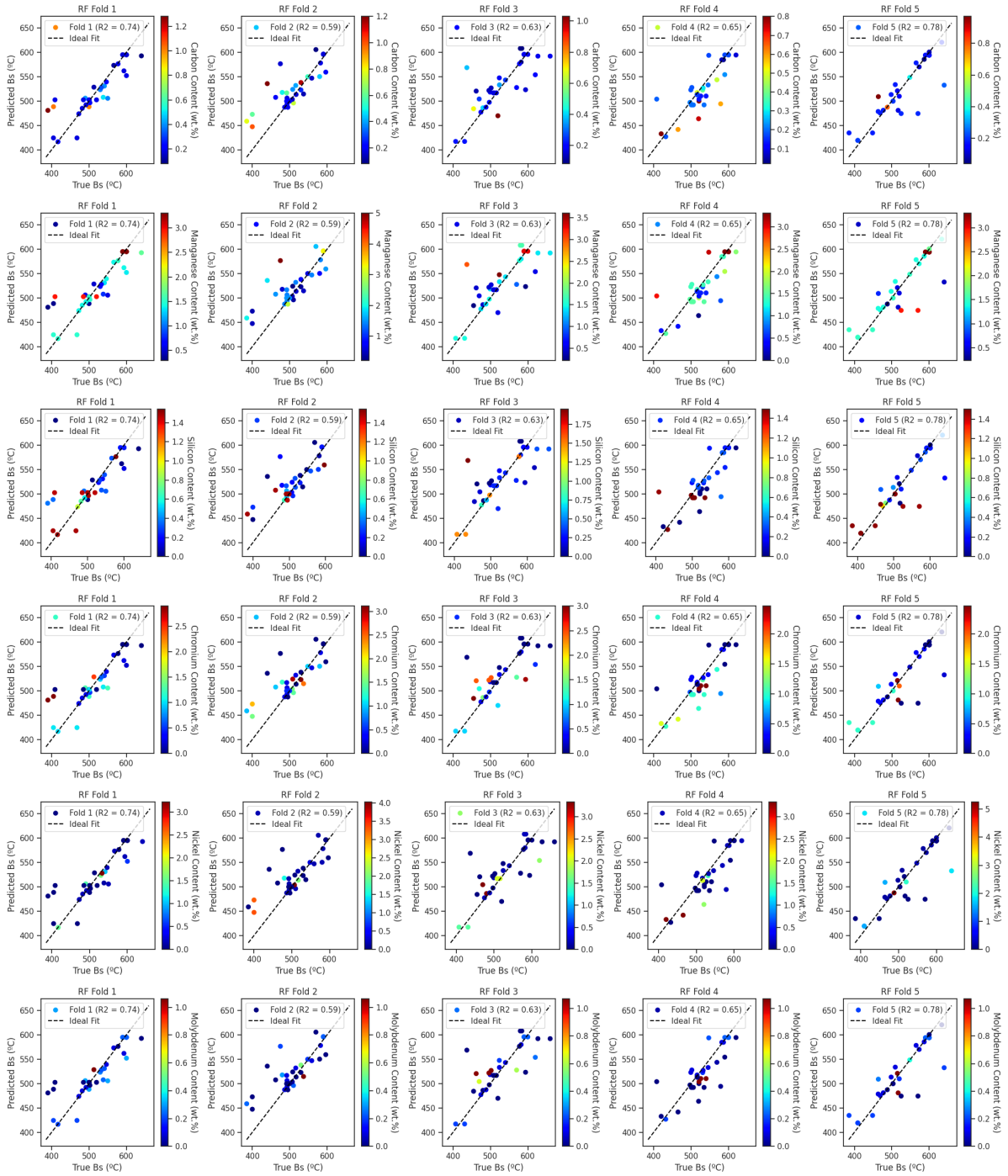

Figure A.16: B_S Predicted with the RF algorithm. The folds are shown as a function of the different chemical components.

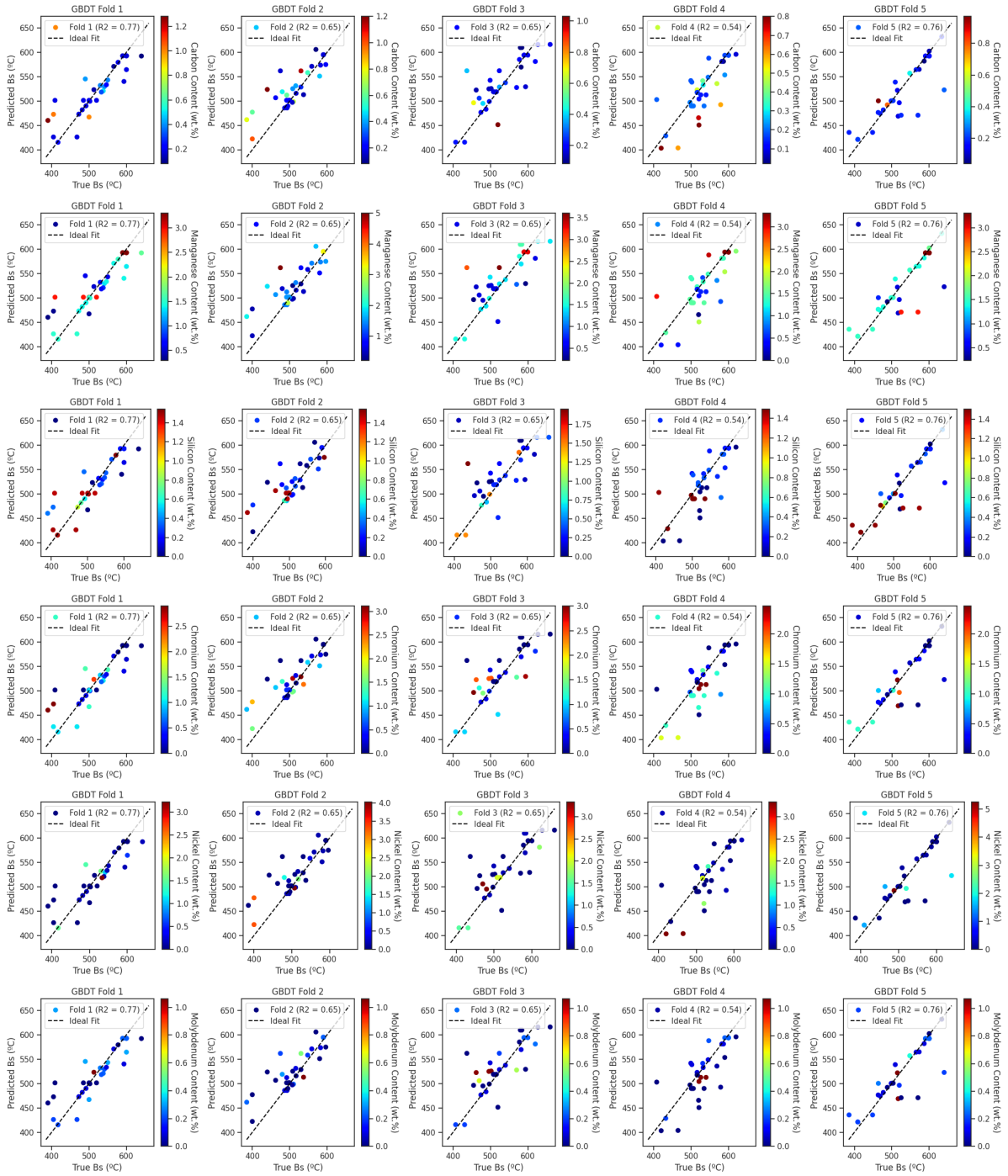

Figure A.17: B_S Predicted with the GBDT algorithm. The folds are shown as a function of the different chemical components.

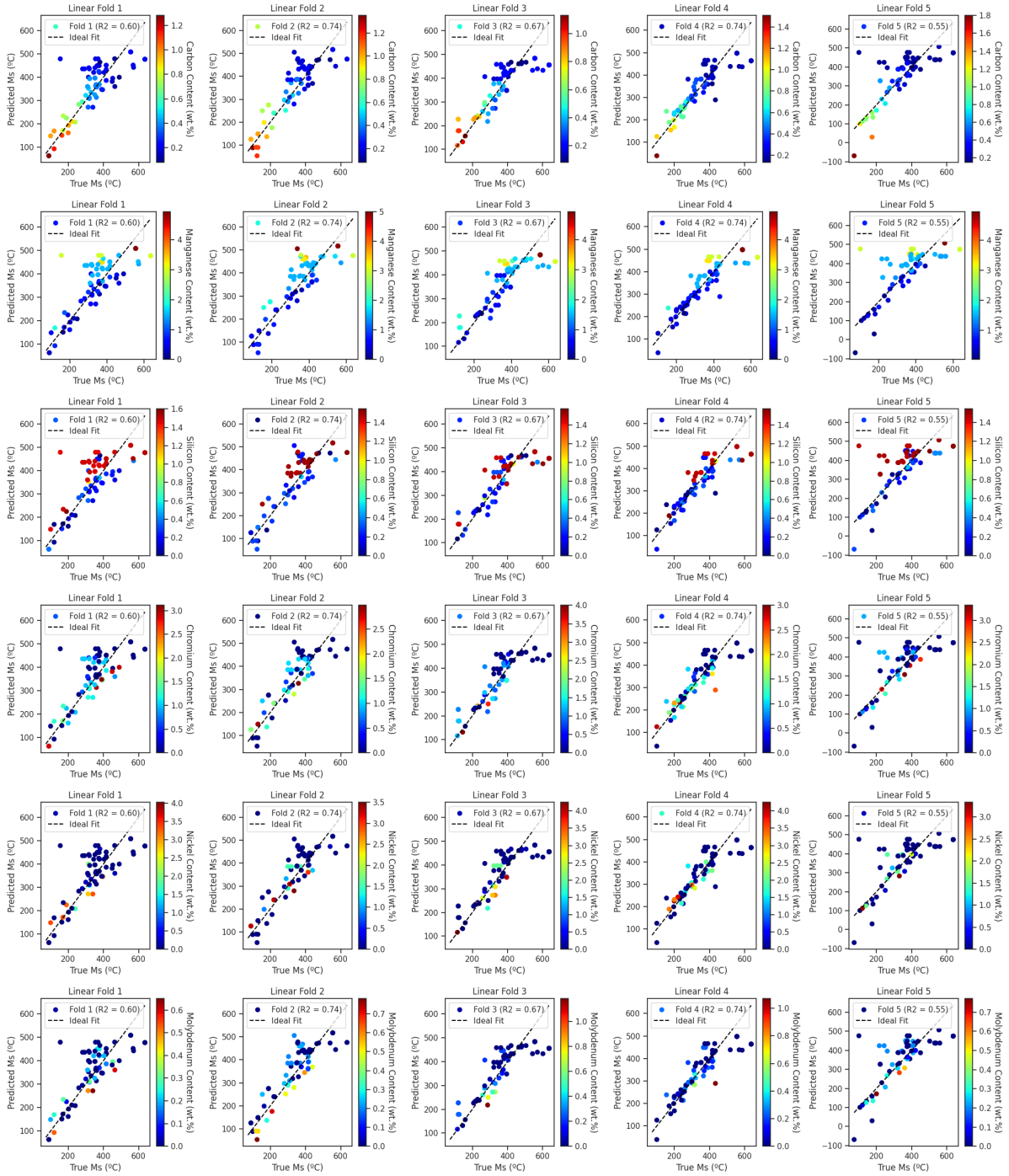

Figure A.18: M_S Predicted with the linear model. The folds are shown as a function of the different chemical components.

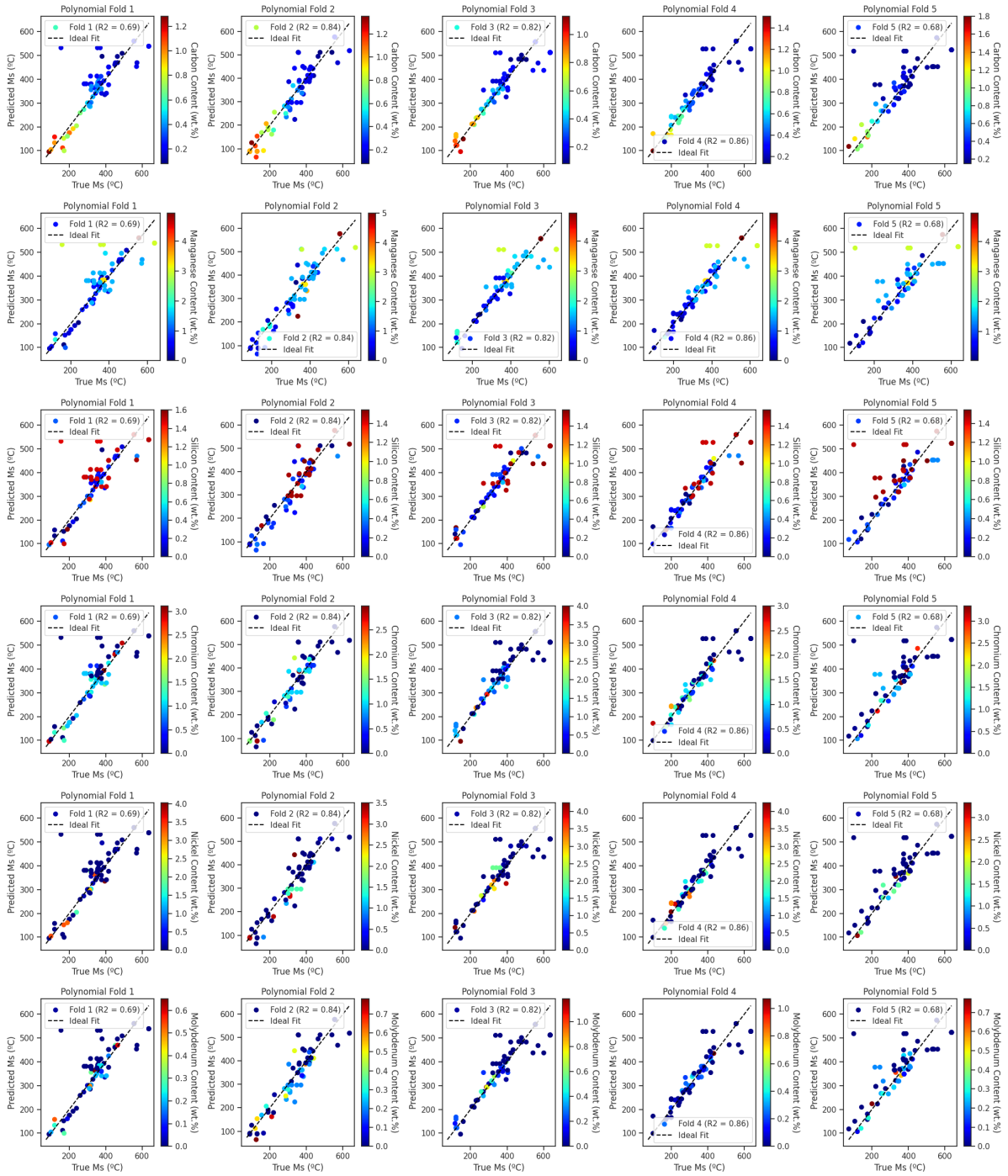

Figure A.19: M_S Predicted with the polynomial model. The folds are shown as a function of the different chemical components.

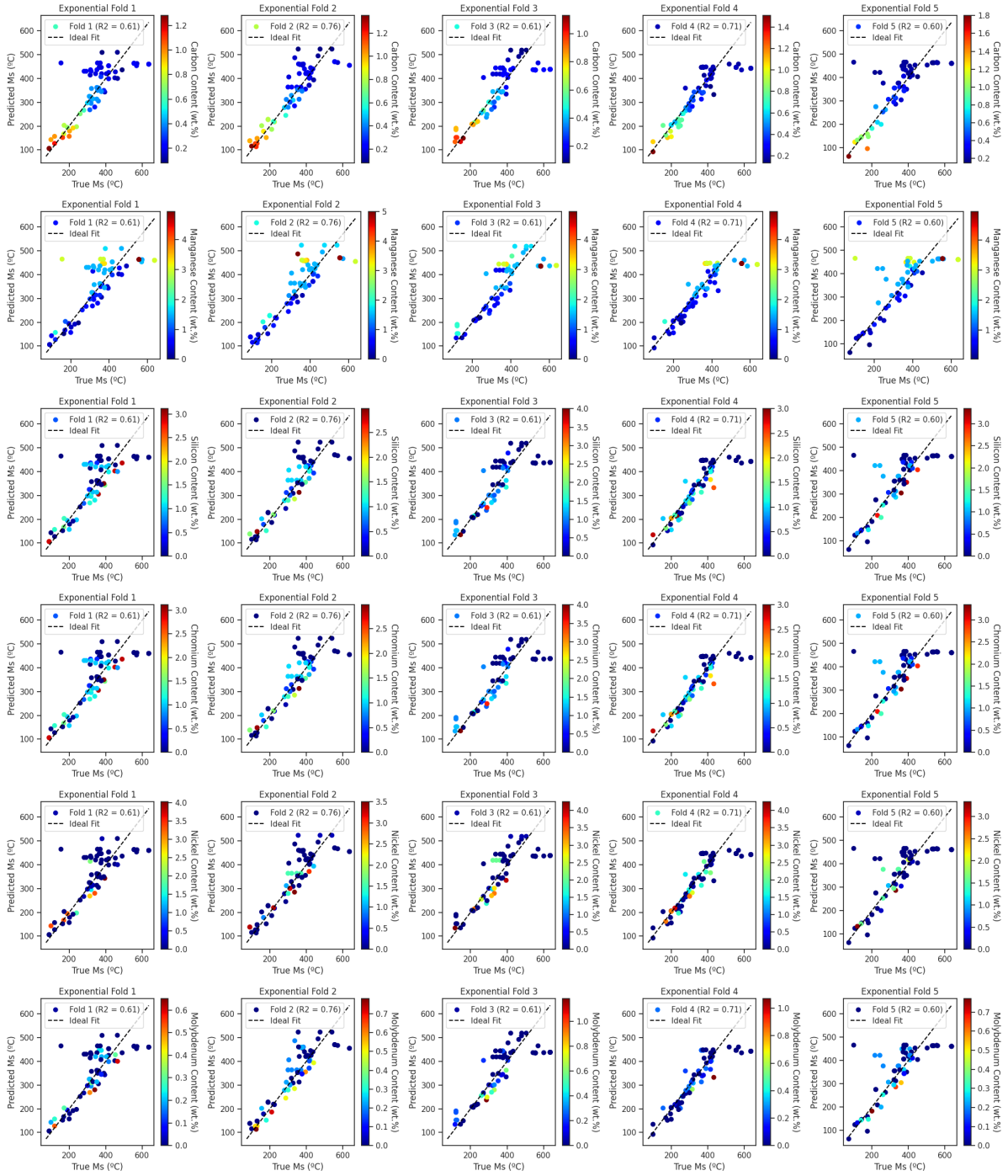

Figure A.20: M_S Predicted with the exponential model. The folds are shown as a function of the different chemical components.

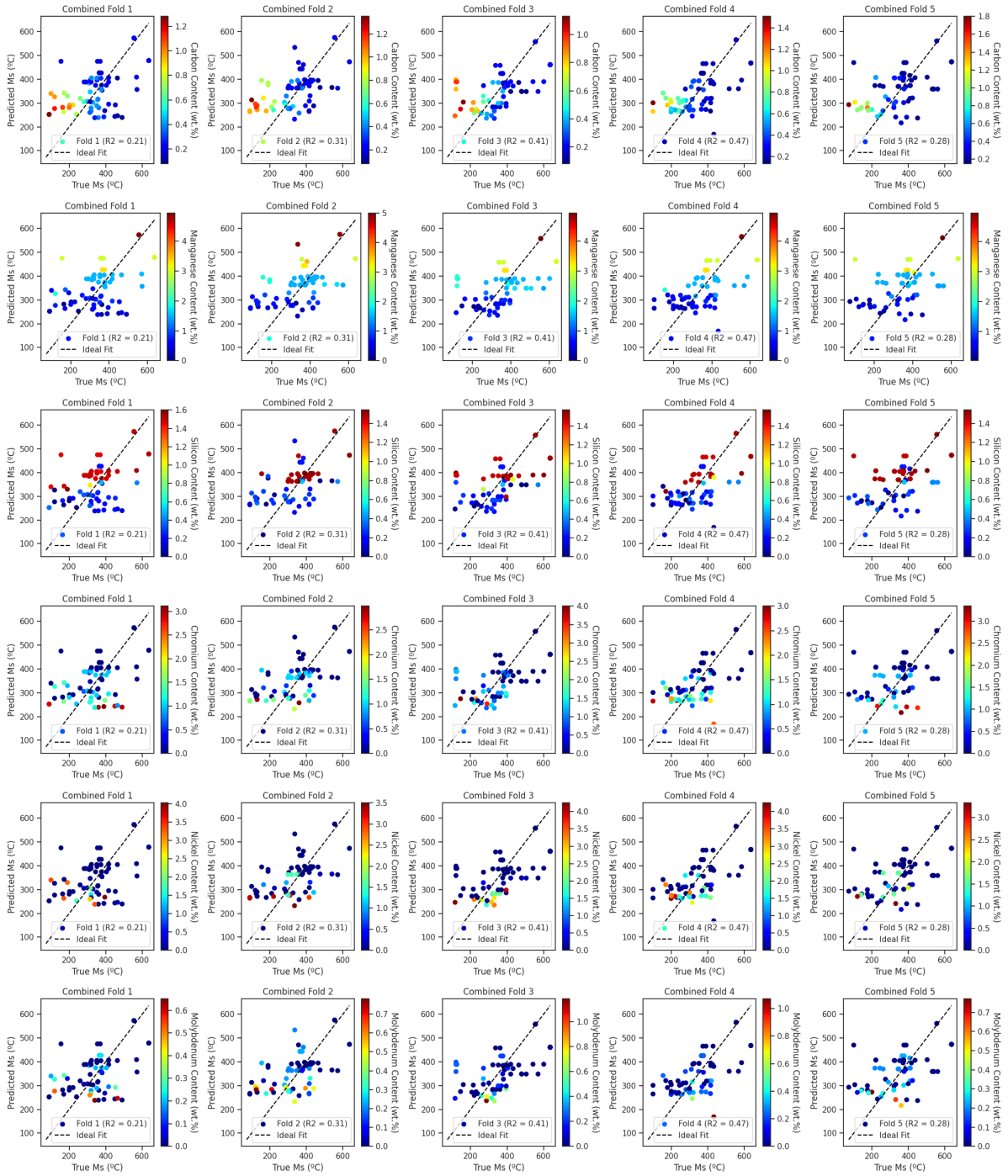

Figure A.21: M_S Predicted with the combined model. The folds are shown as a function of the different chemical components.

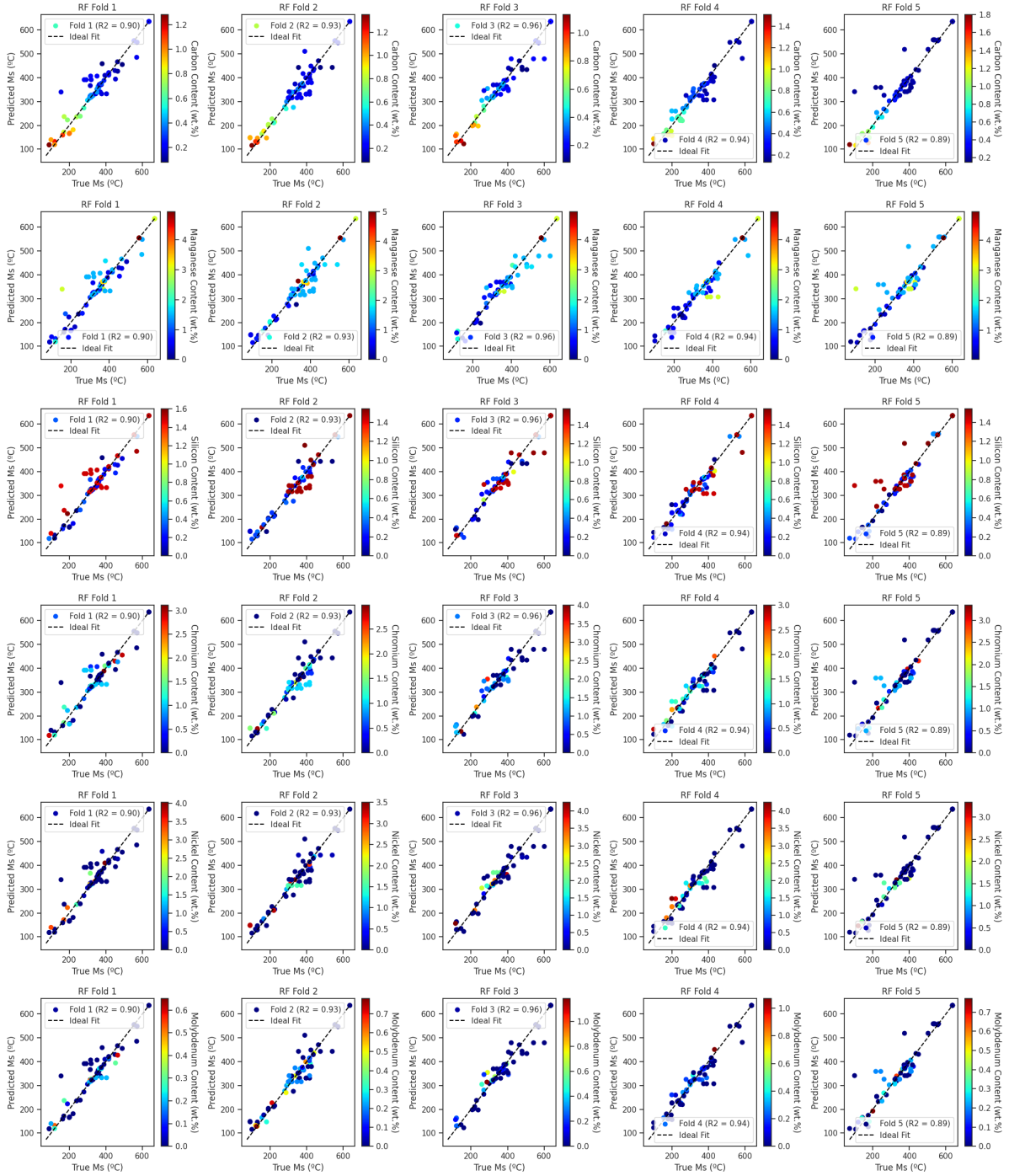

Figure A.22: M_S Predicted with the RF algorithm. The folds are shown as a function of the different chemical components.

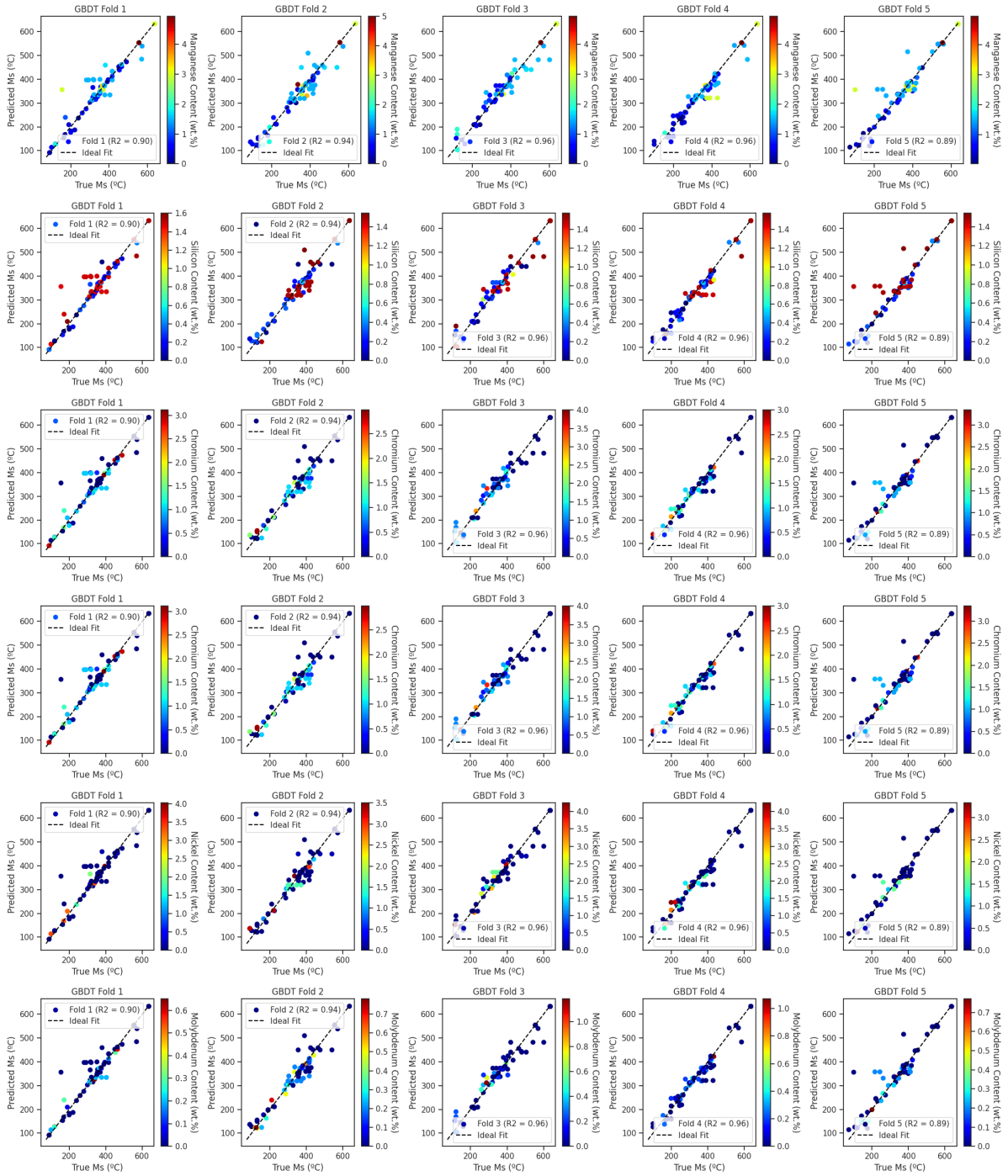

Figure A.23: M_S Predicted with the GBDT algorithm. The folds are shown as a function of the different chemical components.